e-ISSN 2667-9973
p-ISSN 1512-1127

საქართველოს გეოფიზიკური საზოგადოების ჟურნალი

მყარი დედამიწის, ატმოსფეროს, ოკეანისა და კოსმოსური პლაზმის ფიზიკა

ტომი 29 , № 1

JOURNAL OF THE GEORGIAN GEOPHYSICAL SOCIETY

Physics of Solid Earth, Atmosphere, Ocean and Space Plasma

Vol. 29, № 1

Tbilisi

2026

e-ISSN 2667-9973
p-ISSN 1512-1127

საქართველოს გეოფიზიკური საზოგადოების ჟურნალი

მყარი დედამიწის, ატმოსფეროს, ოკეანისა და კოსმოსური პლაზმის ფიზიკა

ტომი 29 , № 1

JOURNAL OF THE GEORGIAN GEOPHYSICAL SOCIETY

Physics of Solid Earth, Atmosphere, Ocean and Space Plasma

Vol. 29 , № 1

Tbilisi
2026

საქართველოს გეოფიზიკური საზოგადოების ჟურნალი

მყარი დედამიწის, ატმოსფეროს, ოკეანისა და კოსმოსური პლაზმის ფიზიკა

მთავარი რედაქტორი: თ. ჭელიძე

მთ. რედაქტორის მოადგილე: ჯ. ქირია; მდივანი: ა. ამირანაშვილი

ჟურნალის შინაარსი:

ჟურნალი მოიცავს მყარი დედამიწის, ატმოსფეროს, ოკეანისა და კოსმოსური პლაზმის ფიზიკის ყველა მიმართულებას. ჟურნალში ქვეყნდება: კვლევითი წერილები, მიმოხილვები, მოკლე ინფორმაციები, დისკუსიები, წიგნების მიმოხილვები, განცხადებები, კონფერენციების მოხსენებები.

JOURNAL OF THE GEORGIAN GEOPHYSICAL SOCIETY

Physics of Solid Earth, Atmosphere, Ocean and Space Plasma

Editor-in-chief: T. Chelidze

Vice-Editor: J. Kiria; Secretary: A. Amiranashvili

Scope of the Journal:

The Journal is devoted to all branches of the Physics of Solid Earth, Atmosphere, Ocean and Space Plasma. Types of contributions are: research papers, reviews, short communications, discussions, book reviews, announcements, conference reports.

ЖУРНАЛ ГРУЗИНСКОГО ГЕОФИЗИЧЕСКОГО ОБЩЕСТВА

Физика Твердой Земли, Атмосферы, Океана и Космической Плазмы

Главный редактор: Т. Челидзе

Зам. гл. редактора: Дж. Кирия; Секретарь: А. Амиранашвили

Содержание журнала:

Журнал Грузинского геофизического общества охватывает все направления физики твердой Земли, Атмосферы, Океана и Космической Плазмы. В журнале публикуются научные статьи, обзоры, краткие информации, дискуссии, обозрения книг, объявления, доклады конференций.

მისამართი:

საქართველო, 0160, თბილისი, ალექსიძის ქ. 1, მ. ნოდიას სახ. გეოფიზიკის ინსტიტუტი
ტელ.: 233-28-67; ფაქსი; (995 32 2332867); ელ. ფოსტა: tamaz.chelidze@gmail.com; avtandilamiranashvili@gmail.com;
geophysics.journal@tsu.ge

გამოქვეყნების განრიგი და ხელმოწერა:

გამოიცემა წელიწადში ორჯერ. მყარი ვერსიის წლიური ხელმოწერის ფასია: უცხოელი ხელმომწერისათვის - 30 დოლარი, საქართველოში - 10 ლარი. ხელმოწერის მოთხოვნა უნდა გაიგზავნოს რედაქციის მისამართით. შესაძლებელია უფასო ონლაინ წვდომა:
http://openjournals.gela.org.ge/index.php/GGS

ჟურნალი ინდექსირებულა Google Scholar-ში:
https://scholar.google.com/citations?hl=en&user=pdG-bMAAAAAJ

Address:

M. Nodia Institute of Geophysics, 1 Alexidze Str., 0160 Tbilisi, Georgia
Tel.: 233-28-67; Fax: (99532) 2332867; e-mail: tamaz.chelidze@gmail.com; avtandilamiranashvili@gmail.com;
geophysics.journal@tsu.ge

Publication schedule and subscription information:

The journal is issued twice a year. The subscription price for print version is 30 $ in year.
Subscription orders should be sent to editor's address. Free online access is possible:
http://openjournals.gela.org.ge/index.php/GGS

The journal is indexed in the Google Scholar:
https://scholar.google.com/citations?hl=en&user=pdG-bMAAAAAJ

Адрес:

Грузия, 0160, Тбилиси, ул. Алексидзе, 1. Институт геофизики им. М. З. Нодиа
Тел: 233-28-67; 294-35-91; Fax: (99532)2332867; e-mail: tamaz.chelidze@gmail.com; avtandilamiranashvili@gmail.com;
geophysics.journal@tsu.ge

Порядок издания и условия подписки:

Журнал издается дважды в год. Годовая подписная цена для печатной версии - 30 долларов США. Заявка о подписке высылается в адрес редакции. Имеется бесплатный онлайн доступ
http://openjournals.gela.org.ge/index.php/GGS

Журнал индексирован в Google Scholar:
https://scholar.google.com/citations?hl=en&user=pdG-bMAAAAAJ

This journal uses Open Journal Systems 2.4.8.3, which is open source journal management and publishing software developed, supported, and freely distributed by the Public Knowledge Project under the GNU General Public License.

(http://openjournals.gela.org.ge/index.php?journal=GGS&page=about&op=aboutThisPublishingSystem)

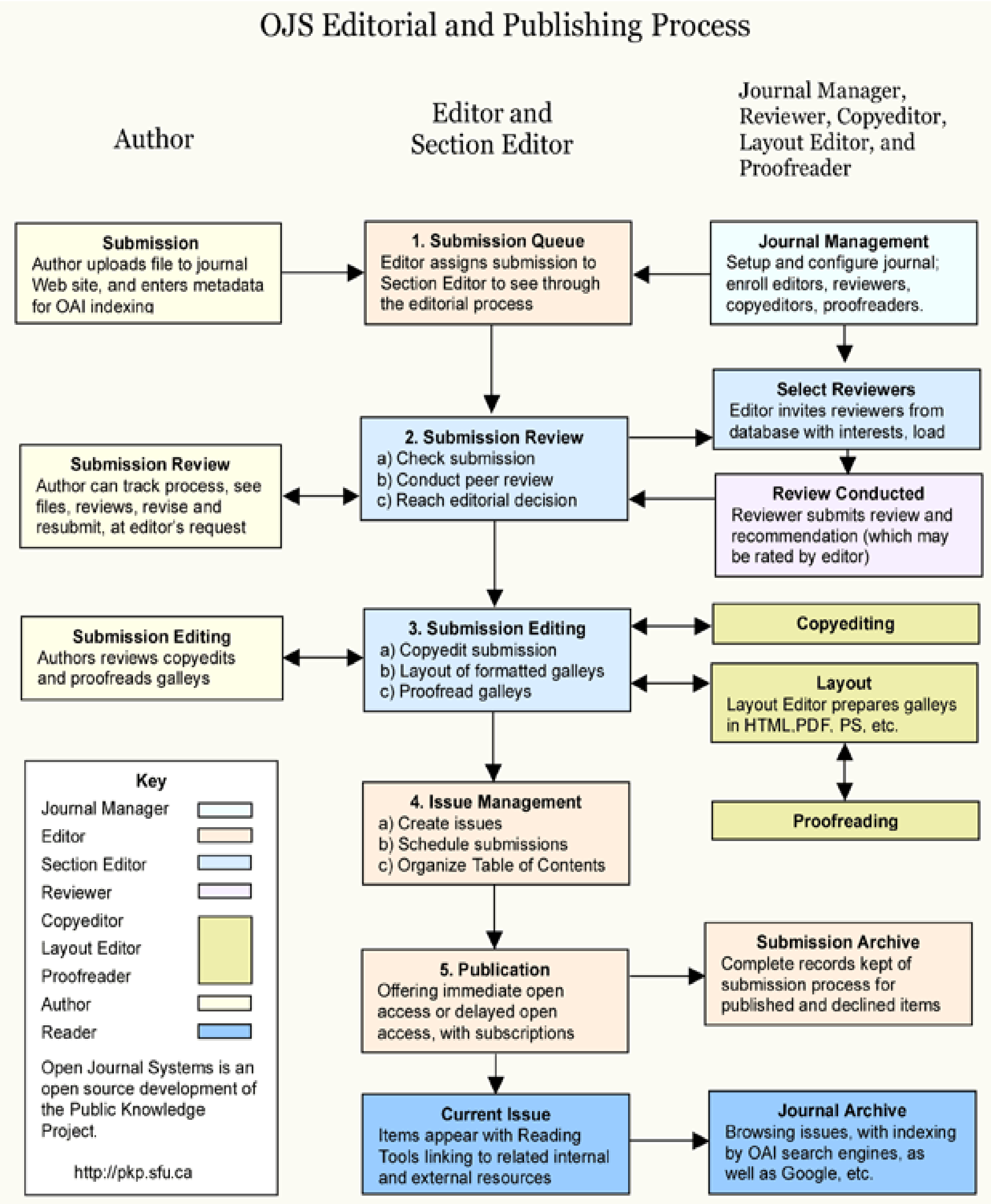

Journal of the Georgian Geophysical Society, e-ISSN: 2667-9973, p-ISSN: 1512-1127
Physics of Solid Earth, Atmosphere, Ocean and Space Plasma, v. 29(1), 2026, pp. 5-11

Delineation of New Models for Seismogenic Areal Sources in the Caucasus

Otar Sh. Varazanashvili

M. Nodia Institute of Geophysics, Iv. Javakhishvili Tbilisi State University, Georgia
e-mail: otar.varazanashvili@tsu.ge

ABSTRACT

New seismogenic areal sources were delineated in the Caucasus based on regional seismotectonic conditions, active faults, observed seismicity patterns, and previously published seismogenic source models. The resulting areal source new zonation provides a framework for the estimation of source-specific recurrence characteristics and seismic hazard contributions.

Keywords: *Probabilistic seismic hazard, seismogenic areal source, tectonic unit, active fault.*

1 Introduction

In connection with the reassessment of the seismic hazard of Georgia and its energy and other facilities, several geological, tectonic, and seismological objectives were addressed. These included the estimation of the maximum expected magnitude (Mwmax), the determination of the Gutenberg-Richter earthquake recurrence relationship and its coefficients (a and b), as well as the delineation of new areal source models for the broader region surrounding Georgia, i.e. the entire Caucasus.

The study area extends from 37.5° to 45.0° N and from 40.0° to 52.0° E, encompassing Georgia, Armenia, Azerbaijan, northeastern Turkey, northwestern Iran, the southern part of the Russian Federation, as well as the eastern Black Sea and western Caspian Sea regions. This area represents one of the most seismically active regions of the Alpine-Himalayan belt. In contrast to previously proposed source models, a new homogeneous areal source model was developed for the entire Caucasus region, providing a consistent framework for regional seismic hazard assessment.

Probabilistic seismic hazard analysis (PSHA) relies on the development of seismogenic source models, as the reliability of hazard estimates largely depends on the adequacy of source characterization. Modern PSHA practice commonly employs several types of seismogenic sources, including areal sources, active fault sources, and background seismicity models, to represent the spatial and temporal distribution of earthquake occurrence. However, individual source types do not always satisfy the assumption of relative tectonic and seismological homogeneity, and in some cases the available earthquake statistics are insufficient for robust estimation of recurrence parameters required for probabilistic seismic hazard assessment. Therefore, a regional areal source model was developed for the Caucasus region based on the integrated interpretation of tectonic units, active fault systems, and observed seismicity. The resulting areal sources represent tectonically coherent regions that provide a suitable framework for the estimation of earthquake recurrence parameters and maximum expected magnitudes. The delineation of the areal sources was based on the geometry of the major tectonic units of the Caucasus, subsequently refined using information on active fault systems and the spatial distribution of seismicity.

2 Input data

As noted above, tectonic units, active faults, and seismicity constitute the principal datasets used for the development of the seismogenic areal source model. The present study is based entirely on information published in internationally recognized scientific literature. In particular, the description and geometry of the principal tectonic units of the Caucasus were adopted from Adamia et al. (2011) [1] and Adamia et al. (2017) [2] (Fig. 1). Information on active fault systems was compiled from Caputo and Gamkrelidze et al. (2000) [3], Adamia et al. (2008) [4], Danciu et al. (2018) [5], and Basili et al. (2024) [6] (Figs. 2-5).

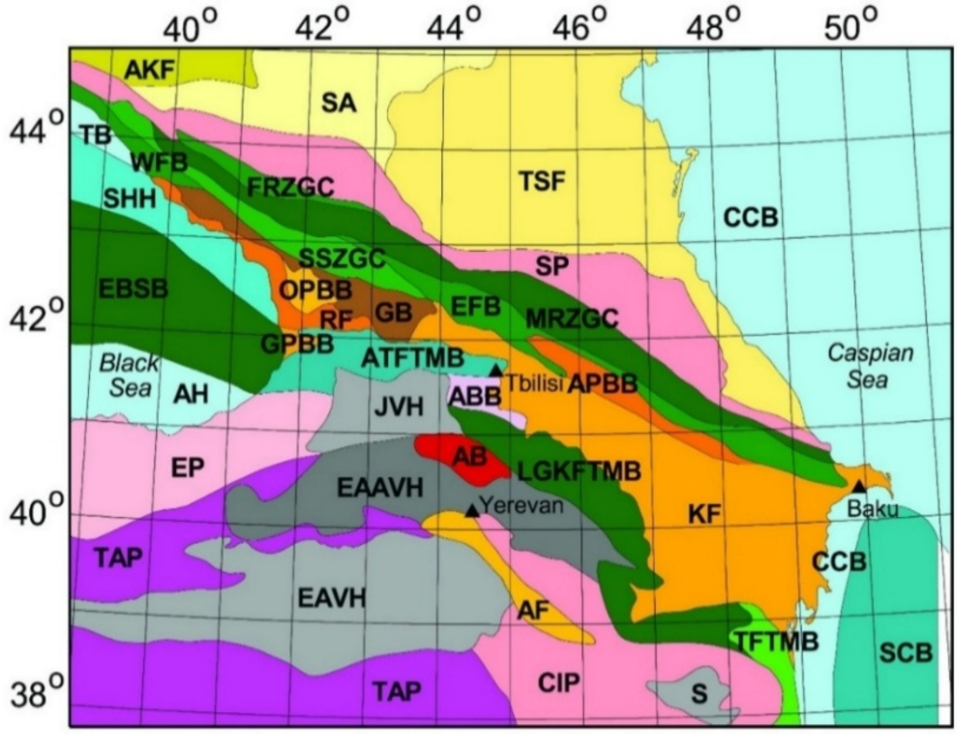

Fig. 1 Tectonic units of the Caucasus according to Adamia et al. (2011, 2017) [1, 2]: AKF – Azov-Kuban Foredeep; SA – Stavropol Arch; TSF – Terek-Caspian Foredeep; SP – Scythian Platform; FEZGC – Fore Range Zone of Great Caucasus; MEZOC – Main Range Zone of Great Caucasus; WFB – Western Flysch Basin; SSZGC – Southern Slope Zone of Great Caucasus; EFB – Eastern Flysch Basin; TB – Tuapse Basin; SHH – Shatsky High; EBSB – Eastern Black Sea Basin; AH – Arkhangelsky High; GB – Georgian Block; OPBB – Odishi Piggyback Basin; RP – Rioni Foreland; GPBB – Guria Piggyback Basin; APBB – Alazani Piggyback Basin; KF – Kura Foreland; ATFTMB – Achara-Trialeti Fold-Thrust Mountain Belt; JVH – Javakheti Volcanic Highland; ABB – Artvin-Bolnisi Block; AB – Armenian Block; LGKFTMB – Loki-Garabagh-Kafan Fold-Thrust Mountain Belt; EP – Eastern Pontides; TAP – Taurus-Anatolian Platform; EAAVH – Eastern Anatolian-Armenian Volcanic Highland; EAVH – Eastern Anatolian Volcanic Highland; AF – Aras Foreland; CIP – Central Iranian Platform; S – Sabalan; TFTMB – Talesh Fold-Thrust Mountain Belt; CCB – Central Caspian Basin; SCB – South Caspian Basin.

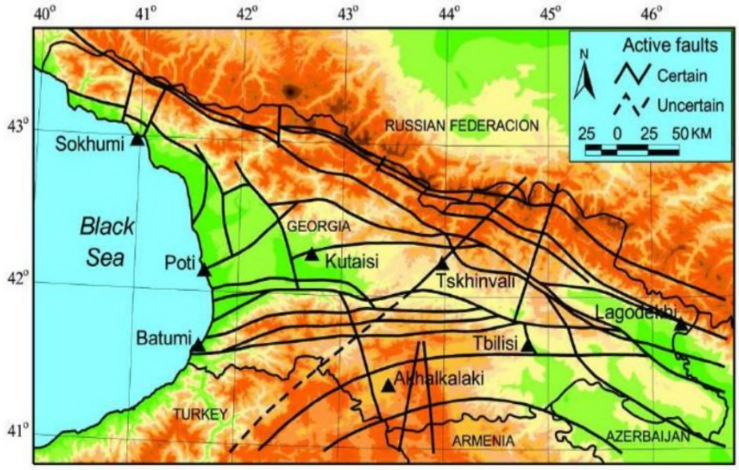

Fig. 2 Active faults in Georgia according to Caputo, Gamkrelidze et al. (2000) [3]

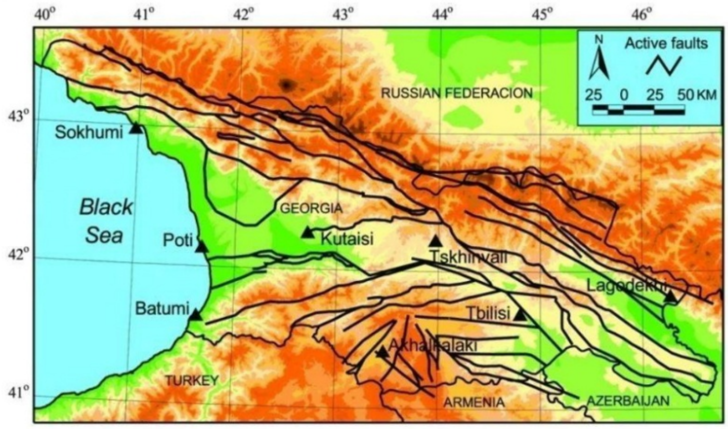

Fig. 3 Active faults in Georgia according to Adamia et al. (2008) [4]

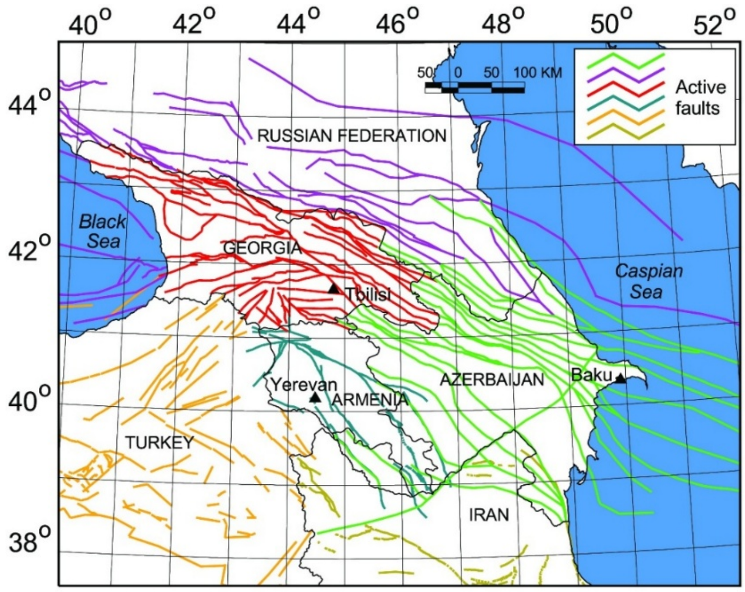

Fig. 4 Active faults in the Caucasus according to the Middle East Seismogenic Source Model – EMME-SSM14 (Danciu et al., 2018) [5]

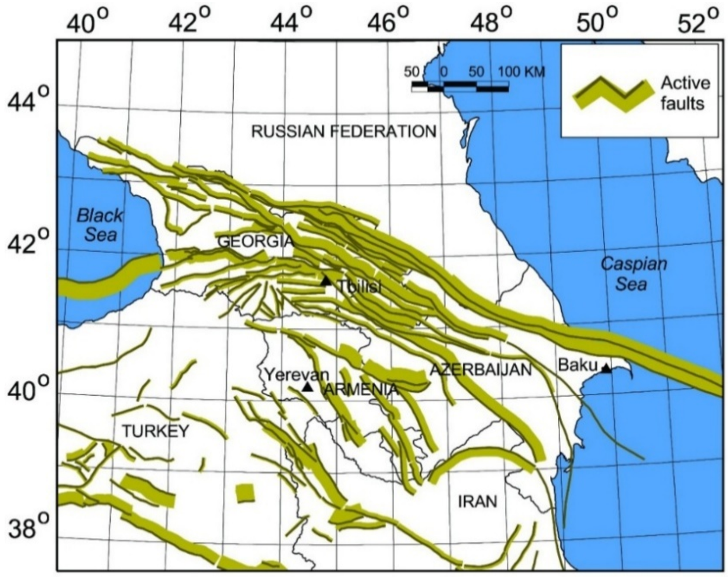

Fig. 5 Active faults in the Caucasus according to the European Fault Source Model – EFSM20 (Basili et al., 2024) [6]

In addition, the newly developed (in M. Nodia Institute of Geophysics of Iv. Javakhishvili Tbilisi State University, IGTSU, 2026) unified earthquake catalogue of the Caucasus was used as the primary seismological dataset for the delineation of the Caucasus areal source model.

3 New models of areal source (AS)

In the process of developing models of such seismogenic areal sources, it should be emphasized that from a methodological point of view, their delineation is based on the zones of tectonic units, active faults within them, and seismicity. The boundaries of areal sources are delineated within tectonic units in such a way as to minimize intersections with active faults. Where possible, the boundaries should not cross active faults; in the case of extensive faults, they should not intersect individual fault segments.

We compared and reconciled geological and seismological data to enable their joint consideration to develop a seismogenic areal source models. The resulting seismogenic areal source models of the Caucasus region defined by regional data on active tectonics and which are correlated with regional observed seismicity.

The seismic potential, or Mwmax, of each seismogenic super source was estimated using several methods presented in Varazanashvili and Tsereteli (2020) [7]. Three of these methods are seismological and two are geological. The final Mwmax values are obtained of averaging the individual values by the five methods.

Specifically, 27 seismogenic areal source (AS) zones have been delineated in the Caucasus region. **AS zone 1** within the study region includes part of Azov-Kuban Lowland and its seismic potential is estimated to be – Mwmax=5.5; **AS zone 2** includes part of Stavropol Arch – Mwmax=6.0; **AS zone 3** includes part of Terek-Caspian Foredeep – Mwmax=7.0; **AS zone 4** includes norten part of Central Caspian Basin – Mwmax=7.0; **AS zone 5** includes western part of Scythian Platform – Mwmax=6.5; **AS zone 6** includes eastern part of Scythian Platform – Mwmax=6.5; **AS zone 7** ncludes Fore Range Zone of Great Caucasus, western part of Main Range Zone of Great Caucasus, Southern Slope Zone of Great Caucasus, Western Flysch Basin, western part of Eastern Flysch Basin – Mwmax=7.5; **AS zone 8** includes eastern part of Main Range Zone of Great Caucasus, Eastern Flysch Basin, western part of Alazani Piggyback Basin – Mwmax=7.5; **AS zone 9** includes Georgian Block, Rioni Foreland, part of Tuapse Basin, Shatsky High – Mwmax=6.5; **AS zone 10** includes part of Georgian Block, Odishi Piggyback Basin – Mwmax=6.5; **AS zone 11** includes Kura Foreland, eastern part of Alazani Piggyback Basin – Mwmax=7.0; **AS zone 12** includes part of Eastern Black Sea Basin, part of Arkhangelsky High – Mwmax=6.5; **AS zone 13** includes part of Kura Foreland part, Guria Piggyback Basin, Achara-Trialeti Fold-Thrust Mountain Belt, part of Javakheti Volcanic Highland –

Mwmax=7.0; **AS zone 14** includes Artvin-Bolnisi Block, part of Loki-Garabagh-Kafan Fold-Thrust Mountain Belt part – Mwmax=7.0; **AS zone 15** includes part of Arkhangelsky High – Mwmax=6.0; **AS zone 16** includes Eastern Pontides – Mwmax=6.0; **AS zone 17** includes Javakheti Volcanic Highland, Armenian Block – Mwmax=7.5; **AS zone 18** includes part of Taurus-Anatolian Platform, part of Eastern Anatolian Volcanic Highland – Mwmax=8.0; **AS zone 19** includes Eastern Anatolian-Armenian Volcanic Highland part, part of Taurus - Anatolian Platform, part of Armenian Block – Mwmax=7.5; **AS zone 20** includes Eastern Anatolian Volcanic Highland, part of Taurus-Anatolian Platform, part of Central Iranian Platform part – Mwmax=8.0; **AS zone 21** includes Aras Foreland, part of Central Iranian Platform – Mwmax=7.0; **AS zone 22** includes part of Taurus-Anatolian Platform part – Mwmax=8.0; **AS zone 23** includes part of Central Iranian Platform part – Mwmax=7.5; **AS zone 24** includes Sabalan – Mwmax=5.5; **AS zone 25** includes part of Loki-Garabagh-Kafan Fold-Thrust Mountain Belt, part of Talesh Fold-Thrust Mountain Belt – Mwmax=7.5; **AS zone 26** includes part of Central Caspian Basin southern – Mwmax=6.5; **AS zone 27** includes South Caspian Basin – Mwmax=6.0 (see Figs. 6 and 7).

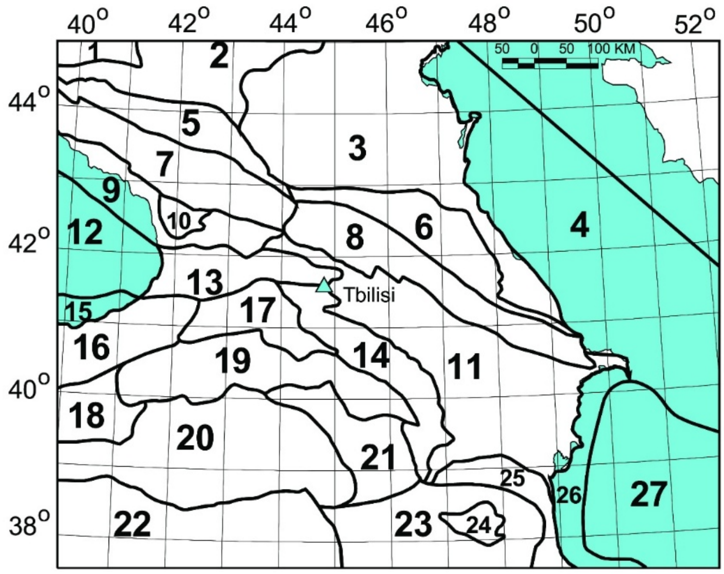

Fig. 6 New seismogenic areal source zones of the Caucasus region.

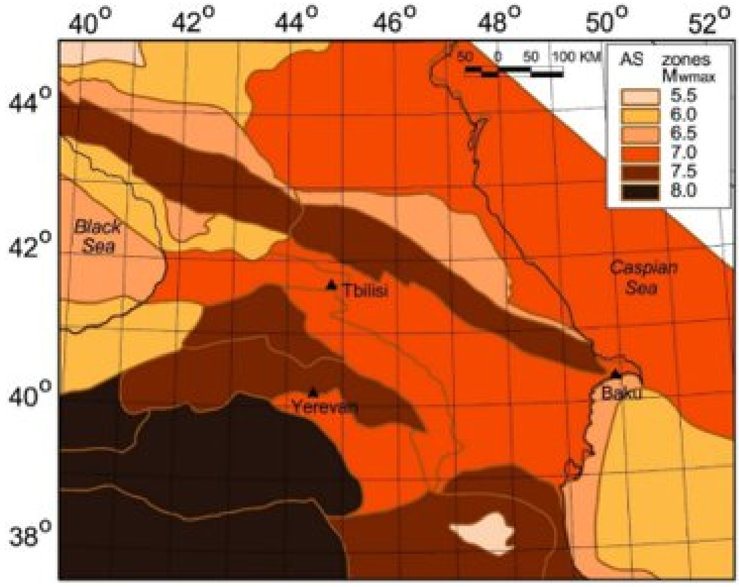

Fig. 7 Seismic potential of seismogenic areal source zones in the Caucasus region.

4 Conclusions

Existing seismogenic source models do not always satisfy the assumption of relative tectonic and seismological homogeneity or provide reliable estimates of the earthquake recurrence parameters required for probabilistic seismic hazard assessment (PSHA).

To address the reassessment of seismic hazard for the territory of Georgia and its critical facilities, a new set of seismogenic areal source models has been developed for the Caucasus region. These models are based on the integrated interpretation of tectonic units, active fault systems, and instrumental and historical seismicity.

The present study is based entirely on geological information published in internationally recognized scientific literature and on the newly developed Unified Earthquake Catalog of the Caucasus (2026), compiled at IGTSU.

As a result of this study, 27 new seismogenic areal source zones were delineated within the Caucasus region. These zones provide a robust framework for determining earthquake recurrence relationships and for conducting probabilistic seismic hazard assessments.

References

[1] Adamia S., Zakariadze G., Chkhotua T., Sadradze N., Tsereteli N., Chabukiani A., Gventsadze A. Geology of the Caucasus: A review. Turkish Journal of Earth Sciences 20 (5), 2011, pp. 489-544. https://doi.org/10.3906/yer-1005-11

[2] Adamia Sh., Alania V., Tsereteli N., Varazanashvili O., Sadradze N., Lursmanashvili N., Gventsadze A. Post-collisional tectonics and seismicity of Georgia. Tectonic Evolution, Collision, and Seismicity of Southwest Asia: In Honor of Manuel Berberian's Forty-Five Years of Research Contributions, Geological Society of America Special Paper, 525, 2017, pp. 535-572.

[3] Caputo M., Gamkrelidze I., Malvezzi V., Sgrigna V., Shengelaia G., Zilpimiani D. Geostructural basis and geophysical investigations for the seismic hazard assessment and prediction in the Caucasus. Il Nuovo Cimento, vol. 23C (2), 2000, pp.191-215.

[4] Adamia Sh., Mumladze T., Sadradze N., Tsereteli E., Tsereteli N., Varazanashvili O. Late Cenozoic tectonics and geodynamics of Georgia (SW Caucasus). Georgian International Journal of Sciences and Technology (Nova Science Publisher), 1(1), 2008, 77–107.

[5] Danciu L., Şeşetyan K., Demircioglu M., Gülen L., Zare M., Basili R., Elias A., Adamia Sh., Tsereteli N., Yalçin H., Utkucu M., Asif Khan M., Sayab M., Hessami Kh., Rovida A. N., Stucchi M., Burg J. P., Karakhanian A., Babayan H., Avanesyan M., Mammadli T., Al-Qaryouti M., Kalafat D., Varazanashvili O., Erdik M., Giardini D. The 2014 earthquake model of the Middle East: seismogenic sources. Bulletin of Earthquake Engineering, 16(8), 2018, pp. 3465-3496.

[6] Basili R., Danciu L., Beauval C., Sesetyan K., Vilanova S. P., Adamia Sh., Arroucau P., Atanackov J., Baize S., Canora C., Caputo R., Carafa M. M. C., Cushing E. M., Custódio S., Demircioglu Tumsa M. B., Duarte J. C., Ganas A., García-Mayordomo J., Gómez de la Peña L., Gràcia E., Jamšek Rupnik P., Jomard H., Kastelic V., Maesano F. E., Martín-Banda R., Martínez-Loriente S., Neres M., Perea H., Šket Motnikar B., Tiberti M. M., Tsereteli N., Tsironi V., Vallone R., Vanneste K., Zupančič P., Giardini D. The European fault-source model 2020 (EFSM20): geologic input data for the European Seismic Hazard Model 2020, Nat. Hazards Earth Syst. Sci., 24, 2024, pp. 3945–3976. https://doi.org/10.5194/nhess-24-3945-2024

[7] Varazanashvili O., Tsereteli N. Models for area seismic source definition and parameterization for Georgia and the Surrounding Region. Journal of the Georgian Geophysical Society, ISSN 1512-1127, Vol. 23(1), 2020, pp. 5-19. https://ggs.openjournals.ge/index.php/GGS/article/view/3315

სეისმოგენური არეალური წყაროების ახალი მოდელების გამოყოფა კავკასიაში

ო. ვარაზანაშვილი

რეზიუმე

ახალი სეისმოგენური არეალური წყაროები გამოიყო კავკასიაში რეგიონული სეისმოტექტონიკური პირობების, დანაკვირვები სეისმურობის, აქტიური რღვევებისა და ადრე გამოქვეყნებული სეისმური წყაროს მოდელების საფუძველზე. შედეგად მიღებული არეალური წყაროს ახალი ზონირება უზრუნველყოფს კონკრეტულ წყაროებში განმეორებადობის სპეციფიკური მახასიათებლებისა და სეისმურ საშიშროებაში წვლილის შეფასებას.

საკვანძო სიტყვები: სავარაუდო სეისმური საფრთხე, სეისმოგენური არეალის წყარო, ტექტონიკური ერთეული, აქტიური რღვევა.

Выделение новых моделей сейсмогенных площадных источников на Кавказе

О. Варазанашвили

Резюме

Новые площадные сейсмогенные источники были выделены в Кавказе на основе региональных сейсмотектонических условий, активных разломов, наблюдаемых закономерностей сейсмичности и ранее опубликованных моделей сейсмогенных источников. Полученное в результате новое зонирование площадных источников обеспечивает основу для оценки специфических характеристик повторяемости конкретных источников и вклада в сейсмической опасности.

Ключевые слова: Вероятностная сейсмическая опасность, сейсмогенный площадной источник, тектоническая единица, активный разлом.

Journal of the Georgian Geophysical Society, e-ISSN: 2667-9973, p-ISSN: 1512-1127
Physics of Solid Earth, Atmosphere, Ocean and Space Plasma, v. 29(1), 2026, pp. 12–20

Archaeogeoradiolocation Near-Surface Survey of the Area Surrounding Svetitskhoveli Cathedral

Davit T. Odilavadze, Tamaz L. Chelidze T., Olga V. Yavolovskaya

M. Nodia Institute of Geophysics of I. Javakhishvili Tbilisi State University, Tbilisi, Georgia
odildavit@gmail.com

ABSTRACT

Georadiolocation work was carried out in the vicinity of Svetitskhoveli Cathedral in 2025 with a georadar Zond 12e and 500 MHz receiving-transmitting shielded antenna. Interpretation of georadar sections revealed radio features of anthropogenic objects at depths of 1m and up to 3m. Radio features of objects with both cylindrical and angular surfaces were recorded at depths of 4-6m. Interpretation of separate georadiolocation sections conducted with a 150MHz dipole antenna revealed radio features of continuous layered, anthropogenic objects at depths of 1-3m. The radio feature of an object with a cylindrical segment was partially identified at depths of 6-7m. According to the results of the geo-radiolocation work performed, the surveyed area is loaded with archaeological sites

Keywords: *archaeogeoradiolocation, radargram, radio face.*

Historical situation of the research area

Svetitskhoveli Cathedral — the main patriarchal cathedral of the Georgian Orthodox Church, the mother church of Georgia, the place of the enthronement (enthronement) of the Catholicos-Patriarchs of Georgia, the burial place of many medieval Georgian kings, their family members and patriarchs. It is a monument of Georgian architecture of the 11th century, one of the four great cathedrals (Oshki, Bagrati Cathedral, Alaverdi) [1 - 9], ɫocated 20km from Tbilisi, in the city of Mtskheta. The Lord's Robe and the cloak of St. Elijah the Prophet are buried in Svetitskhoveli, the UNESCO World Cultural Heritage Site.

Svetitskhoveli is the largest historical church building in Georgia that has survived to this day. It was the religious center of Christian Georgia for centuries. King Mirian, who converted Georgia to Christianity in the 4th century, built the first church here on the advice of Saint Nino, which has not survived to this day.

Before the adoption of Christianity, pagan centers existed on the territory of Svetitskhoveli, including the idol of the sun and the tombs of the kings of Kartli, where rituals were performed in honor of the deities of Mtskheta-Caucasus; after Christianity, Christian churches were built on the remains of pagan buildings, symbolically uniting pagan and Christian Georgia, where the Svetitskhoveli Temple, "connecting heaven and earth", stands.

Pagan period:

Idol of the sun: On the site of the Svetitskhoveli Temple, there was an idol of the sun, which symbolically meant "connecting heaven and earth".

Royal necropolis: This area was the tombs of the kings of Kartli (Iberia), which gave it a special religious significance in Georgia during the pagan period.

Rituals: Rituals of worship of deities (including Mtskheta-Caucasus deities) were performed here.

Christian period (and its connection with paganism):

Spread of Christianity: After the proclamation of Christianity as the state religion in Georgia by Nino, Mtskheta remains the religious center of Georgia.

Construction of the temple: Instead of pagan idols, the first churches were built on this very site, and eventually the Svetitskhoveli Cathedral, which symbolically represents the connection between the pagan past and the Christian future.

Archaeological excavations: Archaeological excavations conducted on the territory of Svetitskhoveli have revealed the remains of buildings of different times, including signs of the pagan period.

Svetitskhoveli is therefore not only a Christian sanctuary, but also historically the place where Georgian statehood and religious center stay from the pagan era to the Christian era.

Svetitskhoveli Cathedral is surrounded by a square-shaped fence (121.6m; X 110.5m). It was built in 1787 by the order of the king Erekle II.

Archaeogeoradiolocation instruments and placement of georadiolocation profiles

Archaeogeoradiolocation[10 - 20] works were carried out to record the radio features of near-surface archaeological sites in the vicinity of the Svetitskhoveli Cathedral. Georadiolocation profiles/cuts were conducted around the temple, a schematic diagram of their placement is shown in Scheme 1, with a 500MHz frequency shielded georadar „Zond 12e" receiving-transmitting antenna, soft Prizm 2.7.

Three parallel georadar profiles were also conducted with a 150MHz frequency dipole receiving-transmitting radar antenna, the schematic layout of which is given in the Scheme -2.

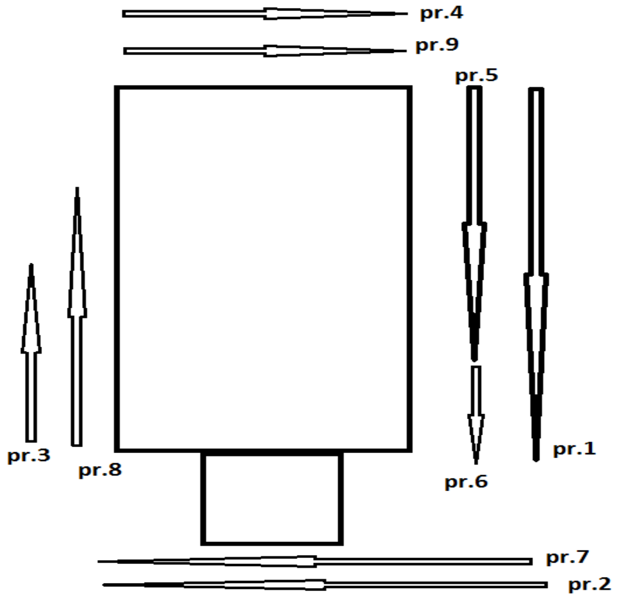

Scheme 1. Schematic drawing of a 500 MHz transceiver with a shielded antenna deployed around Svetitskhoveli.

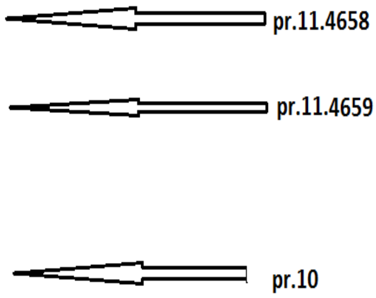

Scheme 2. Schematic drawing of the profiles taken in the part of the Svetitskhoveli Monastery courtyard covered with moss.

Results and conclusion

Below are the plots of geo-radiolocation profiles around the Svetitskhoveli Monastery.

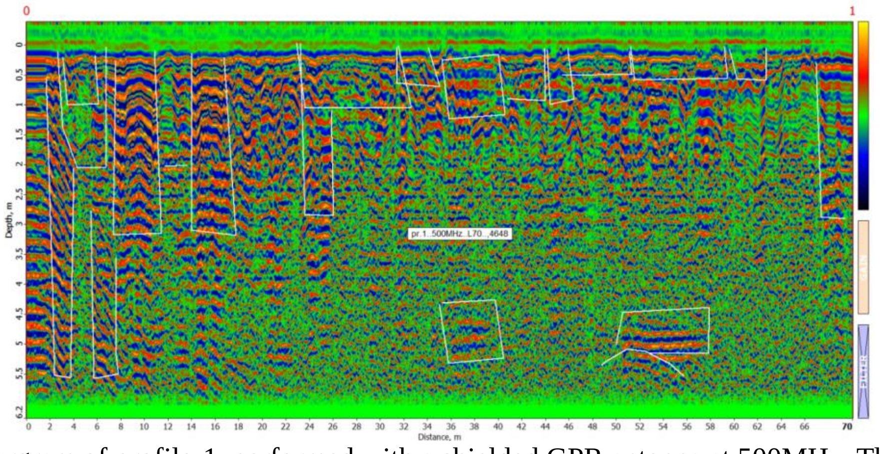

Fig. 1. The radargram of profile-1, performed with a shielded GPR antenna at 500MHz. The length of the profile is 70m, its approximate location is given in the Scheme 1.

In Fig. 1, on the radar image of profile-1, at a distance of 2-4 meters, a radio image of a possible architectural plane with a slope was marked with lines. At a distance of 4-5 meters, a deformed radio image with a depression was marked. The radio image of the object marked at a distance of 6-8 meters partially coincides with the radio image of the object recorded at a distance of 2-4 meters. At distances of 8-10 and 24-26 meters, radio images of the remains of the foundation or the remains of a covered wall were marked, their symmetrical placement is striking. At distances of 26-32 meters, a radio image of an object with a type of overlap, presumably of anthropogenic origin, with depressions up to 1 meter. The location of an object with a similar radio image is considered at distances of 46-50 meters. A number of depressions were marked at 1.5 meters. The radio image of a highly reflective object was observed at a distance of 36-40m, with a depth of 4.5-5.5m. It is noteworthy that at distances of 50-56m and 58m, the cylindrical-like object was overlapped by a highly reflective flat object, with an average depth of 5m.

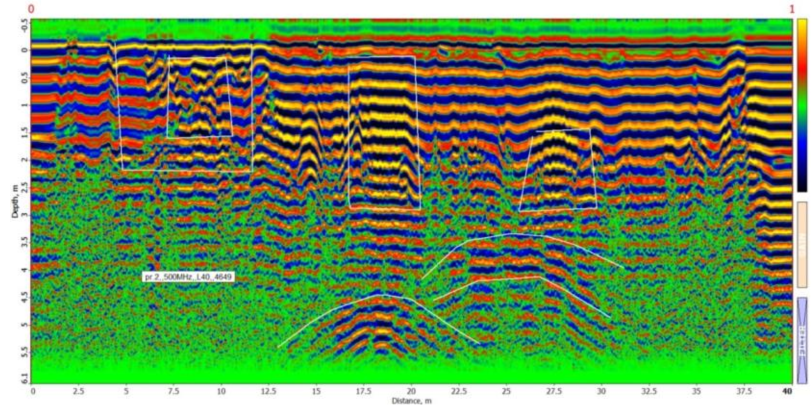

Fig. 2. The radargram of a profile-2 made with a shielded antenna of a georadar, 500MHz. The length of the profile is -40m, its approximate location is given in Scheme 1.

Fig. 2, at distances of 6-8m and at a depth of 2m, shows a complex, structured object with a cavity. At a distance of 17-20m, up to a depth of 3m, a radio image of a presumably foundation remnant is recorded, which surrounds the cylindrical, tubular cavity object, marked with a white hyperbolic line at distances of 16-20m. The radio image of the object recorded at a distance of 23-27m, which surrounds the 3.5-5m depth, is important. At a distance of 26-28m, at a depth of 2-3m, a radio image of an object with a diameter of up to 1m was noted.

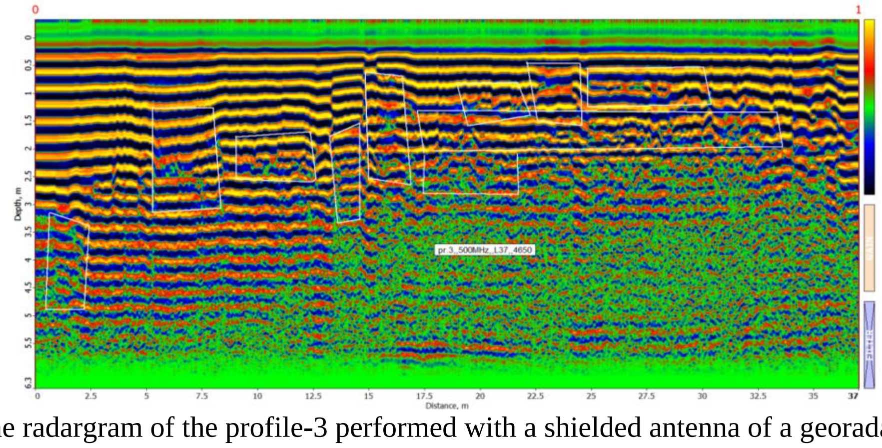

Fig. 3. The radargram of the profile-3 performed with a shielded antenna of a georadar, 500MHz. The length of the profile is 37m, its approximate location is given in Scheme 1.

From the radargram presented in Fig. 3, according to profile-3, a partially deformed cavity radio image is visible from 3m depressions and at 1-2m distances. The texture of the axes of disturbed synphasicity is read at 5-12m distances. A certain structural integrity is created by the combination of the types of objects marked at 15-35m distances.

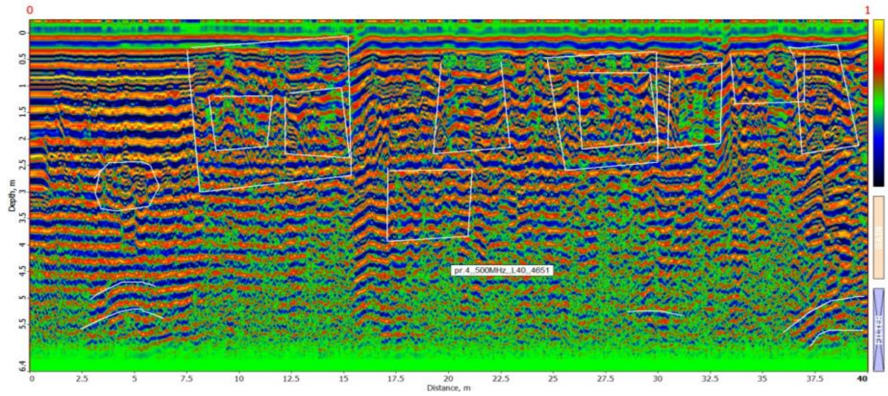

Fig. 4. The profile-4 made with a shielded antenna of a GPR, 500MHz. The length of the profile is 40m, its approximate location is given in the Scheme 1.

Fig. 4, presenting the profile-4, shows the radio images of objects with cavities of probable anthropogenic origin at distances of 7-30m, which are similar to the radio image marked on profile 2 at distances of 7.5-10m. Also interesting are the radio images of cylindrical objects at distances of 5 and 40m, at depths of 5m.

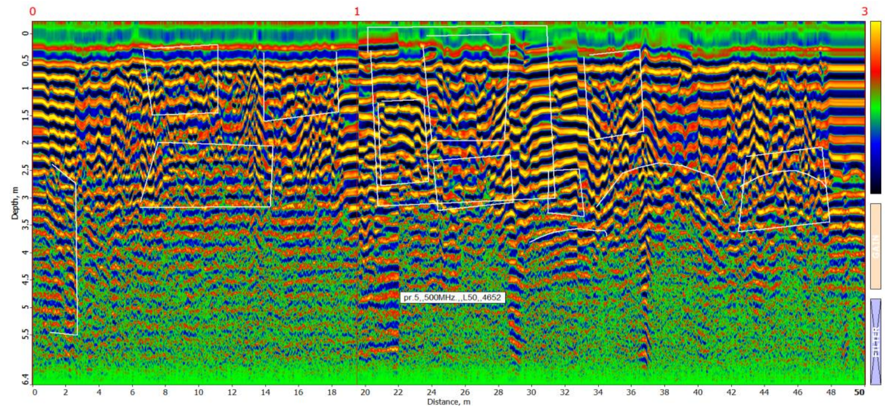

Fig. 5. The profile-5 made with a shielded antenna of a georadar, 500MHz. The length of the profile is 50m, its approximate location is given in the Scheme 1.

From the radargram of Prof-5 presented in Fig. 5, a radio face is read, which coincides with Prof-1 at distances of 1-2m. At distances of 7-11m and 14-19m, objects with similar radio face cavities were noted, perhaps the cavities were partially filled with other material due to the passage of time or external interference. At distances of 8-14m, a radio face of an object with an overlap was noted. A radio face with a structurally uniform face is at distances of 22-30m. There are overlapping radio faces for objects at distances of 38m and 40m.

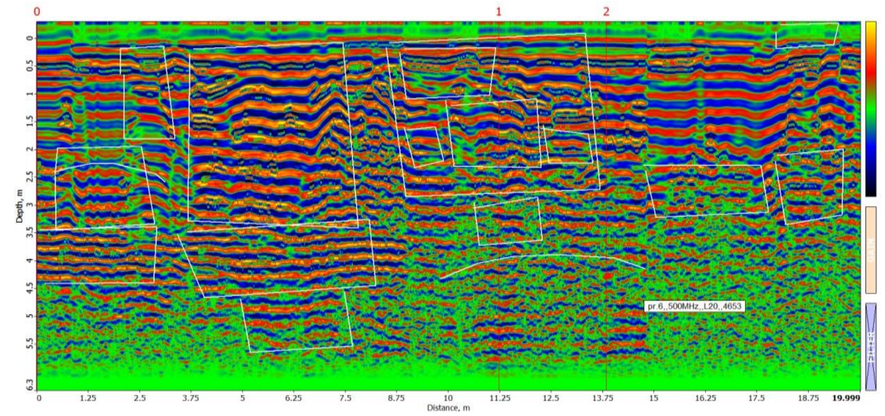

Fig. 6. The profile-6 made with a shielded GPR antenna, 500 MHz. The length of the profile is -20m, its approximate location is given in the Scheme 1.

The profile 6, presented in Fig. 6, shows a number of radio faces that correspond to objects with a cavity at distances of 1, 2, 3m with a deepening of 3.5m. The radio face of a symmetrical object at distances of 9-13m. An object with a possible overlap at distances of 11-13m was marked.

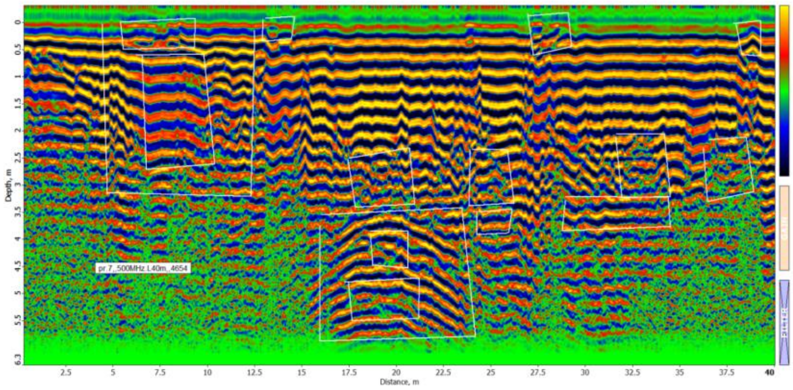

Fig. 7. The profile 7 made with a shielded antenna of a georadar, 500MHz. The length of the profile is -40m, its approximate location is given in the Scheme 1.

From the radargram of profile 7, shown in Fig. 7, 1-2m wide depressions were marked at depths of 0.5-08m and distances of 7.5-14-28-39m. At distances of 5-12.5m and up to 3m depth, a partially concave symmetrical inhomogeneous cavity was recorded from the left. At distances of 20-22-25-32.5-37m we record, on average, 2m wide hollow objects, possibly partially filled with permeable material. At a distance of 15-25m, a clearly expressed complex structured radio face of an object with double, superimposed cameras was noted. The upper part of this radio face coincides with the radio face of the object marked on Prof-2, both in terms of location and dimensions, they must have been continuous intersections of the object. The radio face of a similar object on Prof-2 is weakly readable at a depth of 5m, at distances of 30-32m.

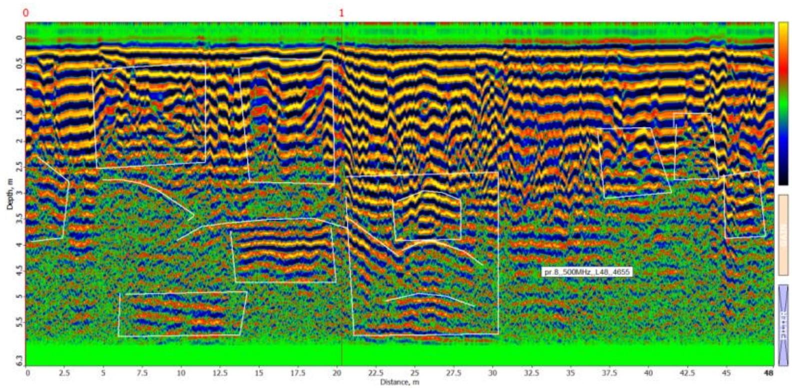

Fig. 8. The profile 8 made with a shielded antenna of a georadar, 500MHz. The length of the profile is -48m, its approximate location is given in the Scheme 1.

Fig. 8 shows the radargram of profile 8, where at distances of 5-11m and a depth of up to 2.5m, a cavity of anthropogenic origin was marked. At distances of 15-20m, there is an area with textural changes, possibly a concave cavity. At distances of 37-40m, cavities of anthropogenic origin are marked. At distances of 22-30m and depths of 3-5.5m, a radio image of a hollow object is presented, it is possible that the cavity is located above a cylindrical object, the left side is partially buried. At distances of 6-12m, a radio image of a horizontally located object with an overlap above was marked. A similar, but heavily deformed, radio image of a symmetrically located object may be seen at distances of 32-37.5m, 4m below the ground.

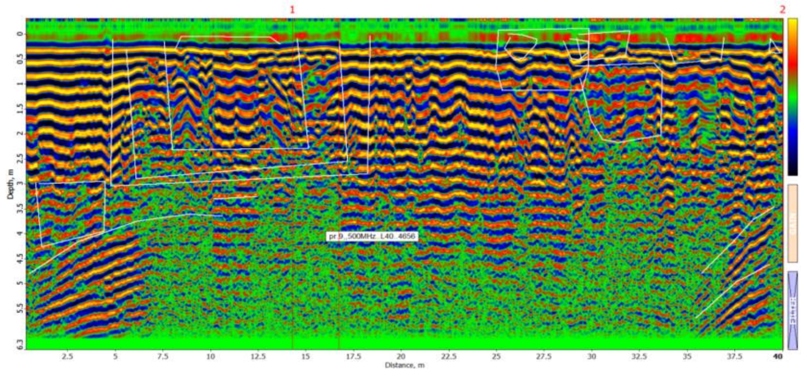

Fig. 9. The profile 9 made with a shielded antenna of a georadar, 500MHz. The length of the profile is -40m, its approximate location is given in the Scheme 1.

Fig. 9 (profile 9) shows a radio image of a practically symmetrical complex-structured object at distances of 5-15m, deepened to 3m. Surface, up to 0.8m indentations are marked at distances of 26-40m. At distances of 0-4m, at depths of 3-4.5m, a radio image of an object containing a deformed cavity was marked. At distances of 0-7m, deepened to 4m, a radio image of an object with strong reflectivity was marked, presumably - part of a structure. There is also a sloping wall, part of the foundation, radio-imaged at distances of 35-40m, and a depression - from 4m down.

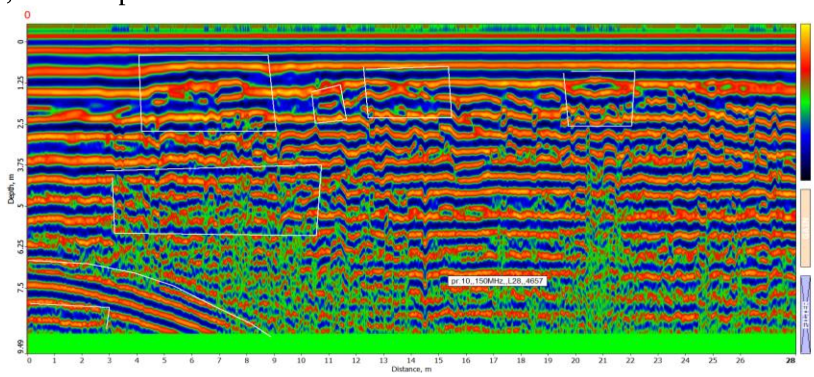

Fig. 10. The profile 10 made with a georadar dipole antenna, 150 MHz. The length of the profile is -28m, its approximate location is given in Scheme 2.

The radargram shown in Fig. 10 (profile 10) revealed the presence of a hollow object of possible anthropogenic origin at a depth of 1-2m and at distances of 4-9m, as well as radio images of various hollow objects at distances of 11-14-21m. At a distance of 11 m, there is a radio image of a pipe-type cross-section, at 14, a radio image of a hollow object 2m wide and 1.5m high, and at 21m, there is also a radio image of an anthropogenic object. At a depth of 3.37m to 6m and at distances of 3m to 10m, a radio image of a converted object with two cavities, presumably an old object, was noted. The radio image of the object, visible at distances of 0-9m from 7m depths, is important.

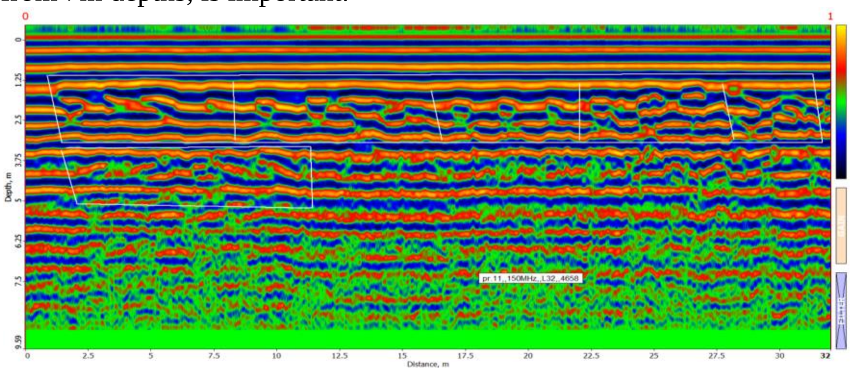

Fig. 11. The profile-11 (4658) made with a georadar dipole antenna, 150MHz. The length of the profile is -32m, , its approximate location is given in Scheme 2.

At distances of 2.5-32m (Fig. 11- profile-11), at depths of 1-3m, the radio faces of structurally uniform objects were marked, for periodically alternating hollow structures. At distances of 2.5-10m, at distances of 3.37-6m, the radio face of a structurally uniform object was marked. It is symmetrical and contains hollows and its radio face extends downwards without interruption.

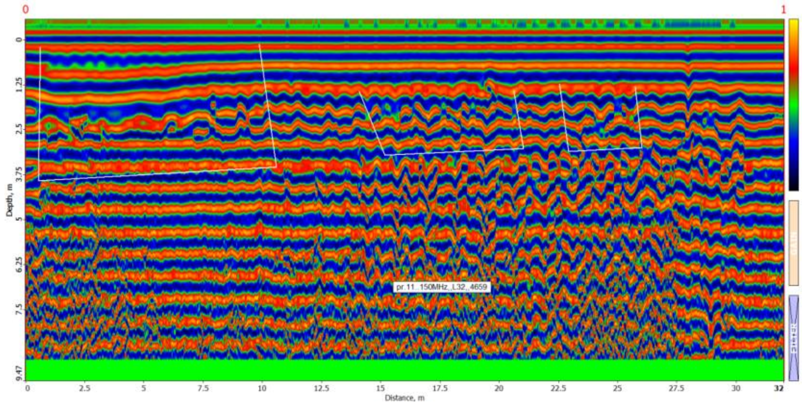

Fig. 12. The profile-12 (4659) made with a georadar dipole antenna, 150MHz. The length of the profile is - 32m, , its approximate location is given in Scheme 2.

Fig. 12 (profile-12) shows a radio image of a symmetrical structure at distances from 3.37 to 10m, similar in size and location to the radio image of the corresponding object marked in Fig. 11. The structure of the subsoil layer is quite heterogeneous, which may be due to the violation of the integrity of the soil at different times.

Conclusion

The following is observed from the profiles 1-11 obtained by interpreting the georadiolocation cuts made with a 500 MHz receiving-transmitting shielded antenna of the georadar;

In the studied area, both at depths of 1m and up to 3m, radio features of anthropogenic objects, fully or partially deformed, are recorded, marked on radargrams with white lines.

In the depths of 4-6m, radio features of objects with both cylindrical and angular surfaces are recorded, marked on radargrams with white lines.

Interpretation of georadiolocation cuts conducted with a 150MHz dipole antenna reveals continuous layered radio features of anthropogenic objects at depths of 1-3m. A radio feature of an object with a possible cylindrical segment was partially recorded from depths of 6-7m.

According to the results of the performed georadiolocation work, the studied area is loaded with archaeological objects.

References

[1] Material from Wikipedia - The Free Encyclopedia.
[2] Beridze V. Old Georgian Architecture, Tbilisi, 1974.
[3] Chubinashvili G. Georgian Architecture in the Middle Ages and Its Three Main Cathedrals, tr.: Aril, Tbilisi, 1925.
[41] Gverdtsiteli R. Mtskheta, Tbilisi, 1962.
[5] Description of Monuments of History and Culture of Georgia. Editorial Board: V. Dolidze, S. Kintsurashvili, U. Sidamonidze, Tbilisi, Vol.5, 1990.
[6] Natroev A. Mtskheta and its Cathedral of Sveti-Tskhoveli. Historical and Archaeological Description. 1900.
[7] Opening of the 11th Century Gate in the Svetitskhoveli Wall. // Journal. Friend of the Monument, No.1 Tbilisi: Soviet Georgia, 1964. — pp. 6-10.
[8] Svetitskhoveli as a resting place. //Journal. Friend of the Monument, No. 69 Tbilisi: Soviet Georgia, 1985. — pp. 25-32.

[9] Kudava B. The burial place of the Georgian king: personal choice, tradition or political decision?, “Historian” (a scientific collection dedicated to the 80th anniversary of the birth of Roin Metreveli), Tbilisi, 2019, pp. 139-167.
[10] Odilavadze D., Goguadze N., Jakhutashvili M., Vepkhvadze S., Kachakhidze M., Kachakhidze N. Results of primary georadiolocation searching of Svetitskhoveli Temple. GESJ: Physics, ISSN 1512-1461 31, No.1(9), 2013.
[11] Ioseliani P. Description of the antiquities of the city Tiflis. 1866, pp. 132-133, (in Russian).
[12] Georgian Soviet Encyclopedia, T. 7, Tbilisi., 1984, p. 440, (in Georgian).
[13] Odilavadze D., Kiria J., Ghlonti N., Yavolovskaya O. The Results of archaeogeoradiolocation investigations of the territory inside the rampart of St. Sophia Church of Khobi. „Moambe”, Bulletin of the Georgian National Academy of Sciences, V.14, n.4, 2020, pp. 51-56.
[14] Chelidze T., Odilavadze D., Pitskhelauri K. Archaeogeophysics in Georgia-New Results, New Prospects. Proceedings of the Georgian National Academy of Sciences. Series of History, Archeology, Ethnology and Art History, №.15, 2013, pp. 24-34.
[15] Odilavadze D.T., Chelidze T.L. A Preliminary GPR investigation of Metekhi Cathedral and the surrounding area. Journal of Georgian Geophysical Society, № 14, 2010, pp. 32-38.
[16] Kofman L., Ronen A., Frydman S. Detection of model voids by identifying reverberation phenomena in GPR records. Journal of Applied Geophysics. (59), 2006, pp. 284-299.
[17] Odilavadze D., Chelidze T., Yavolovskaya O. Some georadiolocation images of cylindrical bodies built with different dielectric fillers, placed in a dielectric environment. International Scientific Conference "Geophysical Processes in the Earth and its Envelopes". Proceedings, ISBN 978-9941-36-147-0, Tbilisi, Georgia, November 16-17, 2023, pp. 217-220.
[18] Odilavadze D., Chelidze T., Ghlonti N., Yavolovskaya O. Determining the presence and structure of a subsurface radioactive burial when interpreting the results of the GPR method by analyzing a three dimensional rotating radio image. Journal of the Georgian Geophysical Society, e-ISSN: 2667-9973, p-ISSN: 1512-1127. Physics of Solid Earth, Atmosphere, Ocean and Space Plasma, v. 25(1), 2022, pp. 21-28.
[19] Odilavadze D., Chelidze T., Yavolovskaya O. The radio image of an object with an elongated, face-fragmented, dielectrically complex structure was studied using the method of georadar physical modeling. Journal of the Georgian Geophysical Society, e-ISSN: 2667-9973, p-ISSN: 1512-1127, Physics of Solid Earth, Atmosphere, Ocean and Space Plasma, v. 27(2), 2024, pp. 15-28.
[20] Odilavadze D., Chelidze T., Yavolovskaya O. Preliminary archaeogeophysical survey of the construction site in the vicinity of the Narikala Citadel. Journal of the Georgian Geophysical Society, e-ISSN: 2667-9973, p- 11.ISSN: 1512-1127. Physics of Solid Earth, Atmosphere, Ocean and Space Plasma, v. 28(1), 2025, pp. 27-35.
[21] Odilavadze D., Chelidze T., Glonti N., Kiria J., Yavolovskaya O. Archaeogeoradiolocation Research of the Territory of the Ninotsminda Monastery Complex. Transactions of Mikheil Nodia Institute of Geophysics, ISSN 1512-1135, vol.LXXVIII, 2025, pp.20-34.

სვეტიცხოველის საკათედრო ტაძრის მიმდებარე ტერიტორიის არქეოგეორადიოლოკაციური ახლოქვეზედაპირული კვლევა

დ. ოდილავაძე, თ. ჭელიძე, ო. იავოლოვსკაია

რეზიუმე

სვეტიცხოვლის საკათედრო ტაძრის გარშემო სიახლოვეში 2025წ ჩატარდა “Zond 12e” გეორადარის 500მჰც მიმღებ-გადამცემი ეკრანირებული ანტენით გეორადიოლოკაციური სამუშაო. გეორადარული ჭრილების ინტერპრეტაციით გამოიკვეთა, როგორც ზედაპირთან ახლო 1 მ, ასევე 3-მდე დაღრმავებებზე ანტროპოგენული წარმოშობის ობიუქტთა რადიოსახეები. დაღრმავებებზე 4-6 მ ფიქსირდება, როგორც ცილინდრული ზედაპირის მქონე

ასევე კუთხოვანი ზედაპირის მქონე ობიექტების რადიოსახეები. 150მჰც სიხშირის დიპოლური ანტენით გატარებული ცალკეული გეორადიოლოკაციური ჭრილების ინტერპრეტაციით იკვეთება 1-3 მ დაღრმავებებზე განგრძობითი ფენობრივი, ანტროპოგენული ობიექტების რადიოსახეები. მოინიშნა, ნაწილობრივ, ცილინდრული სეგმენტის მქონე ობიექტის რადიოსახე 6-7 მ დაღრმავებიდან. შესრულებული გეორადიოლოკაციური სამუშაოს შედეგების მიხედვით, გამოკვლეოლი ტერიტორია, დატვირთულია არქეოლოგიური ობიექტებით.

საკვანძო სიტყვები: არქეოგეორადიოლოკაციური სამუშაოები, გეორადარი, რადიოსახე, რადაროგრამა.

Археогеорадиолокационное приповерхностное обследование территории, прилегающей к кафедральному собору Светицховели.

Д. Одилавадзе, Т. Челидзе, О. Яволовская

Резюме

В 2025 году в окрестностях собора Светицховели были проведены георадиолокационные работы с использованием экранированной приемопередающей антенны георадара «Зонд 12е» с частотой 500МГц. Интерпретация георадарных срезов выявила радиохарактеристики антропогенных объектов на глубинах от 1 до 3 м. На глубинах 4-6м были зарегистрированы радиохарактеристики объектов как с цилиндрической, так и с угловатой поверхностью. Интерпретация отдельных георадиолокационных срезов, проведенная с помощью дипольной антенны с частотой 150МГц, выявила радиохарактеристики сплошных слоистых антропогенных объектов на глубинах 1-3м. На глубинах 6-7м была частично идентифицирована радиохарактеристика объекта с цилиндрическим сегментом.
По результатам проведенных георадиолокационных работ, обследованная территория насыщена археологическими памятниками.

Ключевые слова: археогеорадиолокационные работы, георадар, радио образ, радарограмма.

Journal of the Georgian Geophysical Society, e-ISSN: 2667-9973, p-ISSN: 1512-1127
Physics of Solid Earth, Atmosphere, Ocean and Space Plasma, v. 29(1), 2026, pp. 21-26

Phase Shift Between Water Level and X, Y, Z Components of Gravity Using the Example of Georgian Wells

Genadi N. Kobzev, Tamaz L. Chelidze, George I. Melikadze, Tamar J. Jimsheladze, Tengiz V. Kiria, Aleksandre Sh. Tchankvetadze, Zviadi I. Maghradze, Nino T. Goguadze

M. Nodia Institute of Geophysics of the I. Javakhishvili Tbilisi State University, Georgia

e-mail: kobzev47@gmail.com

ABSTRACT

Various methods are used to detect and record earthquake precursors: measuring the water level and the rate of change, and studying the phase shift of the water level by comparing it with the Z-component of gravity (φZ). However, the X and Y-components of gravity remain obscured. Using the example of wells in Georgia, we will demonstrate the possible relationship between the phase shifts φX, φY and φZ, and, consequently, the informative value of their use.
Key words: *phase shift, water level, tidal X, Y, Z – components.*

Definition. Let φX denote the phase shift between the X-component of gravity (tidalX) and the water level (or its modification). Here tidalX is the North-South component of tidal gravity and tidalY is the East-West component. The phase shifts φY and φZ relate to tidalY and tidalZ, respectively. We will calculate the phase shift for principal semi-diurnal lunar constituent M_2=12.42 h., principal declinational diurnal constituent O_1=25.82 h. and principal solar semidiurnal constituent S_2=12.00 h. For wells in Georgia statements 1, 2 and 3 are *probably* true.

Statement 1. For M_2=12.42 h. the following relationships hold:

a) φY - φX ≈ 90°; b) φZ - φY ≈ 90°.

Statement 2. For O_1=25.82 h. the following relationships hold:

a) φX ≈ φZ; b) φZ - φY ≈ 90°.

Statement 3. For S_2=12.00 h. the following relationships hold:

a) φY – φX≈ 90°; b) φZ – φY≈ 90°.

Below are facts supporting these statements.

Method for calculating phase shift

The Baytap08 program, suggested by D.C. Agnew, is often used to calculate the phase shift. Baytap08 is a modification of the Baytap-G program developed by M. Ishiguro, Y. Tamura, T. Sato, and M. Ooe [1]. This program, using well coordinates, calculates the Z-component of gravity and compares it with water level and atmospheric data. The results of its application to a study of Georgian wells are presented in [2]. The initial data had a sampling period of 1 hour.

Our approach. Gravity values (X, Y, Z components) for a selected well are pre-calculated. A version of the "solid"-program (Dennis Milbert [3]) is used to calculate them. Next, a MatLab-based program, suggested by ChatGPT, is used to compare the selected gravity component with the water level. The basic code is provided below.

Calculation Algorithm

We have water level values measured at 1-minute intervals, for example, from January 1 to December 1, 2025. Starting from the selected date:

1) Take all 1-minute water level values for a 30-day window. 2) Make comparisons, for example, with the X-component of gravity. 3) Assign the resulting value (phase shift in degrees) to our date. 4) Next, increase our selected date by 1 day and repeat the calculations. *Note:* The time interval (window) must be at least 30 days. To calculate the phase shift, we used a portion of the MatLab program provided by ChatGPT, modified to accommodate the input data. Here is a copy of the received text.

```
g_detrended = detrend(g); w_detrended = detrend(w); % Remove the trend (if any)
G = fft(g_detrended); W = fft(w_detrended); % Apply FFT
phase_g = angle(G); phase_w = angle(W); % Obtain phase spectra
N = length(t); % Frequencies (for plotting and analysis)
Fs = 1 / mean(diff(t)); % Sampling frequency (Hz)
f = (0: N-1) *(Fs/N); % Frequency vector
% Select the frequency of interest (for example, the main one - daily)
target_freq = 1 / (24*3600); % 1 time per day in Hz
 [~, idx] = min (abs (f - target_freq)); % Find the index of the nearest frequency
delta_phi = phase_w(idx) - phase_g(idx); % in radians % Calculate the phase shift
delta_phi = angle (exp (1i * delta_phi)); % Bring it into the range [-π, π]
delta_phi_deg = rad2deg(delta_phi); % Conversion to degrees
```

The program returns phase shift values in the range [-180°; +180°]. Therefore, if φ=187°, the program returns φ= -173°. Correction of the obtained data is necessary. When analyzing the tables below, it is useful to remember that if the function $f(x)$ has a period of 360°, then, for example, $f(x\text{-}270°) = f(x\text{-}270°+360°) = f(x+90°)$.

Information about wells

Kobuleti: coordinate 41.802°N, 41.772°E, depth 2000 m, screen 187-640 m.
Lagodekhi: coordinate 41.839°N, 46.282°E, depth 800 m, screen 255-367 m.
Gori: coordinate 41.485°N, 44.111°E, depth 1500 m, screen 960-1200 m.
Marneuli: coordinate 41.436°N, 44.755°E, depth 3505 m, screen 1235-1600 m.
Fig. 1 shows graphs of tidal X, Y, and Z gravity, as well as water level in kPa, for the Kobuleti well. The tidal graphs have different shapes. Calculating the phase shift between the water level and tidal_X for M2, then for tidal_Y and tidal_Z, yields different values. However, their values differ by 90° (see fig.2 and tables).
Below, *minus water* means (-1) **water* data.

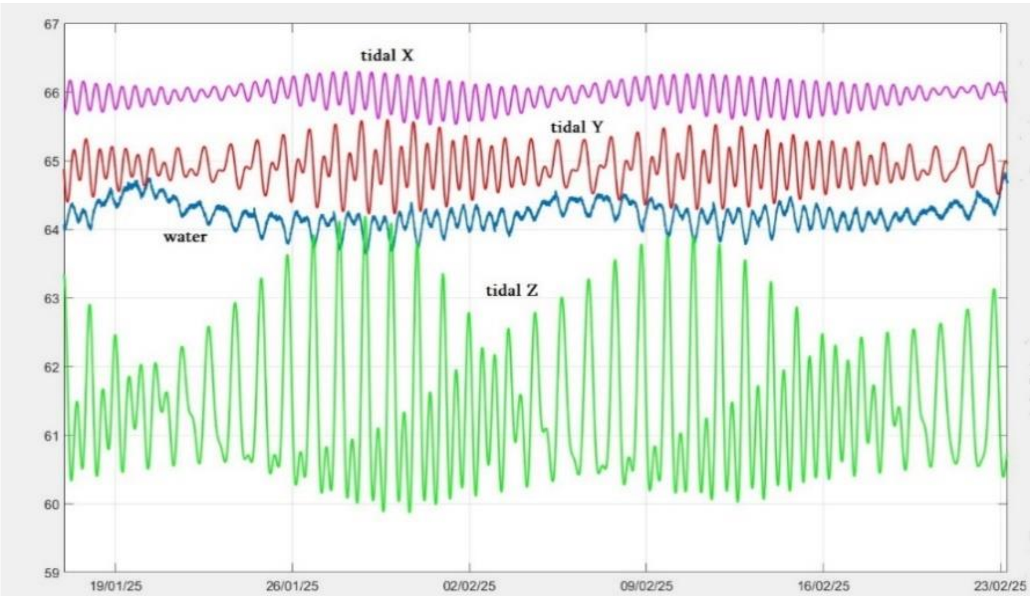

Fig.1. Tidal_X, tidal_Y, tidal_Z, Kobuleti water-k*atmos (blue line), in kPa, 2025

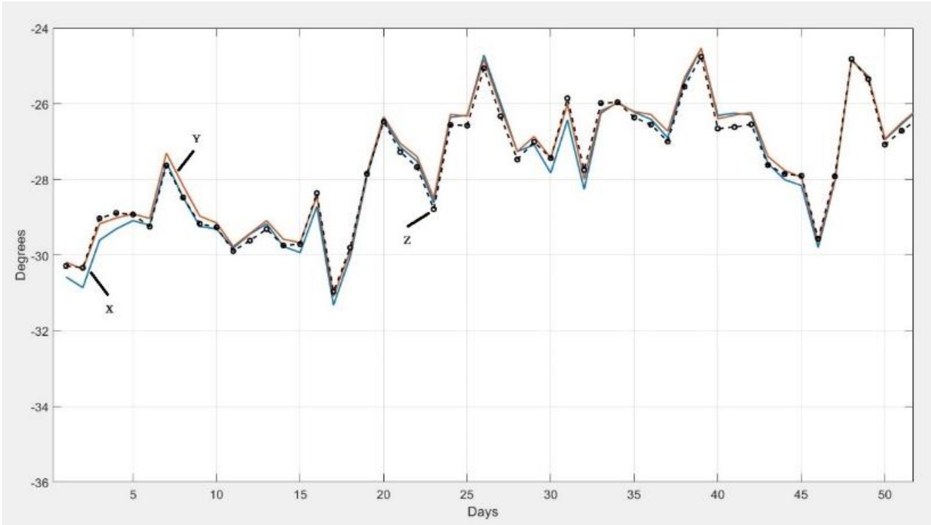

Fig.2. Kobuleti, phase shifts, M_2: φX (blue line), φY-90° (brown); φZ-180° (black, dashed line).
Use water, kPa, from 1 January 2025.

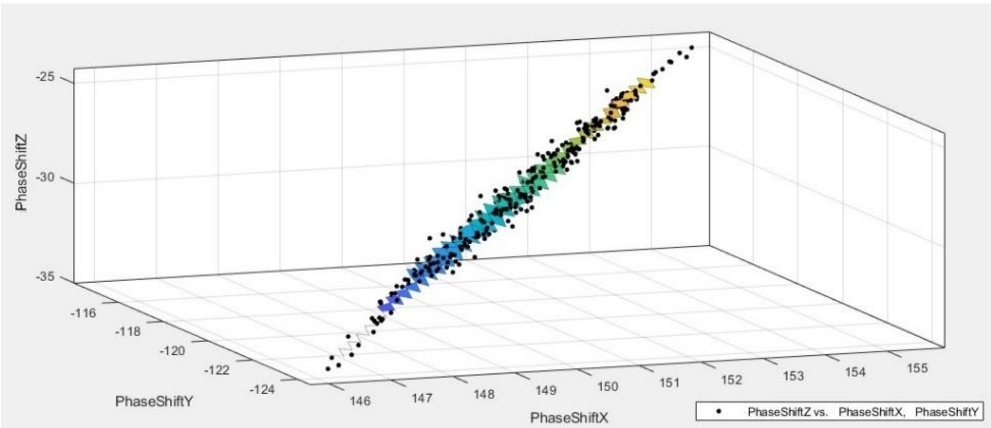

Fig.3. Kobuleti, phase shift X, Y, Z, degrees, M_2. Use minus water, kPa, 1 Jan - 1 Dec 2025

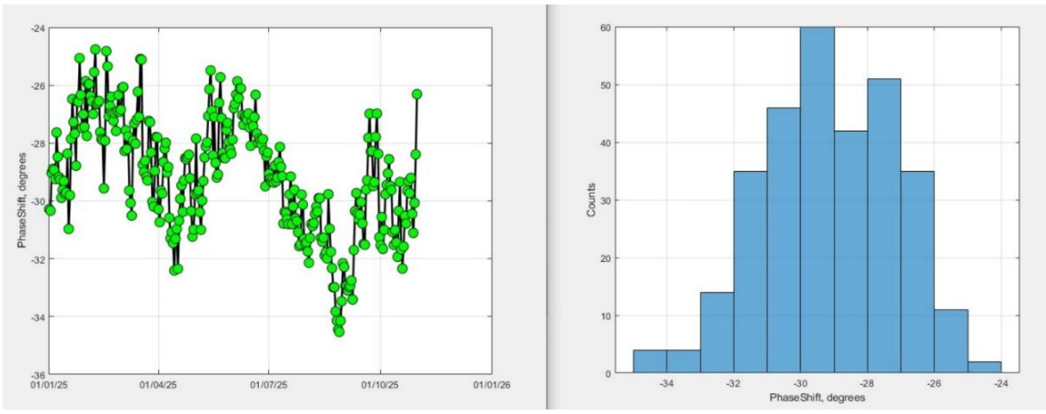

Fig.4. Kobuleti, phase shift Z for M_2, graph and histogram. Use minus water, kPa, 1 Jan - 1 Dec 2025

Information about M_2=12.42 hours

Formula: Y=p1*X+p2. Water data in kPa.

Table 1.1. Phase shifts for Kobuleti, 1 Jan - 1 Dec 2025, target: M_2=12.42 h.

Axes X, degrees	Axes Y, degrees	Water		Minus water	
		p1	p2	p1	p2
φX	φY	1.014	90.41	1.014	-272.2
φX	φZ	1.014	180.4	1.014	-183.8
φY	φX	0.9783	-88.67	0.9783	267.4
φY	φZ	1.0120	89.04	1.0120	91.16
φZ	φX	0.9595	-173.8	0.9595	179.1
φZ	φY	0.9833	-87.24	0.9833	-90.25

Table 1.2. Phase shifts for Lagodekhi, 1 Jan - 20 Sep 2025, target: M_2=12.42 h.

Axes X, degrees	Axes Y, degrees	Water		Minus water	
		p1	p2	p1	p2
φX	φY	1.015	90.94	1.015	-271.8
φX	φZ	1.033	181.8	1.033	-184.2
φY	φX	0.9827	-89.5	0.9827	267.4
φY	φZ	1.018	89.23	1.018	92.5
φZ	φX	0.9633	-175.4	0.9633	178
φZ	φY	0.9807	-87.46	0.9807	-90.94

Table 1.3. Phase shifts for Gori, 9 Mar - 1 Dec 2025, target: M_2=12.42 h.

Axes X, degrees	Axes Y, degrees	Water		Minus water	
		p1	p2	p1	p2
φX	φY	1.007	89.9	1.007	91.24
φX	φZ	1.001	-180.4	1.011	181.5
φY	φX	0.9912	-89.09	0.9912	-90.68
φY	φZ	1.004	-270.6	1.004	90.02
φZ	φX	0.9865	178.0	0.9865	-179.6
φZ	φY	0.9956	269.5	0.9956	-89.69

Table 1.4. Phase shifts for Marneuli, 1 Jan - 1 Nov 2025, target: M_2=12.42 h.

Axes X, degrees	Axes Y, degrees	Water		Minus water	
		p1	p2	p1	p2
φX	φY	1.007	90	1.007	-271.3
φX	φZ	1.017	179.8	1.017	-183.3
φY	φX	0.9886	-88.98	0.9886	269
φY	φZ	1.011	88.74	1.011	90.8
φZ	φX	0.9735	-175	0.9735	180.2
φZ	φY	0.9859	-87.25	0.9859	-89.78

Information about O_1=25.82 hours

Formula: Y=p1*X+p2. Water data in kPa

Table 2.1. Phase shifts for Kobuleti, 1 Jan - 1 Dec 2025, target: O_1=25.82 h.

Axes X, degrees	Axes Y, degrees	Water		Minus water	
		p1	p2	p1	p2
φX	φY	0.9105	-74.36	0.9105	-90.46
φX	φZ	0.9075	15.93	0.9075	-0.7285
φY	φX	0.9829	91.28	0.9829	88.2
φY	φZ	0.9942	90.24	0.9942	89.2
φZ	φX	0.9867	2.409	0.9867	0.007052
φZ	φY	1.001	-90	1.001	-89.74

There is a good relation between φY и φZ. Relation φX => φY is bad, relation φY => φX is good. Relation φX => φZ is bad, relation φZ => φX is good.

Table 2.2. Phase shifts for Lagodekhi, 1 Jan - 20 Sept 2025, target: O_1=25.82 h.

Axes X, degrees	Axes Y, degrees	Water		Minus water	
		p1	p2	p1	p2
φX	φY	0.7181	-49.88	0.7181	-100.6
φX	φZ	0.7041	41.89	0.7041	-11.4
φY	φX	0.9828	90.89	0.9828	87.8
φY	φZ	0.9754	91.03	0.9754	86.61
φZ	φX	0.996	0.809	0.996	0.092
φZ	φY	1.008	-90.9	1.008	-89.44

Relations φX => φY and φX => φZ are bad. Relations φZ => φX and φZ => φY are good.

Table 2.3. Phase shifts for Gori, 9 Mar - 1 Dec 2025, target: O_1=25.82 h

Axes X, degrees	Axes Y, degrees	Water		Minus water	
		p1	p2	p1	p2
φX	φY	0.9319	-76.99	0.9319	-89.25
φX	φZ	0.9353	12.16	0.9353	0.5075
φY	φX	0.9394	95.05	0.9394	84.19
φY	φZ	1.00	89.75	1.00	89.79
φZ	φX	0.9385	10.92	0.9385	-0.143
φZ	φY	0.9956	-88.96	0.9956	-89.76

For *water* data the original values φ were pre-transformed for φX and φZ: if φ <0, then φ replaced by φ+360. For *minus water* φ-values are original. Relations φZ => φX and φZ => φY are good.

Table 2.4. Phase shifts for Marneuli, 1 Jan - 1 Nov 2025, target: O_1=25.82 h

Axes X, degrees	Axes Y, degrees	Water		Minus water	
		p1	p2	p1	p2
φX	φY	0.8612	-65.11	0.8612	-90.1
φX	φZ	0.8504	26.57	0.8504	-0.3605
φY	φX	0.9545	93.94	0.9545	85.75
φY	φZ	0.9837	91.2	0.9837	88.27
φZ	φX	0.9635	6.65	0.9635	0.0936
φZ	φY	1.006	-90.77	1.006	-89.75

For *water* data original values φ transformed for φX и φZ: if φ <0, then φ replaced by φ+360. For *minus water* φ-values are original.

Formula: Y=p1*X+p2. Water data in kPa

Table 2.5. Phase shifts for Marneuli, 1 Jan - 1 Nov 2025, target: S_2=12.00 h

Axes X, degrees	Axes Y, degrees	Water		Minus water	
		p1	p2	p1	p2
φX	φY	0.9905	90.36	0.9905	88.64
φX	φZ	0.9944	-180	0.9944	179
φY	φX	1.009	-91.11	1.009	-89.57
φY	φZ	1.004	-270.7	1.004	89.98
φZ	φX	1.004	180.8	1.004	-180
φZ	φY	0.9958	269.6	0.9958	-89.62

Note. For periodic processes -270°=-270°+360°=+90°.

Conclusions

Analysis of the tables shows that for the selected well, the p1 coefficients for *water* and *minus water* are the same, while the p2 values fluctuate. The p2 coefficients are almost identical for Kobuleti, Lagodekhi and Marneuli, but differ by 360° from the coefficients for Gori. The p2 coefficients confirm the validity of the previously formulated statements 1, 2 and 3.

Note: Control calculations for Gori for the period 1 Jan – 1 Dec, 2021 showed that the p2 values for 2021 and 2025 are almost identical.

Acknowledgements. The scientific research has been funded and performed with financial support of the Shota Rustaveli National Science Foundation within the grant project **FR24-17839**.

References

[1] Tamura Y., Sato T., Ooe M., Ishiguro M. A procedure for tidal analysis with a Bayesian information criterion. Geophys. J. Internat., 104, 1991, pp. 507-516.

[2] Kobzev G.N., Chelidze T.L., Melikadze G.G., Jimsheladze T.J., Kiria T.V., Tchankvetadze A.Sh., Maghradze Z.I., Goguadze N.T. Water Level Phase Shift Relative to Gravity into Georgian Wells. Journal of the Georgian Geophysical Society, e-ISSN: 2667-9973, p-ISSN: 1512-1127. Physics of Solid Earth, Atmosphere, Ocean and Space Plasma, v. 28(1), 2025, pp. 36 - 39.

[3] Milbert D. https://geodesyworld.github.io/SOFTS/solid.htm

ფაზური წანაცვლება წყლის დონესა და გრავიტაციის X, Y, Z კომპონენტებს შორის საქართველოს ჭაბურღილების მაგალითზე

გ. კობზევი, თ. ჭელიძე, გ. მელიქაძე, თ. ჯიმშელაძე, თ. ქირია, ა. ჭანკვეტაძე, ზ. მაღრაძე, ნ. გოგუაძე

რეზიუმე

ნაშრომში განხილულია ფაზური წანაცვლებები ქობულეთის, ლაგოდეხის, გორისა და მარნეულის ჭაბურღილებში წყლის დონესა და გრავიტაციის X, Y და Z კომპონენტებს შორის. გრავიტაციული მიმოქცევის M_2, O_1 და S_2 კომპონენტებისათვის განსაზღვრულია ფაზური წანაცვლებების φX, φY და φZ ურთიერთკავშირი.

საკვანძო სიტყვები: ფაზური წანაცვლება, წყლის დონე, გრავიტაციის X, Y, Z კომპონენტები.

Фазовый сдвиг между уровнем воды и X,Y,Z-компонентами гравитации на примере скважин Грузии

Г. Кобзев, Т. Челидзе, Г. Меликадзе,
Т. Джимшеладзе, Т. Кирия, А. Чанкветадзе, З. Маградзе, Н. Гогуадзе

Резюме

Рассматриваются фазовые сдвиги между уровнем воды в скважинах Кобулети, Лагодехи, Гори, Марнеули и X,Y,Z-компонентами гравитации. Для составляющих гравитации M_2, O_1, S_2 определяется взаимная связь между фазовыми сдвигами $\varphi X, \varphi Y, \varphi Z$.

Ключевые слова: фазовый сдвиг, уровень воды, X,Y,Z-компоненты гравитации.

Journal of the Georgian Geophysical Society, e-ISSN: 2667-9973, p-ISSN: 1512-1127
Physics of Solid Earth, Atmosphere, Ocean and Space Plasma, v. 29(1), 2026, pp. 27–49

Assessment of the Relationship Between Daily and Total Multi-Day Precipitation Sums and Landslide Activation in the Regions of Georgia

[1]Avtandil G. Amiranashvili, [2]Luca Brocca, [1]Tamaz L. Chelidze, [1]Tengiz V. Kiria, [1] David T. Svanadze, [3] Tamar N. Tsamalashvili, [1] Nodar D. Varamashvili

[1]*M. Nodia Institute of Geophysics of I. Javakhishvili Tbilisi State University, Tbilisi, Georgia*
[2]*Research Institute for Geo-Hydrological Protection, Perugia, Italy*
[3]*A. Janelidze Geological Institute of I. Javakhishvili Tbilisi State University, Tbilisi, Georgia*
avtandilamiranashvili@gmail.com

ABSTRACT

A detailed statistical analysis of the relationship between daily and accumulated multi-daily precipitation sums and the number of landslides in 12 regions of Georgia is presented. Landslide data with a known days of activation were used (a total of 519 landslide events from 1968 to 2022). For the analysis, the precipitation sum for the day of landslide activation (P1) was determined, as well as the accumulated precipitation sum for 3 days (P3), 5 (P5), 7 (P7), 10 (P10), 20 (P20) and 30 days (P30) prior to landslide occurrence (including the day with landslide).
Specifically, the following results were obtained. The relationship between average precipitation values (threshold values) and daily precipitation duration during the day of landslide activation and before 3, 5...30 days of landslides activation in Georgia and its individual regions was determined. It was found that, overall, in eastern Georgia (including the Samtskhe-Javakheti region), landslide activation occurs with significantly lower precipitation sums than in western Georgia. The average P1 values are 8.8 and 11.9 mm, respectively, and the P30 values are 75.2 and 156.6 mm. The linear correlation between the number of landslides and the P1...P30 values across the regions of Georgia is high for P1,P3,P20 and P30 and moderate for P5,P7 and P10. For Georgia the sum of precipitation associated with landslides exceeds the general long-term mean daily precipitation sum by approximately 95%. For Georgia as a whole and its Eastern and Western parts, the dependence of the number of landslides on the P1 ... P30 values have the form of a third-degree polynomial (sequentially: slight increase – plateau – strong increase). For P1 values, the precipitation sum plateau, after which a strong increase in the number of landslides begins, covers the range from 6.3 to 30.8 mm, and for P30 – from 62.4 to 189.5 mm (the total relative number of landslides is ≈ 42.1–43.3%).

Keywords: *landslides, natural disaster, atmospheric precipitations, statistical analysis.*

Introduction

Landslides, as a type of natural disaster, are common almost everywhere [1–5], including in Georgia [6–12]. Landslides often lead to the destruction of residential buildings and utility infrastructure, serious damage to roads, railways, and bridges, the failure of various life support systems, significant material damage, threats to human life and health, etc. [9, 10, 13].

For example, according to data from the Geological Department of the Environmental Protection Agency of Georgia, the annual number of activated and newly formed landslides (LS) for the period from 1995 to 2024 ranged from 56 to 1,360, with an average annual value of 581 [10, 12].

Landslide activation is associated with many natural and anthropogenic factors, such as slope steepness, lithology, vegetation cover, seismic activity, construction work near landslide-prone areas, and others. Landslide formation is often accelerated by prolonged, intense, or extreme precipitation [14–15].

In recent years, a number of studies have been conducted in Georgia to identify the short-term (hours, days, months) [16–20] and long-term (years, climate scale) effects of precipitation on landslide and mudflow activation [21–28]. These studies used landslide and mudflow data presented in [9, 10], as well as ground-based, radar, and satellite precipitation data, taking into account their representativeness depending on the distance to the measurement point [29–33]. In particular, in our recent work [28], we conducted an initial statistical assessment of landslide hazard using 11 weighted objective factors (including annual precipitation). Using machine learning methods, we obtained a landslide hazard map that correlates well with observed data, confirming the reliability and robustness of the proposed model even in the case of unbalanced data.

In the paper [20] are assessed the rainfall conditions, which can lead to initiation of mass-movement using limited terrestrial data on the summary rainfall (mm) and its duration (h) obtained in Georgia. It is shown that the landslide activating precipitation threshold line follows the equation: $E=a\cdot D^b$, where E is the volume of accumulated precipitation, D is the duration of rain; a and b are parameters. The parameters of above equation for Georgia and its 10 regions as well as their statistical characteristics are calculated and compared to data for similar climatic zones in the world. The results obtained in this study indicate the prospects for further expansion of work for a more detailed study of the influence of precipitation on the activation of landslides in Georgia.

A detailed statistical analysis of the relationship between monthly and accumulated multi-month precipitation sums and the number of landslides in 12 regions of Georgia is presented. Landslide data with a known month and year of activation were used (a total of 788 landslide events from 1961 to 2022) was presented in [21]. For the analysis, the precipitation sum for the month of landslide activation (P1) was determined, as well as the accumulated precipitation sum for the month of activation and for 1 month (P2), 2 months (P3), …, and 11 months (P12) prior to landslide occurrence.

Specifically, the following results were obtained. The relationship between average precipitation values (threshold values) and monthly precipitation duration during the month of landslide activation and before landslide activation in Georgia and its individual regions was determined. It was found that, overall, in eastern Georgia (including the Samtskhe-Javakheti region), landslide activation occurs with significantly lower precipitation sums than in western Georgia. The average P1 values are 76 and 156 mm, respectively, and the P12 values are 684 and 1588 mm. The linear correlation between the number of landslides and the P1…P12 values across the regions of Georgia is low for P1 and moderate for P2…P12. The sum of precipitation associated with landslides exceeds the general long-term average monthly precipitation by approximately 16%. For Georgia as a whole, the dependence of the number of landslides on the P1 and P12 values has the form of a fifth-order polynomial (sequentially: slight increase – plateau – strong increase). For P1 values, the precipitation sum plateau, after which a strong increase in the number of landslides begins, covers the range from 62 to 149 mm, and for P12 – from 914 to 1588 mm (the number of landslides is ≈ 108–114) [21].

This work is a continuation of previous studies [20, 21] related to the study of the relationship between precipitation and the activation of landslide processes on a time scale of 1, 3, 5, 7, 10, 20 and 30 days (or 24, 72, 120, 168, 240, 480 and 720 hours). 1 day (24 hour): sum of precipitation in the day with landslide occurrence; 3 days (72 hour) -30 days (720 hour): cumulative precipitation sums in the day and up to the day in which the landslide occurred.

Some results of statistical analysis of the relationship between daily and cumulative multi-daily sums of precipitation with the number of landslides in the 12 regions of Georgia are presented below.

Study area, material and methods

Study area is Georgia and their 12 regions (Abkhazeti; Samegrelo-Zemo Svaneti; Guria; Adjara; Samtskhe-Javakheti; Kvemo Kartli; Tbilisi; Kakheti; Mtskheta-Mtianeti; Shida Kartli; Imereti; Racha-Lechkhumi and Kvemo Svaneti) – Table 1, Fig. 1.

Data on the number of landslides with the known days of their activation were taken from the catalog [9]. Period of observation - from 1968 to 2022; landslide occurrence height – from 5 (Abkh) to 3773 (M-M) m; number of landslides - from 5 (KK) to 89 (Adj), total – 519 (Table 1, Fig. 1).

Data National Environmental Agency about daily sum of atmospheric precipitations for 68 meteorological stations are used. List of meteorological stations, their coordinates and locations in Table 2 and Fig. 2 are presented. Data from 80 meteorological stations on daily precipitation values for the period from 1960 to 1989 were also used for comparison with data on precipitation associated with landslides.

In the proposed work the analysis of data is carried out with the use of the standard statistical analysis methods [34].

The following designations will be used below: Max - maximal values; Min - minimal values; Mean - average values; P_M - average values of precipitation related to landslide processes; P* - average values of precipitation in 1960-1989; St Dev - standard deviation; St Err – standard error; R^2 – coefficient of determination; R – coefficient of linear correlation; R' - index of correlation for nonlinear equations; 99%(+/-) - 99% confidence interval of the mean; Lat - north latitude, N°; Lon - east longitude, E°; H – altitude above sea level, m; landslide – LS; P (or E for precipitations duration D in hour) - precipitation sum, mm; P1 – precipitation sum in day with LS activation, mm; P3, P5, P7, P10, P20 and P30 - cumulative precipitation sums in the day with landslide and 3…30 days up to landslide occurrence cumulative precipitation sums in the day and up to the day in which the landslide occurred; N(LS) – number of landslides; Eastern Georgia – E Geo; Western Georgia - W Geo.

Landslide activation thresholds were determined using two empirical methods.

1)The precipitation amount for Georgia, its eastern and western parts, and regions was determined by the precipitation amount for 30 consecutive days prior to the landslide and on the day of the landslide (30 days in total). The threshold equations are:

$P = a \cdot x + b$, where P is the total precipitation amount (mm), x is the duration (days), a is the slope of the threshold curve, and b is the free term of the equation;

$E = a \cdot D^b$, where E is the total precipitation amount (mm), D is the duration (hours), a and b are parameters.

The a and b coefficients were determined for average precipitation values.

2) The precipitation threshold for Georgia and its eastern and western parts was estimated by determining the number of landslides in seven precipitation ranges in ascending order. N(LS) = f(P), where N(LS) is the relative number of landslides, in %; f(P) is the precipitation function. All equations are represented by third-degree polynomials.

Table 1. Study regions, period and number of years of observation, number of landslides and their heights for known days of their occurrence in Georgia.

Region	Region, Abbr.	Observation period	Number of years	Number of landslides	Landslide occurrence height, m		
					Min	Max	Mean
1.Abkhazeti	Abkh	1968-1980	3	48	5	637	217
2.Samegrel	S-ZS	1979-2022	12	58	33	2278	696
3.Guria	Gur	2009-2022	11	40	30	1135	233
4.Adjara	Adj	1968-2022	11	89	15	1846	639
5.Samtskhe-	S-J	1973-2022	12	47	797	2468	1282
6.Kvemo	KK	2002-2022	5	5	668	1295	868
7.Tbilisi	Tb	2001-2022	11	47	435	1376	773
8.Kakheti	Kakh	2016-2022	5	9	500	1974	968
9.Mtskheta-	M-M	2013-2022	9	22	455	3773	1476
10.Shida	Sh K	2007-2022	10	16	548	986	781
11.Imereti	Im	1968-2022	13	75	29	980	416
12.Racha-Lechkhumi	R-L KS	2005-2022	13	63	372	1576	906
Georgia	Geo	1968-2022	28	519	5	3773	694

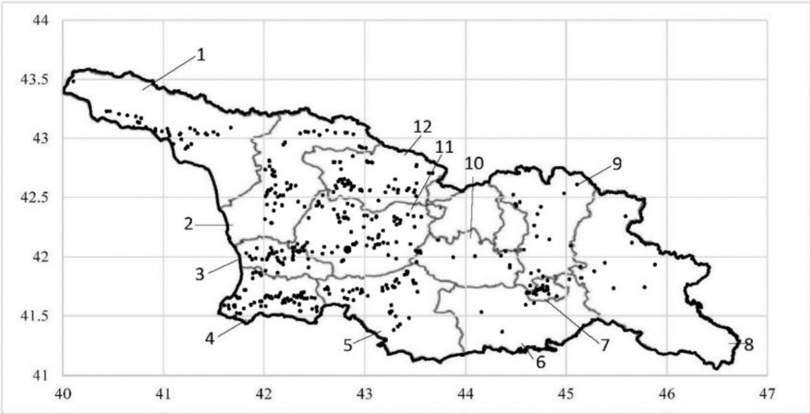

Fig. 1. Landslide distribution map for known days of occurrence. The numbers indicating the contours of the regions correspond to the numbers before the names of the regions in Table 1.

Table 2. List of meteorological stations whose precipitation data were used for known days of landslide occurrence. AWS - automatic weather station

Station	Lon, N°	Lat, E°	H, m	Station	Lon, N°	Lat, E°	H, m
Abastumani	41.75	42.83	1265	Legakhare	42.6	42.17	267
Achadara	43.04	40.99	1280	Luji	42.85	43.02	2587
Akhalkalaki	41.41	43.49	1716	Magaroskari	42.29	44.87	958
Akhaltsikhe	41.64	42.99	989	Martvili	42.38	42.28	176
Alpana	42.56	42.83	560	Martvili AWS	42.38	42.28	176
Ambrolauri	42.52	43.15	544	Mestia AWS	43.04	42.73	1441
Babushera	42.87	41.14	6	Mirveti	41.53	41.72	60
Bakhmaro AWS	41.85	42.32	1926	Mukhrani_AWS	41.93	44.58	550
Bakuriani	41.74	43.52	1665	Nokalakevi	42.36	42.19	115
Batumi_Airport	41.6	41.61	11	Orbeti_AWS	41.66	44.53	1306
Bichvinta	43.15	40.34	4	Orpiri_AWS	42.35	42.86	457
Borjomi	41.84	43.38	790	Pasanauri	42.35	44.69	1070
Chkhalta	43.1	41.68	544	Sabueti_Mta	42.03	43.47	1242
Chkhari AWS	42.27	43.02	465	Sachkhere	42.33	43.41	455
Chokhatauri	42.02	42.24	144	Sagarejo	41.74	45.33	802
Dimi AWS	42.12	42.85	200	Samgori	41.72	44.9	549
Dusheti_AWS	42.09	44.71	1038	Samtredia	42.16	42.34	28
Gagra	43.28	40.27	7	Samtredia_AWS	42.2	42.42	42
Glola	42.7	43.64	1280	Senaki	42.27	42.06	34
Gordi AWS	42.47	42.58	988	Senaki_AWS	42.31	42.12	388
Gori	41.98	44.11	609	Shovi	42.7	43.68	1509
Gudauri_AWS	42.5	44.51	2915	Sokhumi	43.01	41.04	116
Gudauta	43.1	40.64	46	Tbilisi	41.76	44.76	427
Gvandra	43.04	40.92	109	Telavi	41.92	45.48	568
Keda	41.6	41.94	256	Tianeti	42.11	44.97	1099
Khaishi	42.94	42.19	730	Tkibuli	42.35	43	593
Kharagauli AWS	42.03	43.23	597	Tsageri_AWS	42.64	42.79	621
Khashuri	41.99	43.6	690	Tsalka	41.6	44.09	1458
Khertvisi	41.48	43.29	1250	Tseva_AWS	42.12	43.17	448
Khulo	41.64	42.31	946	Tskaltubo_AWS	42.35	42.66	452
Kobi AWS	42.56	44.52	1973	Uravi_AWS	42.65	43.32	1742
Kobuleti	41.85	41.78	7	Zemo Chaladidi	42.22	41.79	4
Kutaisi	42.26	42.7	113	Zestafoni	42.1	43.05	160
Lata	43.03	41.48	299	Zugdidi	42.51	41.87	118

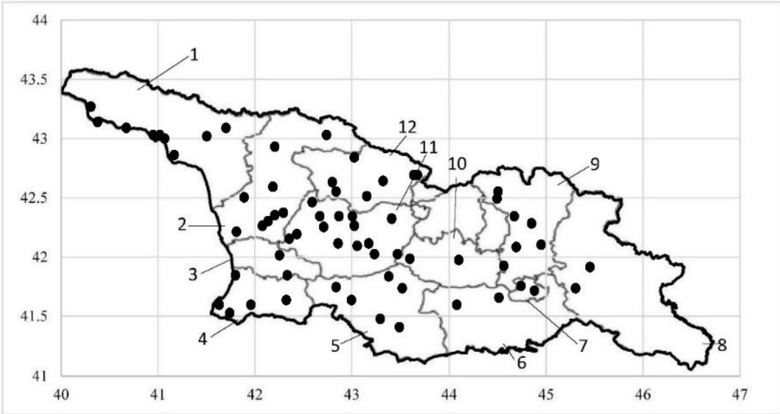

Fig. 2. Distribution map of meteorological stations for known days of landslide occurrence.

The degree of correlation was determined in accordance with [34]: very high correlation ($0.9 \leq R \leq 1.0$); high correlation ($0.7 \leq R < 0.9$); moderate correlation ($0.5 \leq R < 0.7$); low correlation ($0.3 \leq R < 0.5$); negligible correlation ($0 \leq R < 0.3$).

Results and discussion

Results in Tables 3 – 23 and Fig. 3 - 14 are presented. In Tables 3-18 statistical characteristics of the cumulative sum of precipitation related to landslide processes in Georgia, its regions as well as in its eastern and western parts are presented.

Table 3. Statistical characteristics of the cumulative sum of precipitation related to landslide processes in Georgia.

	Cumulative precipitation sum, mm. (1 - Day of landslide occurrence).						
Day	1	3	5	7	10	20	30
Min	0	0	0	0	0	0.1	1.8
Max	222.6	366.6	366.6	416.4	416.4	702.2	798.6
P_M	10.8	22.3	31.4	40.4	54.1	98.4	132.7
St Dev	22.1	39.5	44.5	51.3	59.1	90.5	105.0
St Err	1.0	1.7	2.0	2.3	2.6	4.0	4.6
Count	519	519	519	519	519	519	519
99%(+/-)	2.5	4.5	5.0	5.8	6.7	10.2	11.9
P*	3.3	9.9	16.5	23.1	33.0	65.9	98.9
P_M/P*	3.27	2.25	1.90	1.75	1.64	1.49	1.34

Georgia. P1 values vary from 0.0 mm (252 cases out of those observed) to 222.6 mm, with an average value of 10.8 mm; P30 values vary from 1.8 mm to 798.6 mm, with an average value of 132.7 mm (Table 3, catalog [9]).

The ratio P_M/P* varies from 1.34 (for P30) to 3.27 (for P1). Generally, cumulative sum of landslide-related (mean) precipitation in Georgia is higher than their average long-term values in 1960-1989 (P*). An example is shown in Fig. 3. The P_M/P* average value is 1.95.

Fig. 4 and 5 show examples of distribution maps of P5 and P30 values in the territory of Georgia. In particular, as can be seen from these Figures and Table 4, the distribution of P5 and P30 values in the study area is extremely uneven. Values of P5 vary from 0.0 mm (65 cases out of those observed) to 366.6 mm (Im, Kveda Gordi, landslides activation in October 07, 2013), with an average value of 31.4 mm (Table 3, Fig. 4, catalog [9]); P30 values vary from 1.8 mm (Sh K, Kaspi, February 01, 2019; Kakh, Manavi, January 14, 2020) to 798.6 mm (Adj, Keda, village lower Agara, October 16, 2017), with an average value of 132.7 mm (Table 3, Fig. 5, catalog [9]).

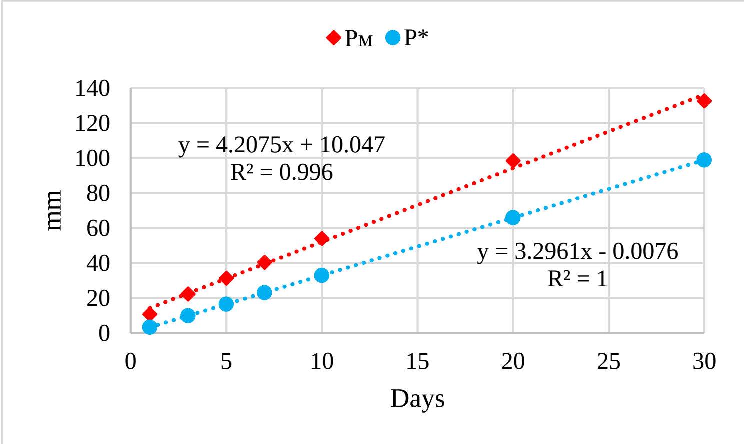

Fig. 3. Cumulative sum of landslide-related (P_M) and average (P*) precipitation in Georgia (very high correlation).

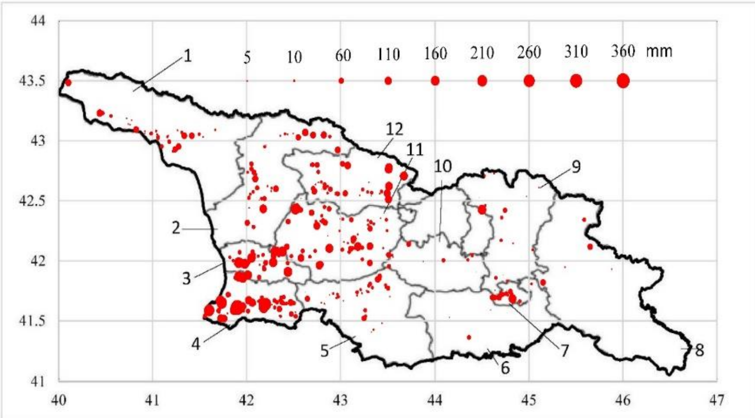

Fig. 4. Map of distribution of 5 days cumulative precipitation up to landslide occurrence (P5). (Total including the day of the landslide).

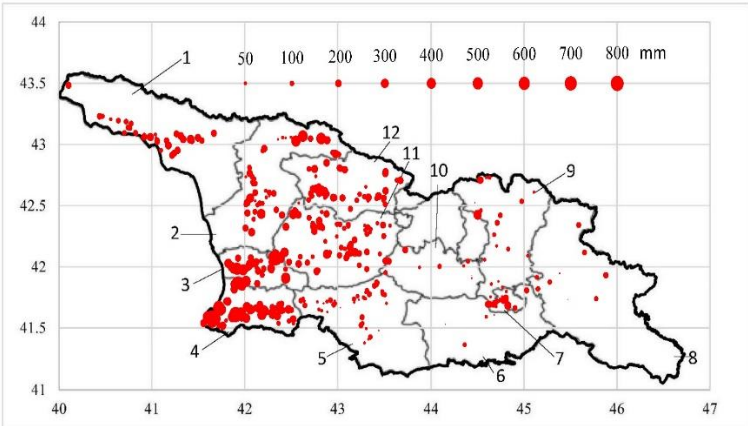

Fig. 5. Map of distribution of 30 days cumulative precipitation up to landslide occurrence (P30). (Total including the day of the landslide).

In Tables 4-18 statistical characteristics of the cumulative sum of precipitation related to landslide processes in 12 regions of Georgia, as well as in its eastern and western parts are presented.

Table 4. Statistical characteristics of the cumulative sum of precipitation related to landslide processes in Abkhazeti.

	Cumulative precipitation sum, mm. (1 - Day of landslide occurrence).						
Day	1	3	5	7	10	20	30
Min	0	0	0	0	0.05	4.6	35.5
Max	37.8	78.4	87.2	127.9	194.7	267.3	273.3
P_M	4.1	12.5	22.8	32.3	44.3	93.9	122.9
St Dev	9.1	20.2	24.5	31.4	41.2	52.6	54.7
St Err	1.3	2.9	3.6	4.6	6.0	7.7	8.0
Count	48	48	48	48	48	48	48
99%(+/-)	3.4	7.6	9.2	11.8	15.5	19.8	20.5
P*	4.4	13.2	22.0	30.8	44.0	88.1	132.1
P_M/P*	0.93	0.95	1.04	1.05	1.01	1.07	0.93

Abkhazeti. P1 values vary from 0.0 mm (31 cases out of those observed) to 37.8 mm (Amtqeli, August 05, 1980), with an average value of 4.1 mm; P30 values vary from 35.5 mm (Aleksandrovka, July 20, 1980) to 273.3 mm (Zenobani, August 13, 1980), with an average value of 122.9 mm (Table 4, catalog [9]).

The ratio P_M/P* varies from 0.93 (for P1 and P30) to 1.07 (for P20). Generally, in Abkhazeti the specified parameters practical not differ from each other. The P_M/P* average value is 1.00.

Table 5. Statistical characteristics of the cumulative sum of precipitation related to landslide processes in Samegrelo-Zemo Svaneti.

	Cumulative precipitation sum, mm. (1 - Day of landslide occurrence).						
Day	1	3	5	7	10	20	30
Min	0	0	0	0	0	2	7
Max	52.6	75.4	126.0	205.7	226.9	285.4	448.9
P_M	6.5	16.3	22.0	34.7	48.8	97.1	133.7
St Dev	12.0	22.8	29.3	38.9	47.7	71.6	99.7
St Err	1.6	3.0	3.9	5.2	6.3	9.5	13.2
Count	58	58	58	58	58	58	58
99%(+/-)	4.1	7.8	10.0	13.3	16.3	24.4	34.0
P*	4.5	13.6	22.6	31.7	45.3	90.6	135.8
P_M/P*	1.44	1.20	0.97	1.09	1.08	1.07	0.98

Samegrelo-Zemo Svaneti. P1 values vary from 0.0 mm (34 cases out of those observed) to 52.6 mm (Mestia-Mulakhi-Ushguli road, village near Mulakhi, September 07, 2017), with an average value of 6.5 mm; P30 values vary from 7.0 mm (Chkvaleri, September 24, 2015) to 448.9 mm (Mestia-Mulakhi-Ushguli road, village near Mulakhi, September 07, 2017), with an average value of 133.7 mm (Table 5, catalog [9]).

The ratio P_M/P* varies from 0.97 (for P5) to 1.44 (for P1). Generally, cumulative sum of landslide-related precipitation in Samegrelo-Zemo Svaneti is slightly higher than their average long-term values. The P_M/P* average value is 1.12.

Table 6. Statistical characteristics of the cumulative sum of precipitation related to landslide processes in Guria.

	Cumulative precipitation sum, mm. (1 - Day of landslide occurrence).						
Day	1	3	5	7	10	20	30
Min	0	0	0	0	0	3	13.6
Max	70	160	187.4	208	244.3	498.2	498.7
P_M	12.2	31.0	44.9	58.2	75.5	132.0	179.6
St Dev	20.6	46.9	53.9	61.2	70.3	112.6	115.7
St Err	3.3	7.5	8.6	9.8	11.3	18.0	18.5
Count	40	40	40	40	40	40	40
99%(+/-)	8.5	19.3	22.3	25.2	29.0	46.4	47.7
P*	5.0	15.0	25.1	35.1	50.1	100.3	150.5
P_M/P*	2.44	2.07	1.79	1.66	1.51	1.32	1.19

Guria. P1 values vary from 0.0 mm (20 cases out of those observed) to 70.0 mm (Bayleti, Zoti, October 16, 2017), with an average value of 12.2 mm; P30 values vary from 13.6 mm (Mtispiri, August 09, 2015) to 498.7 mm (Konchkati, September 24, 2022), with an average value of 179.6 mm (Table 6, catalog [9]).

The ratio P_M/P^* varies from 1.19 (for P30) to 2.44 (for P1). Generally, cumulative sum of landslide-related precipitation in Guria is higher than their average long-term values. The P_M/P^* average value is 1.71.

Table 7. Statistical characteristics of the cumulative sum of precipitation related to landslide processes in Adjara.

	Cumulative precipitation sum, mm. (1 - Day of landslide occurrence).						
Day	1	3	5	7	10	20	30
Min	0	0	0	0	0	3	26.2
Max	222.6	366.6	366.6	416.4	416.4	702.2	798.6
P_M	20.3	41.1	55.1	65.8	82.6	154.5	210.3
St Dev	35.0	65.3	70.5	80.7	93.1	143.3	161.8
St Err	3.7	7.0	7.5	8.6	9.9	15.3	17.2
Count	89	89	89	89	89	89	89
99%(+/-)	9.6	17.9	19.4	22.1	25.6	39.4	44.4
P*	5.7	17.0	28.4	39.8	56.8	113.7	170.6
P_M/P^*	3.56	2.42	1.94	1.65	1.45	1.36	1.23

Adjara. P1 values vary from 0.0 mm (31 cases out of those observed) to 222.6 mm (Keda, village lower Agara, October 16, 2017), with an average value of 20.3 mm; P30 values vary from 26.2 mm (Ghorjomeladzeebi, July 14, 2021) to 798.6 mm (Keda, village lower Agara, October 16, 2017), with an average value of 210.3 mm (Table 7, catalog [9]).

The ratio P_M/P^* varies from 1.23 (for P30) to 3.56 (for P1). Generally, cumulative sum of landslide-related precipitation in Adjara is higher than their average long-term values. The P_M/P^* average value is 1.95.

Table 8. Statistical characteristics of the cumulative sum of precipitation related to landslide processes in Samtskhe-Javakheti.

	Cumulative precipitation sum, mm. (1 - Day of landslide occurrence).						
Day	1	3	5	7	10	20	30
Min	0	0	0	0	0	2.9	6.35
Max	60.0	62.0	69.3	74.4	76.8	97.9	121.0
P_M	5.3	9.7	13.8	16.9	20.9	40.5	60.7
St Dev	11.1	12.6	16.2	18.0	20.0	24.1	33.5
St Err	1.6	1.9	2.4	2.6	2.9	3.6	4.9
Count	47	47	47	47	47	47	47
99%(+/-)	4.2	4.8	6.1	6.8	7.6	9.1	12.7
P*	2.0	6.0	10.0	14.0	20.1	40.2	60.2
P_M/P^*	2.65	1.62	1.38	1.21	1.04	1.01	1.01

Samtskhe-Javakheti. P1 values vary from 0.0 mm (19 cases out of those observed) to 60.0 mm (Borjomi, August 04, 2016), with an average value of 5.3 mm; P30 values vary from 6.35 mm (Adigeni, February 06, 2020) to 121.0 mm (Aspindza, May 27, 1976), with an average value of 60.7 mm (Table 8, catalog [9]).

The ratio P_M/P^* varies from 1.01 (for P20 and P30) to 2.65 (for P1). Generally, cumulative sum of landslide-related precipitation in Samtskhe-Javakheti is higher than their average long-term values. The P_M/P^* average value is 1.42.

Table 9. Statistical characteristics of the cumulative sum of precipitation related to landslide processes in Kvemo Kartli.

	Cumulative precipitation sum, mm. (1 - Day of landslide occurrence).						
Day	1	3	5	7	10	20	30
Min	0	0	0	1.6	1.6	1.6	5
Max	1.0	20.2	33.8	38.0	58.8	101.2	131.8
P_M	0.2	4.4	10.4	20.1	27.1	47.2	55.6
St Dev	0.4	8.9	14.3	16.5	25.3	42.3	52.6
St Err	0.2	4.4	7.2	8.3	12.6	21.1	26.3
Count	5	5	5	5	5	5	5
99%(+/-)	0.6	11.4	18.4	21.3	32.6	54.4	67.7
P*	1.7	5.2	8.6	12.1	17.2	34.5	51.8
P_M/P*	0.12	0.85	1.21	1.66	1.58	1.37	1.07

Kvemo Kartli. P1 values vary from 0.0 mm (4 cases out of those observed) to 1.0 mm (Sagharasheni, April 11, 2019), with an average value of 0.2 mm; P30 values vary from 5.0 mm (Gomareti, February 09, 2022) to 131.8 mm (Martkhopi, September 02, 2002), with an average value of 55.6 mm (Table 9, catalog [9]).

The ratio P_M/P* varies from 0.12 (for P1) to 1.66 (for P7). Generally, cumulative sum of landslide-related precipitation in Kvemo Kartli is slightly higher than their average long-term values. The P_M/P* average value is 1.12.

Table 10. Statistical characteristics of the cumulative sum of precipitation related to landslide processes in Tbilisi.

	Cumulative precipitation sum, mm. (1 - Day of landslide occurrence).						
Day	1	3	5	7	10	20	30
Min	0	0	0	0	0	0.1	6.2
Max	93.5	126.2	129.4	214.2	221.5	228.6	237.6
P_M	12.4	16.4	20.3	26.1	43.4	71.8	84.9
St Dev	21.2	24.5	25.1	34.1	35.7	49.3	46.6
St Err	3.1	3.6	3.7	5.0	5.3	7.3	6.9
Count	47	47	47	47	47	47	47
99%(+/-)	8.1	9.3	9.5	13.0	13.6	18.7	17.7
P*	1.7	5.0	8.3	11.6	16.5	33.1	49.6
P_M/P*	7.29	3.28	2.45	2.25	2.63	2.17	1.71

Tbilisi. P1 values vary from 0.0 mm (24 cases out of those observed) to 93.5 mm (Krtsanisi ravine, May 13, 2012), with an average value of 12.4 mm; P30 values vary from 6.2 mm (Vere valley, new road, January 10, 2017) to 237.6 mm (Krtsanisi ravine, May 13, 2012), with an average value of 84.9 mm (Table 10, catalog [9]).

The ratio P_M/P* varies from 1.71 (for P30) to 7.29 (for P1). Generally, cumulative sum of landslide-related precipitation in Tbilisi is significantly higher than their average long-term values. The P_M/P* average value is 3.11.

Table 11. Statistical characteristics of the cumulative sum of precipitation related to landslide processes in Kakheti.

	Cumulative precipitation sum, mm. (1 - Day of landslide occurrence).						
Day	1	3	5	7	10	20	30
Min	0	0	0	0	0	1.8	1.8
Max	30.1	62.4	66.4	83.2	95.55	123.9	133.1
P_M	6.7	13.0	22.7	31.5	36.1	58.8	80.1
St Dev	10.6	21.3	27.6	31.8	32.6	44.1	46.0
St Err	3.8	7.5	9.7	11.2	11.5	15.6	16.3
Count	9	9	9	9	9	9	9
99%(+/-)	9.7	19.4	25.1	28.9	29.7	40.2	41.9
P*	2.0	6.1	10.2	14.2	20.3	40.7	61.0
P_M/P*	3.35	2.13	2.23	2.22	1.78	1.44	1.31

Kakheti. P1 values vary from 0.0 mm (4 cases out of those observed) to 30.1 mm (Gombori Pass, near Ujarma Castle, October 03, 2017), with an average value of 6.7 mm; P30 values vary from 1.8 mm (Manavi, January 14, 2020) to 133.1 mm (Kvareli, May 13, 2022), with an average value of 80.1 mm (Table 11, catalog [9]).

The ratio P_M/P^* varies from 1.31 (for P30) to 3.35 (for P1). Generally, cumulative sum of landslide-related precipitation in Kakheti is significantly higher than their average long-term values. The P_M/P^* average value is 2.07.

Table 12. Statistical characteristics of the cumulative sum of precipitation related to landslide processes in Mtskheta-Mtianeti.

	Cumulative precipitation sum, mm. (1 - Day of landslide occurrence).						
Day	1	3	5	7	10	20	30
Min	0	0	0	0	0	4.4	7.3
Max	59.6	154.8	157.6	176.2	180.4	230.4	329
P_M	8.2	16.8	22.3	29.2	39.7	56.0	81.2
St Dev	15.6	35.3	38.2	45.7	49.1	56.0	75.0
St Err	3.4	7.7	8.3	10.0	10.7	12.2	16.4
Count	22	22	22	22	22	22	22
99%(+/-)	8.8	19.9	21.5	25.7	27.6	31.5	42.2
P*	2.5	7.4	12.3	17.2	24.6	49.2	73.8
P_M/P^*	3.28	2.27	1.81	1.70	1.61	1.14	1.10

Mtskheta-Mtianeti. P1 values vary from 0.0 mm (12 cases out of those observed) to 59.6 mm (Gudauri-Kobi highway way, August 09, 2018), with an average value of 8.2 mm; P30 values vary from 7.3 mm (Gudauri-Kobi highway way, March 03, 2017) to 329.0 mm (Gudauri-Kobi highway way, August 09, 2018), with an average value of 81.2 mm (Table 12, catalog [9]).

The ratio P_M/P^* varies from 1.10 (for P30) to 3.28 (for P1). Generally, cumulative sum of landslide-related precipitation in Mtskheta-Mtianeti is higher than their average long-term values. The P_M/P^* average value is 1.84.

Table 13. Statistical characteristics of the cumulative sum of precipitation related to landslide processes in Shida Kartli.

	Cumulative precipitation sum, mm. (1 - Day of landslide occurrence).						
Day	1	3	5	7	10	20	30
Min	0	0	0	0	0	0.4	1.8
Max	39.4	39.7	55.1	70.7	86.3	164.7	170.9
P_M	6.8	11.2	16.9	21.2	31.8	57.5	76.1
St Dev	11.3	13.4	18.3	20.6	28.7	44.8	53.6
St Err	2.9	3.5	4.7	5.3	7.4	11.6	13.8
Count	16	16	16	16	16	16	16
99%(+/-)	7.5	8.9	12.2	13.7	19.1	29.8	35.7
P*	1.7	5.1	8.5	11.9	17.0	34.1	51.2
P_M/P^*	4.00	2.20	1.99	1.78	1.87	1.69	1.49

Shida Kartli. P1 values vary from 0.0 mm (8 cases out of those observed) to 39.4 mm (Abano, June 16, 2016), with an average value of 6.8 mm; P30 values vary from 1.8 mm (Kaspi, February 01, 2019) to 170.9 mm (Chumateleti, March 15, 2022), with an average value of 76.1 mm (Table 13, catalog [9]).

The ratio P_M/P^* varies from 1.49 (for P30) to 4.00 (for P1). Generally, cumulative sum of landslide-related precipitation in Shida Kartli is significantly higher than their average long-term values. The P_M/P^* average value is 2.14.

Table 14. Statistical characteristics of the cumulative sum of precipitation related to landslide processes in Imereti.

	Cumulative precipitation sum, mm. (1 - Day of landslide occurrence).						
Day	1	3	5	7	10	20	30
Min	0	0	0	0	0	23.2	32
Max	100.7	180.4	189.8	203.3	258.8	409.4	414.4
P_M	10.8	25.4	37.8	47.9	62.0	105.1	142.5
St Dev	21.5	38.9	42.1	45.8	52.0	78.0	79.6
St Err	2.5	4.5	4.9	5.3	6.0	9.1	9.3
Count	75	75	75	75	75	75	75
99%(+/-)	6.4	11.6	12.6	13.7	15.6	23.4	23.8
P*	3.7	11.1	18.5	25.9	37.0	74.0	111.0
P_M/P*	2.92	2.29	2.04	1.85	1.68	1.42	1.28

Imereti. P1 values vary from 0.0 mm (32 cases out of those observed) to 100.7 mm (Khoni, July 08, 2016), with an average value of 10.8 mm; P30 values vary from 32.0 mm (Kinchkha, May 21, 2013) to 414.4 mm (Samtredia, noga; Samtredia, village partial field, May 21, 2013), with an average value of 142.5 mm (Table 14, catalog [9]).

The ratio P_M/P* varies from 1.28 (for P30) to 2.92 (for P1). Generally, cumulative sum of landslide-related precipitation in Imereti is higher than their average long-term values. The P_M/P* average value is 1.93.

Table 15. Statistical characteristics of the cumulative sum of precipitation related to landslide processes in Racha-Lechkhumi and Kvemo Svaneti.

	Cumulative precipitation sum, mm. (1 - Day of landslide occurrence).						
Day	1	3	5	7	10	20	30
Min	0	0	0	0	0	8.4	19.3
Max	84.5	114.5	128.5	159.0	159.0	203.7	224.9
P_M	11.7	20.6	28.3	35.2	51.8	92.9	123.6
St Dev	23.4	31.9	36.5	40.1	43.5	55.6	58.2
St Err	3.0	4.0	4.6	5.1	5.5	7.1	7.4
Count	63	63	63	63	63	63	63
99%(+/-)	7.7	10.4	11.9	13.1	14.2	18.2	19.0
P*	3.2	9.5	15.8	22.1	31.6	63.2	94.7
P_M/P*	3.66	2.17	1.79	1.59	1.64	1.47	1.31

Racha-Lechkhumi and Kvemo Svaneti. P1 values vary from 0.0 mm (33 cases out of those observed) to 84.5 mm (Patara Ghebi, Ghebi, Nakieti, Shovi, July 29, 2020), with an average value of 11.7 mm; P30 values vary from 19.3 mm (Likheti, August, 13, 2017) to 224.9 mm (Komandeli, October 01, 2021), with an average value of 123.6 mm (Table 15, catalog [9]).

The ratio P_M/P* varies from 1.31 (for P30) to 3.66 (for P1). Generally, cumulative sum of landslide-related precipitation in Racha-Lechkhumi and Kvemo Svaneti is higher than their average long-term values. The P_M/P* average value is 1.95.

Table 16. Statistical characteristics of the cumulative sum of precipitation related to landslide processes in Eastern Georgia.

	Cumulative precipitation sum, mm. (1 - Day of landslide occurrence).						
Day	1	3	5	7	10	20	30
Min	0	0	0	0	0	0.1	1.8
Max	93.5	154.8	157.6	214.2	221.5	230.4	329.0
P_M	8.8	14.1	18.9	24.1	33.2	57.1	75.2
St Dev	16.4	22.4	24.6	30.3	33.6	45.4	50.6
St Err	1.4	1.9	2.0	2.5	2.8	3.8	4.2
Count	146	146	146	146	146	146	146
99%(+/-)	3.5	4.8	5.3	6.5	7.2	9.7	10.8
P*	2.0	6.0	10.0	13.9	19.9	39.9	59.8
P_M/P*	4.40	2.35	1.89	1.73	1.67	1.43	1.26

Eastern Georgia. P1 values vary from 0.0 mm (181 cases out of those observed) to 93.5 mm (Tbilisi, Krtsanisi ravine, May 13, 2012), with an average value of 8.8 mm; P30 values vary from 1.8 mm (Shida Kartli, Kaspi, February 01, 2019; Kakheti, Manavi, January 14, 2020) to 329.0 mm (Mtskheta-Mtianeti, Gudauri-Kobi highway way, August 09, 2018), with an average value of 75.2 mm (Table 16, catalog [9]).

The ratio Pм/P* varies from 1.26 (for P30) to 4.40 (for P1). Generally, cumulative sum of landslide-related precipitation in Eastern Georgia is significantly higher than their average long-term values. The Pм/P* average value is 2.10.

Table 17. Statistical characteristics of the cumulative sum of precipitation related to landslide processes in Western Georgia.

	Cumulative precipitation sum, mm. (1 - Day of landslide occurrence).						
Day	1	3	5	7	10	20	30
Min	0	0	0	0	0	2	7
Max	222.6	366.6	366.6	416.4	416.4	702.2	798.6
Pм	11.9	26.1	37.1	47.5	62.8	115.5	156.6
St Dev	24.2	44.2	49.5	56.3	65.0	98.3	112.6
St Err	1.3	2.3	2.6	2.9	3.4	5.1	5.8
Count	373	373	373	373	373	373	373
99%(+/-)	3.2	5.9	6.6	7.5	8.7	13.1	15.0
P*	4.4	13.3	22.1	30.9	44.2	88.4	132.5
Pм/P*	2.70	1.96	1.68	1.54	1.42	1.31	1.18

Western Georgia. P1 values vary from 0.0 mm (71 cases out of those observed) to 222.6 mm (Adjara, Keda, village lower Agara, October 16, 2017), with an average value of 11.9 mm; P30 values vary from 7.0 mm (Samegrelo-Zemo Svaneti, Chkvaleri, September 24, 2015) to 798.6 mm (Adjara, Keda, village lower Agara, October 16, 2017), with an average value of 156.6 mm (Table 17, catalog [9]).

The ratio Pм/P* varies from 1.18 (for P30) to 2.70 (for P1). Generally, cumulative sum of landslide-related precipitation in Western Georgia is higher than their average long-term values. The Pм/P* average value is 1.68.

Thus, on average, for individual regions of Georgia (with the exception of Abkhazeti, Pм/P* average value is 1.00, Table 4), Georgia as a whole and its eastern and western parts cumulative sum of landslide-related precipitation is higher, чем their average long-term values (Table 3, Tables 5-17, Fig. 3). The lowest value of the average ratio Pм/P* is observed in Samegrelo-Zemo Svaneti (Table 5) and Kvemo Kartli (Table 9) - 1.12 each, the greatest - in Tbilisi (3.11, Table 10). In Georgia this ratio is 1.95 (Table 3), in its eastern and western parts – 2.10 and 1.68 respectively (Tables 16 and 17).

A refinement of the results of work [20] shows that in order of increasing precipitation amount, based on P30 values, regions of Georgia can be grouped as follows (Tables 4-15): 1 – Kvemo Kartli (55.6 mm); 2 - Samtskhe-Javakheti (60.7 mm), 3- Shida Kartli (76,1 mm), 4-Kakheti (80.1 mm), 5- Mtskheta-Mtianeti (81.2 mm), 6- Tbilisi (84.9 mm), 7- Abkhazeti (122.9 mm), 8- Racha-Lechkhumi and Kvemo Svaneti (123.6 mm), 9- Samegrelo-Zemo Svaneti (133.7 mm), 10-Imereti (142.5 mm), 11- Guria (179.6 mm), 12- Adjara (210.3 mm).

In general, in eastern Georgia (including the Samtskhe-Javakheti region), landslide activation occurs with significantly lower precipitation amounts than in the west. Average P1 values are 8.8 and 11.9 mm, respectively, while P30 values are 75.2 and 156.6 mm (Tables 16,17).

In Fig. 6 graphs of connection of associated with landslide processes mean values of the cumulative sum of precipitation by individual regions of Georgia with mean values of the cumulative sum of precipitation for Georgia are presented. These relationships are linear. The corresponding regression equation coefficients are presented in Table 18.

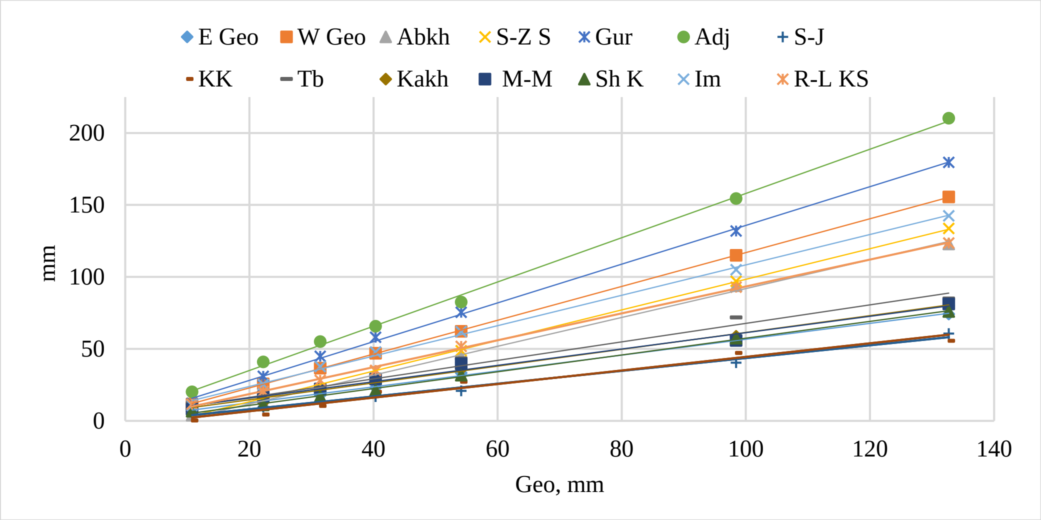

Fig. 6. Connection of associated with landslide processes (data from Tables 3-15) mean values of the cumulative sum of precipitation by individual regions of Georgia with mean values of the cumulative sum of precipitation for Georgia (linear regression, R≥0.94, very high correlation).

Table 18. The coefficients of the linear regression equation between mean values of the cumulative sum of precipitation by individual regions of Georgia with mean values of the cumulative sum of precipitation for Georgia (Fig. 6).

	Y = a·x + b			Y = a·x + b	
Region	a	b	Region	a	b
E Geo	0.5519	1.5341	KK	0.4723	-2.7517
W Geo	1.1754	-0.6005	Tb	0.643	3.4833
Abkh	1.0024	-8.323	Kakh	0.5842	2.9957
S-Z S	1.0628	-7.9381	M-M	0.5681	4.5294
Gur	1.3451	1.2306	Sh K	0.5841	-0.9199
Adj	1.537	4.287	Im	1.0556	2.8193
S-J	0.4446	-0.8057	R-L KS	0.935	-0.0996

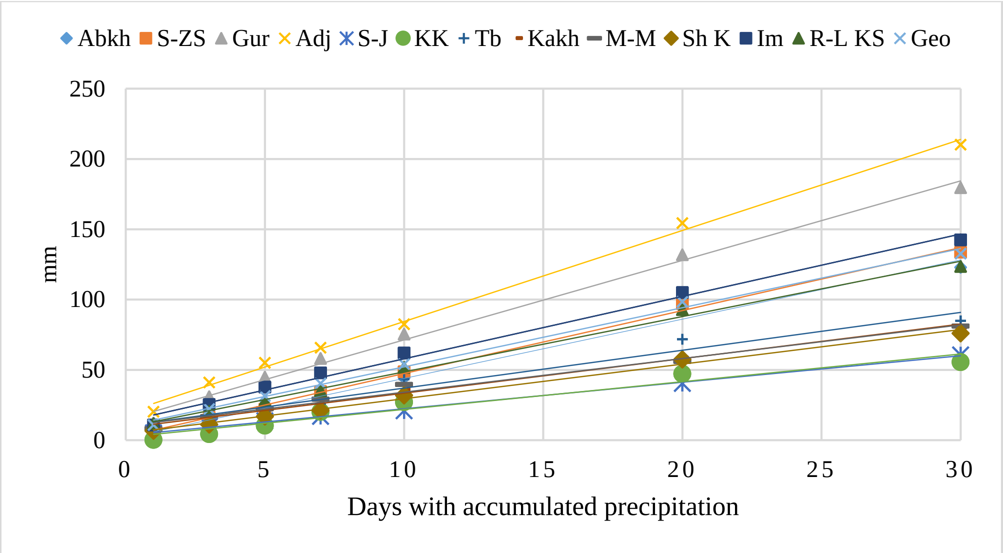

Fig. 7. Dependence of average precipitation values (threshold values) on precipitation duration in days on the day of landslide activation and before landslide activation in Georgia and its individual regions (linear regression).

In Fig. 7 graphs of dependence of average precipitation values (threshold values) on precipitation duration in days on the day of landslide activation and before landslide activation in Georgia and its individual regions in the linear approximation. In Fig. 8 graphs of dependence of average precipitation values (threshold values) on precipitation duration in hours on the day of landslide activation and before landslide activation in Georgia and its individual regions in the power approximation (data from Tables 3-15).

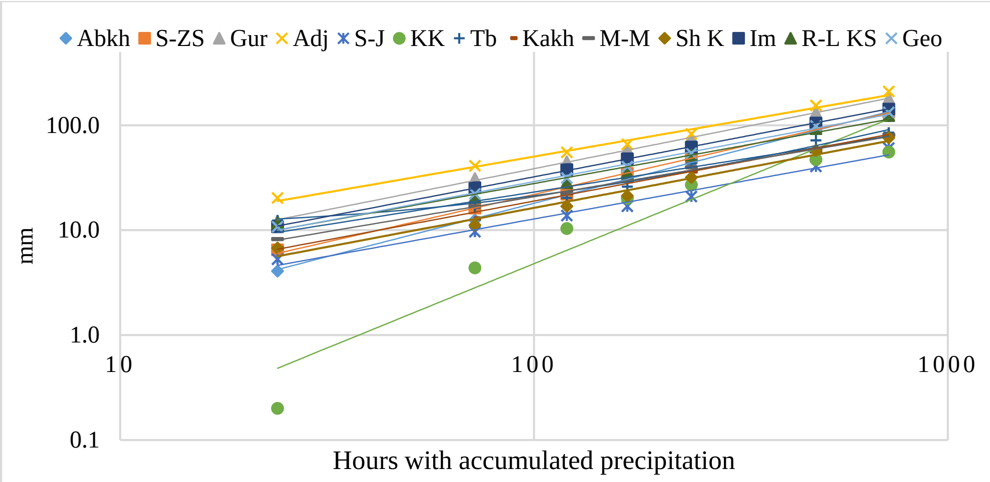

Fig. 8. Dependence of average precipitation values (threshold values) on precipitation duration in hours on the day of landslide activation and before landslide activation in Georgia and its individual regions (power regression).

The corresponding regression equation coefficients are presented in Table 19. For comparison, the same Table also provides previously calculated coefficients of the power regression equations for Georgia and its 10 regions for 174 cases of landslides [20].

Table 19. Coefficients of regression equation dependence of average precipitation values (threshold values) on precipitation duration in days and hours on the day of landslide activation and before landslide activation in Georgia and its individual regions.

Regions	Data from Tables 3-15				Data according to [20]	
	Regression equations					
	$P=a \cdot x+b$		$E=a \cdot D^b$			
	Regression equation coefficients					
	a	b	a	b	a	b
R^2, R, R'	$(0.9479 \le R^2 \le 0.9982)$, R ≥0.97		$(0.9017 \le R^2 \le 0.9998)$, R'≥0.95		$(0.761 \le R^2 \le 0.995)$, R' ≥ 0.87	
Abkh	4.21	1.78	0.17	1.02	No data	No data
S-ZS	4.48	2.66	0.34	0.91	1.63	0.71
Gur	5.66	14.76	1.04	0.78	6.77	0.57
Adj	6.48	19.62	2.16	0.68	9.7	0.5
S-J	1.88	3.54	0.48	0.71	1.29	0.56
KK	1.97	2.18	0.003	1.61	No data	No data
Tb	2.69	10.07	1.32	0.62	2.71	0.5
Kakh	2.45	8.90	0.63	0.74	2.61	0.53
M-M	2.39	10.21	0.96	0.67	0.88	0.69
Sh K	2.46	4.94	0.53	0.74	1.36	0.64
Im	4.44	13.46	0.99	0.76	3.94	0.55
R-L KS	3.94	9.27	1.03	0.71	1.13	0.7
Geo	4.21	10.03	0.93	0.75	3.88	0.55

In particular, the values of the coefficients of a and b in in the equation $E=a \cdot D^b$ vary in a wide range for different regions of Georgia according to the climate zones from the subtropical regions (Abkhazeti, Adjara, Guria) to areas with a continental climate (Shida Kartli, Kakheti, etc., Table 19). Note, as in [20], the data on the values of a and b coefficients (Table 19) in some cases agree satisfactorily with similar data obtained by their authors for various regions of the world [35-37].

Fig. 9 shows dependence of average precipitation values (threshold values) on precipitation duration in days on the day of landslide activation and before landslide activation in Eastern and Western Georgia. Fig. 10 shows dependence of average precipitation values (threshold values) on precipitation duration in hours on the day of landslide activation and before landslide activation in the same parts of Georgia.

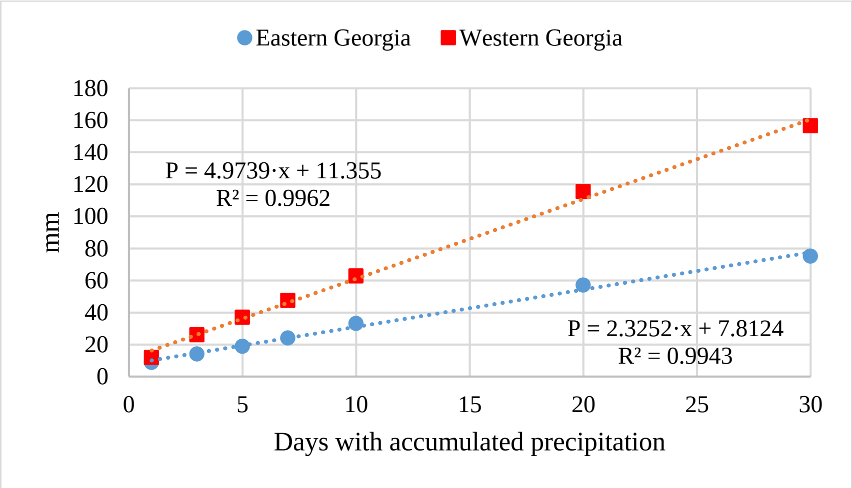

Fig. 9. Dependence of average precipitation values (threshold values) on precipitation duration in days on the day of landslide activation and before landslide activation in Eastern and Western Georgia (R ≈ 1.00, very high correlation).

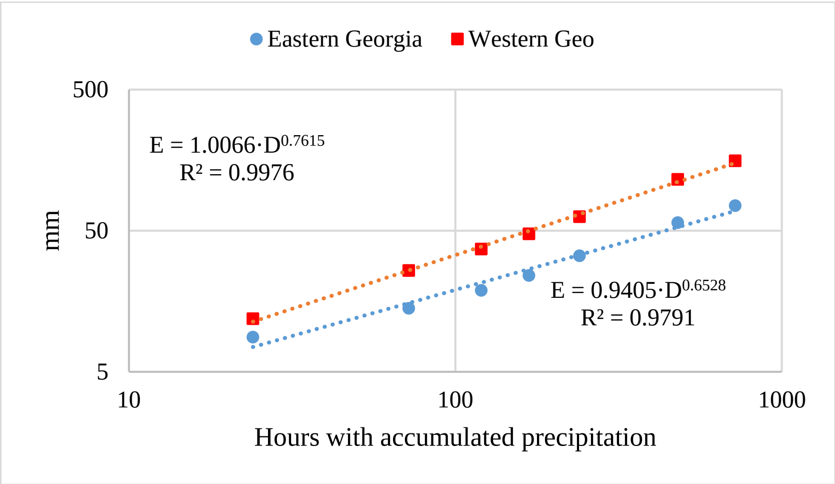

Fig. 10. Dependence of average precipitation values (threshold values) on precipitation duration in hours on the day of landslide activation and before landslide activation in Eastern and Western Georgia (R' ≥ 0.99, very high correlation).

In the first case (Fig. 9), a linear relationship is observed between the parameters under study; in the second (Fig. 10), a power-law relationship is observed. Depending on the task at hand, both relationships can be used (e.g., comparison with similar works by various authors [35-37], etc.).

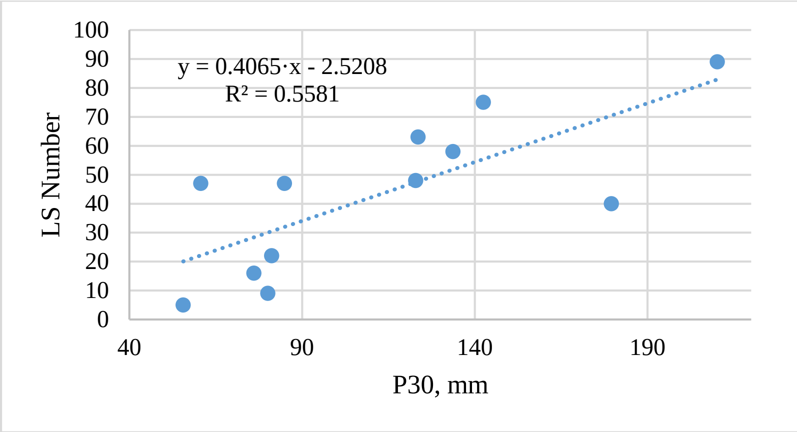

Fig. 11. Example of linear correlation and regression between the number of landslides and the cumulative sum of precipitation for 30 days related to landslide processes by regions of Georgia (data from Tables 4-15).

Fig. 11 shows an example of a graph of linear correlation and regression between the number of landslides and P30 values by region of Georgia. In Table 20 data on coefficients of the linear regression equation between the number of landslides (Y) and the cumulative sum of precipitation of different days (x) related to landslide processes by regions of Georgia are presented

Table 20. Coefficients of the linear regression equation between the number of landslides (Y) and the cumulative sum of precipitation of different days (x) related to landslide processes by regions of Georgia (data from Tables 4-15).

Cumulative precipitation sum	Coefficients of the linear regression equation Y = a·x + b		R	Degree of correlation
P1	3.5964	11.76	0.70	high
P3	1.8775	9.1242	0.72	high
P5	1.3571	7.3696	0.68	moderate
P7	1.1149	4.3125	0.64	moderate
P10	0.9703	-2.3436	0.69	moderate
P20	0.5546	-3.292	0.74	high
P30	0.4065	-2.5208	0.75	high

In general, the linear correlation between the number of landslides and the values of P1…P30 by the regions of Georgia for change from 0.64 (P7, moderate correlation) to 0.75 (P30, high correlation)

Fig. 12-14, as an examples, present graphs of dependences the relative number of landslides (N(LS), %) from P1 values, respectively, for territory of Georgia and its Eastern and Western parts. Averaging was performed over seven ranges of P1 values in ascending order. The relationship between N(LS) values and P1, as well as P3, P5... P30, is a third-degree polynomial. The corresponding regression equation coefficients are presented in Table 21.

Table 21. Coefficients of the regression equation between the relative number of landslides (N(LS), %) and the cumulative sum of precipitation for 1, 3, 5, 7, 10, 20 and 30 days (x) related to landslide processes by Georgia and its eastern and western parts. $R' \geq 0.99$ (very high correlation)

Region	Cumulative precipitation sum	Regression equation
Georgia	P1	$N(LS) = 0.0001x^3 - 0.0126x^2 + 0.3121x + 12.007$
	P3	$N(LS) = 4E\text{-}05x^3 - 0.0052x^2 + 0.1974x + 12.008$
	P5	$N(LS) = 3E\text{-}05x^3 - 0.004x^2 + 0.1726x + 11.835$
	P7	$N(LS) = 4E\text{-}05x^3 - 0.0044x^2 + 0.1743x + 10.808$
	P10	$N(LS) = 1E\text{-}05x^3 - 0.0031x^2 + 0.2052x + 10.405$
	P20	$N(LS) = 3E\text{-}06x^3 - 0.0009x^2 + 0.0944x + 10.538$

	P30	$N(LS) = 7E\text{-}06x^3 - 0.0025x^2 + 0.3125x + 2.1577$
Eastern Georgia	P1	$N(LS) = 0.0003x^3 - 0.0213x^2 + 0.4195x + 12.075$
	P3	$N(LS) = 0.0002x^3 - 0.014x^2 + 0.309x + 12.204$
	P5	$N(LS) = 0.0002x^3 - 0.0137x^2 + 0.3348x + 11.986$
	P7	$N(LS) = 0.0003x^3 - 0.0192x^2 + 0.4168x + 10.738$
	P10	$N(LS) = 7E\text{-}05x^3 - 0.0068x^2 + 0.22x + 11.492$
	P20	$N(LS) = 1E\text{-}05x^3 - 0.0023x^2 + 0.1329x + 11.199$
	P30	$N(LS) = 1E\text{-}05x^3 - 0.0019x^2 + 0.1293x + 10.636$
Western Georgia	P1	$N(LS) = 8E\text{-}05x^3 - 0.0081x^2 + 0.2771x + 11.952$
	P3	$N(LS) = 3E\text{-}05x^3 - 0.0049x^2 + 0.1942x + 11.863$
	P5	$N(LS) = 2E\text{-}05x^3 - 0.0035x^2 + 0.1739x + 11.625$
	P7	$N(LS) = 3E\text{-}05x^3 - 0.0036x^2 + 0.1662x + 10.631$
	P10	$N(LS) = 7E\text{-}06x^3 - 0.0016x^2 + 0.1179x + 11.392$
	P20	$N(LS) = 2E\text{-}06x^3 - 0.0008x^2 + 0.0991x + 9.8761$
	P30	$N(LS) = 1E\text{-}06x^3 - 0.0005x^2 + 0.0907x + 8.7936$

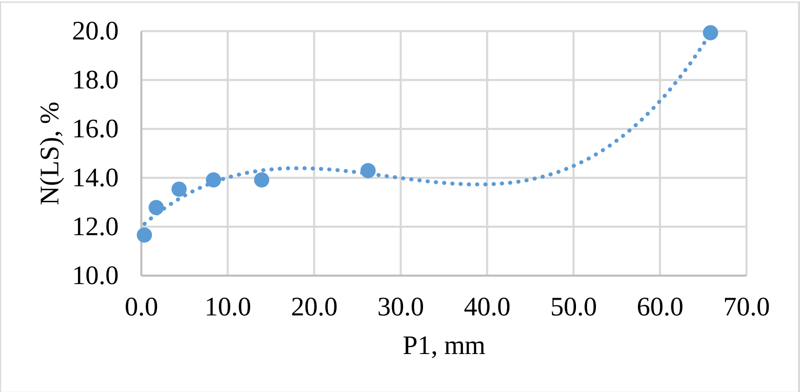

Fig. 12. Relationship between the relative number of landslides (%) and the 1-day total precipitation in the territory of Georgia (critical precipitation threshold).

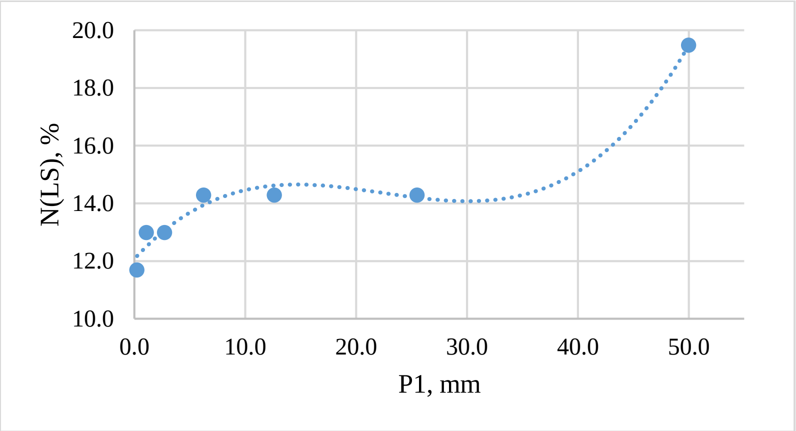

Fig. 13. Relationship between the relative number of landslides (%) and the 1-day total precipitation in the territory of Eastern Georgia (critical precipitation threshold).

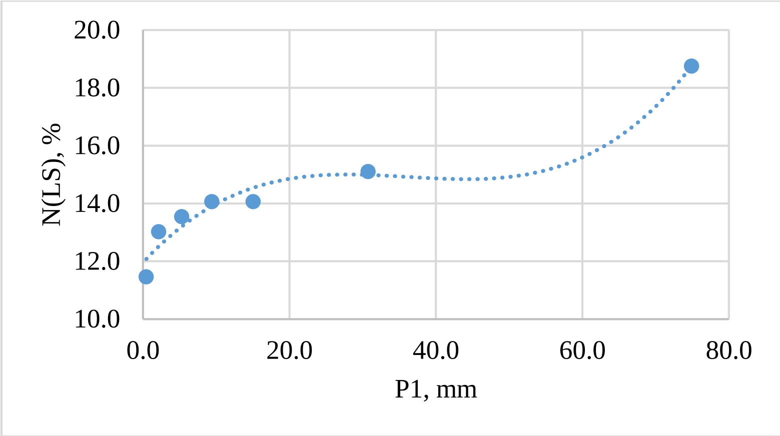

Fig. 14. Relationship between the relative number of landslides (%) and the 1-day total precipitation in the territory of Western Georgia (critical precipitation threshold).

Finally, Tables 21 and 22 presents data on critical threshold of 1, 3, 5, 7, 10, 20 and 30 - days precipitation sum for the activation of landslide processes in Georgia and its Eastern and Western parts (threshold start, threshold end, max precipitation sum).

Table 22. Critical threshold of 1, 3, 5 and 7-days precipitation sum for the activation of landslide processes in Georgia and its Eastern and Western parts

Region	Parameter	Threshold Start	Threshold End	Sum N(LS), %	Max	Sum N(LS), %
		P1, mm				
Georgia	Average	8.4	26.3	42.1	65.9	19.9
	99%(+/-)	0.6	2.2		10.3	
Eastern Georgia	Average	6.3	25.5	42.9	50.0	19.5
	99%(+/-)	1.2	4.6		10.0	
Western Georgia	Average	9.4	30.8	43.2	74.9	18.8
	99%(+/-)	0.7	3.4		13.0	
Region	Parameter	P3, mm				
Georgia	Average	13.7	36.5	42.1	99.4	19.7
	99%(+/-)	0.8	2.3		15.6	
Eastern Georgia	Average	11.4	28.4	42.0	59.4	19.0
	99%(+/-)	1.4	2.8		18.2	
Western Georgia	Average	14.7	39.7	41.8	109.6	20.4
	99%(+/-)	1.0	3.1		17.0	
Region	Parameter	P5, mm				
Georgia	Average	18.3	43.4	42.0	108.3	20.2
	99%(+/-)	0.8	2.3		15.0	
Eastern Georgia	Average	11.7	31.9	42.9	60.1	19.0
	99%(+/-)	1.9	2.5		11.8	
Western Georgia	Average	21.2	51.4	42.4	125.2	19.8
	99%(+/-)	1.1	3.1		18.1	
Region	Parameter	P7, mm				
Georgia	Average	21.3	44.9	39.1	109.8	25.8
	99%(+/-)	1.0	1.7		14.3	
Eastern Georgia	Average	12.6	31.3	40.6	56.4	23.3
	99%(+/-)	2.1	2.3		9.2	
Western Georgia	Average	25.6	52.1	39.3	125.0	25.7
	99%(+/-)	1.3	2.1		17.3	

Table 23. Critical threshold of 10, 20, and 30-day precipitation sum for the activation of landslide processes in Georgia and its Eastern and Western parts.

Region	Parameter	Threshold Start	Threshold End	Sum N(LS), %	Max	Sum N(LS), %
		P10, mm				
Georgia	Average	33.5	68.5	43.5	148.8	19.8
	99%(+/-)	1.0	2.1		17.9	
Eastern Georgia	Average	23.4	52.1	41.4	81.1	20.7
	99%(+/-)	1.9	4.1		18.7	
Western Georgia	Average	39.0	81.8	42.1	169.0	19.7
	99%(+/-)	1.3	3.1		21.3	
Region	Parameter	P20, mm				
Georgia	Average	67.3	124.7	42.0	234.4	20.2
	99%(+/-)	1.8	4.0		27.6	
Eastern Georgia	Average	40.3	78.6	41.8	129.5	19.9
	99%(+/-)	1.5	5.4		17.7	
Western Georgia	Average	81.1	142.5	42.1	265.2	20.1
	99%(+/-)	2.7	3.8		34.5	
Region	Parameter	P30, mm				
Georgia	Average	88.3	141.2	42.4	262.7	27.0
	99%(+/-)	2.1	3.3		25.3	
Eastern Georgia	Average	62.4	100.5	41.8	150.0	19.9
	99%(+/-)	3.9	3.4		22.4	
Western Georgia	Average	118.0	189.5	42.1	330.1	20.1
	99%(+/-)	3.1	4.1		37.1	

As can be seen from Fig. 12-14 and Tables 22, 23, for the P1 values, the precipitation plateau after which a rapid increase in the number of landslides begins covers the range from 6.3 to 30.8 mm, while for P30 it covers the range from 62.4 to 189.5 mm (total relative number of landslides ≈ 42.1-43.2%).

Conclusion

In the near future, the results of this study are planned to be used to assess the role of various factors in the activation of landslide processes (geological structure, topography, distance from roads and rivers, precipitation amount, etc.) using artificial intelligence methods in both steady-state and dynamic modes.

The results of this study may also be useful for hybrid risk assessment and the application of an integrated hybrid approach to forecasting various disaster-related events [38].

Acknowledgments

This work was supported by Shota Rustaveli National Science Foundation of Georgia (SRNSFG), Grant number FR-23-5466, "Machine Learning Approach to the Landslide Activation Prediction in Georgia".

References

[1] Li H., Samsudin N. A. A Systematic Review of Landslide Research in Urban Planning Worldwide. Nat Hazards, 121, 2025, pp. 6391–6411. https://doi.org/10.1007/s11069-024-07064-4

[2] Akosah S., Gratchev I. Systematic Review of Post-Wildfire Landslides. GeoHazards, 6(1):12, 2025, https://doi.org/10.3390/geohazards6010012

[3] Dalğıç S., Karimov E. Investigation of landslide mechanism in the Balaban landslide area using 3D numerical modelling. Int. Journal of Sustainability and Risk Control, Vol.1, No 2(2), Baku, Azerbaijan, September 2025, pp. 31-35.

[4] Matossian A., Baghdasaryan H., Avagyan A., Igityan H., Gevorgyan M., Havenith H. New Landslide Inventory for the Armenian Lesser Caucasus: Slope Failure Morphologies and Seismotectonic Influences on Large Landslides. Geosciences, 10, 111, 2020.

[5] Alcántara-Ayala I. Landslides in a Changing World. Landslides, 2025. https://doi.org/10.1007/s10346-024-02451-1
[6] Varazanashvili O., Tsereteli N., Amiranashvili A., Tsereteli E., Elizbarashvili E., Dolidze J., Qaldani L., Saluqvadze M., Adamia Sh., Arevadze N., Gventcadze A. Vulnerability, hazards and multiple risk assessment for Georgia. Natural Hazards, Vol. 64, Number 3, 2012, pp. 2021-2056. DOI: 10.1007/s11069-012-0374-3, http://www.springerlink.com/content/9311p18582143662/fulltext.pdf.
[7] Fourth National Communication of Georgia Under the United Nations Framework Convention on Climate Change. Chapter 4.9 Geological Hazards in Georgia, Tbilisi, 2021, pp. 278-286.
[8] Gaprindashvili, M., Tsereteli, E., Gaprindashvili, G., Kurtsikidze, O. Landslide and mudflow hazard assessment in Georgia. In: Bonali, F.L., Pasquaré Mariotto, F., Tsereteli, N. (eds) Building Knowledge for Geohazard Assessment and Management in the Caucasus and other Orogenic Regions. NATO Science for Peace and Security Series C: Environmental Security. Springer, Dordrecht, 2021. https://doi.org/10.1007/978-94-024-2046-3_14
[9] Varazanashvili O., Gaprindashvili G., Elizbarashvili E., Basilashvili, Ts., Amiranashvili A., Fuchs S. The First Natural Hazard Event Database for the Republic of Georgia (GeNHs). Catalog, 2023, 270 p. https://openscience.ge/server/api/core/bitstreams/12d32a4e-11dc-4b5c-8878-7c1bf091039d/content; DOI: 10.13140/RG.2.2.12474.57286
[10] Geological bulletins. 2015-2025, (in Georgian). https://nea.gov.ge/c/Departments/Geology
[11] Amiranashvili A., Elizbarashvili E., Gaprindashvili G., Varazanashvili O., Fuchs S. Statistical analysis of parameterized landslide data in Georgia from 1900 to 2022. Reliability: Theory and Applications, ISSN 1932-2321, Special Issue № 6 (81), Part-2, Vol. 19, 2024, pp. 812 - 818. https://doi.org/10.24412/1932-2321-2024-681-812-818
[12] Amiranashvili A., Brocca L., Chelidze T., Svanadze D., Tsamalashvili T., Varamashvili N. Statistical analysis of the annual number of registered landslides and mudflows in Georgia in 1995-2024. 1st International Scientific Conference "Modern problems in Geophysics". Proceedings, ISBN 978-9941-36-434-1, ISSN 3088-4349, Tbilisi, Georgia, November 6-8, 2025. Publish House of Iv. Javakhishvili Tbilisi State University, Tbilisi, 2025, pp. 35-38.
[13] Froude M., Petley D. Global fatal landslide occurrence from 2004 to 2016. Nat. Hazards Earth Syst. Sci., 18, 2018, pp. 2161–2181.
[14] Segoni S., Piciullo L., Gariano S.L. A Review of the Recent Literature on Rainfall Thresholds for Landslide Occurrence. Landslides, 15, 2018, pp. 1483–1501, DOI: 10.1007/s10346-018-0966-4.
[15] Gonzalez F.C.G., Cavacanti M.D.C.R., Nahas Ribeiro W., Mendonça M.B., Haddad A.N. A systematic review on rainfall thresholds for landslides occurrence. Heliyon, 10, 2024, https://doi.org/10.1016/j.heliyon.2023.e23247
[16] Amiranashvili A., Chelidze T., Svanadze D., Tsamalashvili T., Tvauri G. Abnormal precipitation before the landslide in Akhaldaba (A Suburb of Tbilisi, Georgia) on June 13, 2015 according to radar measurements. Journal of the Georgian Geophysical Society, e-ISSN: 2667-9973, p-ISSN: 1512-1127, Physics of Solid Earth, Atmosphere, Ocean and Space Plasma, v. 26(1), 2023, pp. 30–41.
[17] Amiranashvili A., Brocca L., Chelidze T., Svanadze D., Tsamalashvili T., Varamashvili N. Analysis of the precipitation regime that triggered the landslide in Nergeeti (Imereti, Georgia) on February 7, 2024. Int. Sc. Conf. "Complex Geophysical Monitoring in Georgia: History, Modern Problems, Promoting Sustainable Development of the Country", Proceedings, ISBN 978-9941-36-272-9, Publish house of Iv. Javakhishvili Tbilisi State University, Tbilisi, Georgia, October 17-19, 2024, pp. 155 – 158. http://dspace.gela.org.ge/bitstream/123456789/10619/1/39_MM-180.pdf
[18] Beglarashvili N., Elizbarashvili I., Jamrishvili N., Janelidze I., Pipia M., Tavidashvili Kh. Analysis of heavy precipitation in the Adigeni and Chokhatauri municipaliities on July 21, 2025 based on satellite measurements. 1st International Scientific Conference "Modern problems in Geophysics". Proceedings, ISBN 978-9941-36-434-1, ISSN 3088-4349, Tbilisi, Georgia, November 6-8, 2025. Publish House of Iv. Javakhishvili Tbilisi State University, Tbilisi, 2025, pp. 125-128.
[19] Amiranashvili A., Chelidze T., Dalakishvili L., Svanadze D., Tsamalashvili T., Tvauri G. Preliminary results of a study of the relationship between the monthly mean sum of atmospheric precipitation and landslide cases in Georgia. Journal of the Georgian Geophysical Society, ISSN: 1512-1127, Physics of Solid Earth, Atmosphere, Ocean and Space Plasma, v. 23(2), 2020, pp. 37 – 41.
[20] Chelidze T., Amiranashvili A., Svanadze D., Tsamalashvili T., Tvauri G. Terrestrial and satellite-based assessment of rainfall triggered landslides activity in Georgia, Caucasus. Bull. Georg. Nat. Acad. Sci., vol. 17, no. 2, 71-77, 2023, http://science.org.ge/bnas/vol-17-2.html

[21] Amiranashvili A., Brocca L., Chelidze T., Kiria T., Svanadze D., Tsamalashvili T., Varamashvili N. Statistical Analysis of the Relationship Between Monthly and Cumulative Multi-Month Sums of Precipitation with the Number of Landslides in the Regions of Georgia. Transactions of Mikheil Nodia Institute of Geophysics, ISSN 1512-1135, vol. LXXVIII, Publish House of Ivane Javakhishvili Tbilisi State University, Tbilisi, 2025, pp. 49-66. http://dspace.gela.org.ge/bitstream/123456789/10809/1/7_Tr_IG_78_2025.pdf

[22] Amiranashvili A., Brocca L., Chelidze T., Kiria T., Svanadze D., Tsamalashvili T., Varamashvili N. Intra-Annual Distribution of Landslide Recurrence in Georgia and its Relationship with Monthly and Cumulative Multi-Month Sums of Precipitation. Journal of the Georgian Geophysical Society, e-ISSN: 2667-9973, p-ISSN: 1512-1127, Physics of Solid Earth, Atmosphere, Ocean and Space Plasma, v.28(2), 2025, pp. 25-30. https://ggs.openjournals.ge/index.php/GGS/article/view/10453

[23] Amiranashvili A., Chelidze T., Dalakishvili L., Svanadze D., Tsamalashvili T., Tvauri G. Preliminary results of a study of the relationship between the variability of the mean annual sum of atmospheric precipitation and landslide processes in Georgia. Int. Sc. Conf. „Modern Problems of Ecology", Proc., ISSN 1512-1976, v. 7, Tbilisi-Telavi, Georgia, 26-28 September, 2020, pp. 202-206.

[24] Chelidze, T., Tsamalashvili, T., Fandoeva, M. Mass-movement stationary hazard maps of Georgia including precipitation triggering effect: fuzzy logic approach. Bull. Georg. Nat. Acad. Sci., vol. 16, no. 2, 56-63, 2022, http://science.org.ge/bnas/t16-n2/07_Chelidze_Geophysics.pdf

[25] Amiranashvili A., Chelidze T., Svanadze D., Tsamalashvili T., Tvauri G. Some results of a study of the relationship between the mean annual sum of atmospheric precipitation and re-activated and new landslide cases in Georgia taking into account of climate change. Journal of the Georgian Geophysical Society, e-ISSN: 2667-9973, p-ISSN: 1512-1127, Physics of Solid Earth, Atmosphere, Ocean and Space Plasma, v. 25(2), 2022, pp. 38–48. https://openjournals.ge/index.php/GGS/article/view/5959, DOI: https://doi.org/10.48614/ggs2520225959

[26] Amiranashvili A., Chelidze T., Svanadze D., Tsamalashvili T., Tvauri G. Study of the relationship between the mean annual sum of atmospheric precipitation and re-activated and new mudflow cases in Georgia. Journal of the Georgian Geophysical Society, e-ISSN: 2667-9973, p-ISSN: 1512-1127, Physics of Solid Earth, Atmosphere, Ocean and Space Plasma, v. 26(1), 2023, pp. 19–29. https://ggs.openjournals.ge/index.php/GGS/article/view/6958;
DOI: https://doi.org/10.48614/ggs2620236958

[27] Amiranashvili A., Brocca L., Chelidze T., Svanadze D., Tsamalashvili T., Varamashvili N. Statistical analysis of the number of damaging landslides in municipalities and regions of Georgia and their relationship with atmospheric precipitation in 2015-2024. Reliability: Theory and Applications, ISSN 1932-2321, Special Issue No. 9 (87), Volume 20, November 2025, pp. 255-264.

[28] Chelidze T., Kiria T., Amiranashvili A., Svanadze D., Tsamalashvili T., Varamashvili N. Landslide Hazard Maps of Georgia Using Machine Learning Approach. Bulletin of the National Academy of Sciences of Georgia, ISSN: 0132 - 1447, vol. 20(194), no. 2, 2026, pp. 23-29. http://science.org.ge/bnas/t20-n2/03_Chelidze_Geophysics.pdf

[29] Amiranashvili A., Chelidze T., Svanadze D., Tsamalashvili T., Tvauri G. On the representativeness of data from meteorological stations in Georgia for annual and semi-annual sum of atmospheric precipitation around of these stations. Int. Sc. Conf. „Natural Disasters in the 21st Century: Monitoring, Prevention, Mitigation". Proceedings, ISBN 978-9941-491-52-8, Tbilisi, Georgia, December 20-22, 2021. Publish house of Iv. Javakhishvili Tbilisi State University, Tbilisi, 2021, pp. 79 - 83. http://openlibrary.ge/bitstream/123456789/9566/1/20_Conf_ND_2021.pdf

[30] Amiranashvili A., Chelidze T., Svanadze D., Tsamalashvili T., Varamashvili N. About the representativeness of data from meteorological stations in Georgia for monthly sum of atmospheric precipitation around of these stations. Journal of the Georgian Geophysical Society, e-ISSN: 2667-9973, p-ISSN: 1512-1127, Physics of Solid Earth, Atmosphere, Ocean and Space Plasma, v. 27(1), 2024, pp. 52–57. https://ggs.openjournals.ge/index.php/GGS/article/view/7983

[31] Amiranashvili A., Chelidze T., Svanadze D., Tsamalashvili T., Tvauri G. Comparison of data from ground-based and satellite measurements of the monthly sum of atmospheric precipitation on the example of Tbilisi city in 2001-2020. Int. conf. of young scientists "Modern Problems of Earth Sciences". Proceedings, ISBN 978-9941-36-044-2, Publish House of Iv. Javakhishvili Tbilisi State University, Tbilisi, November 21-22, 2022, pp. 154-158. http://openlibrary.ge/bitstream/123456789/10251/1/37_YSC_2022.pdf

[32] Amiranashvili A., Chelidze T., Svanadze D., Tsamalashvili T., Varamashvili N. Comparison of satellite

and ground-based data on semi-annual and annual sum of atmospheric precipitation for 26 points in Georgia in 2001-2020. Int. Sc. Conf. “Complex Geophysical Monitoring in Georgia: History, Modern Problems, Promoting Sustainable Development of the Country”, Proceedings, ISBN 978-9941-36-272-9, Publish House of Iv. Javakhishvili Tbilisi State University, Tbilisi, Georgia, October 17-19, 2024, pp. 159 – 163. http://www.openlibrary.ge/bitstream/123456789/10618/1/40_MM-180.pdf
[33] Amiranashvili A.G., Brocca L., Chelidze T.L., Svanadze D.T., Tsamalashvili T.N., Varamashvili N.D. Statistical Analysis of Annual and Semi-Annual Sum of Atmospheric Precipitation Data for 59 Municipalities (11 Regions) of Georgia with Landslide Hazard Zones from 2015 to 2024. Journal of the Georgian Geophysical Society, e-ISSN: 2667-9973, p-ISSN: 1512-1127 Physics of Solid Earth, Atmosphere, Ocean and Space Plasma, v. 28(1), 2025, pp. 50 - 63. https://ggs.openjournals.ge/index.php/GGS/article/view/9249
[34] Hinkle D. E., Wiersma W., Jurs S. G. Applied statistics for the behavioral sciences. Boston, MA, Houghton Mifflin Company, ISBN: 0618124055; 9780618124053, 2003, 756 p.
[35] Guzzetti F., Peruccacci S., Rossi M., Stark C.P. Rainfall thresholds for the initiation of landslides in central and southern Europe. Meteorol. Atmos. Phys. 98, 2007, pp. 239-267.
[36] Gariano S. L., Petrucci O., Guzzetti F. Changes in the occurrence of rainfall-induced landslides in Calabria, southern Italy, in the 20th century. Nat. Hazards Earth Syst. Sci., 15, 2015, pp. 2313–2330, https://doi.org/10.5194/nhess-15-2313-2015.
[37] Dikshit A., Sarkar R., Pradhan B., Acharya S., Dorji, K. Estimating rainfall thresholds for landslide occurrence in the Bhutan Himalayas. Water, 11(8), 2019, 1616 https://doi.org/10.3390/w11081616.
[38] Aliyev V., Pkhovelishvili M., Archvadze N., Gasitashvili Z. Hybrid risk review. Int. Journal of Sustainability and Risk Control, Baku, Azerbaijan, Vol.1, No 1(1), June 2025, pp. 12-23.

საქართველოს რეგიონებში ყოველთვიურ და კუმულაციურ მრავალთვიან ნალექების რაოდენობასა და მეწყრის გააქტიურებას შორის კავშირის შეფასება

ა. ამირანაშვილი, ლ. ბროკა, თ. ჭელიძე, თ. ქირია,
დ. სვანაძე , თ. წამალაშვილი, ნ. ვარამაშვილი

რეზიუმე

წარმოდგენილია საქართველოს 12 რეგიონში დღიური და დაგროვილი მრავალდღიანი ნალექების რაოდენობასა და მეწყერების რაოდენობას შორის ურთიერთკავშირის დეტალური სტატისტიკური ანალიზი. გამოყენებული იქნა მონაცემები მეწყერების შესახებ ცნობილი გააქტიურების დღით (სულ 519 მეწყერის მოვლენა 1968 წლიდან 2022 წლამდე). ანალიზისთვის განისაზღვრა ნალექების რაოდენობა მეწყერის გააქტიურების დღეს (P1), ასევე დაგროვილი ნალექების რაოდენობა მეწყერამდე 3 დღის (P3), 5 დღის (P5), 7 დღის (P7), 10 დღის (P10), 20 დღის (P20) და 30 დღის (P30) განმავლობაში (მეწყერის დღის ჩათვლით).
კერძოდ, მიღებული იქნა შემდეგი შედეგები. დადგინდა კავშირი ნალექების საშუალო მნიშვნელობებსა (ზღვრულ მნიშვნელობებსა) და დღიური ნალექების ხანგრძლივობას შორის მეწყერის გააქტიურების დღეს და მეწყერის გააქტიურებამდე 3, 5 და 30 დღის განმავლობაში საქართველოში და მის ცალკეულ რეგიონებში. აღმოჩნდა, რომ აღმოსავლეთ საქართველოში (სამცხე-ჯავახეთის რეგიონის ჩათვლით) მეწყერის გააქტიურება ხდება ნალექების მნიშვნელოვნად დაბალი რაოდენობით, ვიდრე დასავლეთ საქართველოში. P1 საშუალო მნიშვნელობებია შესაბამისად 8.8 და 11.9 მმ, ხოლო P30 მნიშვნელობებია 75.2 და 156.6 მმ. საქართველოს რეგიონებში მეწყერების რაოდენობასა და P1…P30 მნიშვნელობებს შორის წრფივი

კორელაცია მაღალია P1, P3, P20 და P30-სთვის და ზომიერი P5, P7 და P10-სთვის. საქართველოსთვის, მეწყერებთან დაკავშირებული ნალექების რაოდენობა დაახლოებით 95%-ით აღემატება დღიური ნალექების საერთო გრძელვადიან საშუალო მაჩვენებელს. მთლიანად საქართველოსთვის და მისი აღმოსავლეთ და დასავლეთ ნაწილებისთვის, მეწყერების რაოდენობის დამოკიდებულებას P1…P30 მნიშვნელობებზე აქვს მესამე ხარისხის პოლინომის ფორმა (თანმიმდევრულად: უმნიშვნელო ზრდა - პლატო - ძლიერი ზრდა). P1 მნიშვნელობებისთვის, ნალექების პლატო, რომლის შემდეგაც იწყება მეწყერების რაოდენობის მკვეთრი ზრდა, მოიცავს დიაპაზონს 6.3-დან 30.8 მმ-მდე, ხოლო P30-ისთვის - 62.4-დან 189.5 მმ-მდე (მეწყერების საერთო ფარდობითი რაოდენობა ≈ 42.1–43.3%-ია).

საკვანძო სიტყვები: მეწყერი, სტიქიური უბედურება, ატმოსფერული ნალექები, სტატისტიკური ანალიზი.

Оценка связи суточных и накопленных многосуточных сумм осадков с активизацией оползней в регионах Грузии

А. Амиранашвили, Л. Брокка, Т. Челидзе, Т. Кириа,

Д. Сванадзе, Т. Цамалашвили, Н. Варамашвили

Резюме

Представлен подробный статистический анализ связи между суточным и накопленными многодневными количеством осадков и числом оползней в 12 регионах Грузии. Использовались данные об оползнях с известным днем активации (всего 519 оползневых событий с 1968 по 2022 год). Для анализа была определена сумма осадков в день активации оползня (P1), а также накопленная сумма осадков за 3 дня (P3), 5 (P5), 7 (P7), 10 (P10), 20 (P20) и 30 дней (P30) до возникновения оползня (включая день с оползнем).
В частности, были получены следующие результаты. Была определена связь между средними значениями осадков (пороговыми значениями) и продолжительностью суточных осадков в день активации оползня и за 3, 5...30 дней до активации оползней в Грузии и ее отдельных регионах. Было установлено, что в целом в восточной Грузии (включая регион Самцхе-Джавахети) активизация оползней происходит при значительно меньших суммах осадков, чем в западной Грузии. Средние значения P1 составляют 8.8 и 11.9 мм соответственно, а значения P30 — 75.2 и 156.6 мм. Линейная корреляция между количеством оползней и значениями P1…P30 по регионам Грузии высокая для P1, P3, P20 и P30 и умеренная для P5, P7 и P10. Для Грузии сумма осадков, связанных с оползнями, превышает общую долгосрочную среднюю суточную сумму осадков примерно на 95%. Для Грузии в целом и ее восточной и западной частей зависимость количества оползней от значений P1…P30 имеет вид полинома третьей степени (последовательно: незначительный рост — плато — сильный рост). Для значений P1 плато суммы осадков, после которого начинается резкое увеличение числа оползней, охватывает диапазон от 6.3 до 30.8 мм, а для P30 – от 62.4 до 189.5 мм (общее относительное число оползней составляет ≈ 42.1–43.3%).

Ключевые слова: оползни, стихийное бедствие, атмосферные осадки, статистический анализ.

Journal of the Georgian Geophysical Society, e-ISSN: 2667-9973, p-ISSN: 1512-1127
Physics of Solid Earth, Atmosphere, Ocean and Space Plasma, v. 29(1), 2026, pp. 50 - 59

Retrospective Analysis of Landslides Processes in Akhaldaba (A Suburb of Tbilisi, Georgia) on June 13-14, 2015

[1]Avtandil G. Amiranashvili, [1]Tamaz L. Chelidze, [1]Tengiz V. Kiria,
[1] David T. Svanadze, [3] Tamar N. Tsamalashvili, [1] Nodar D. Varamashvili

[1]M. Nodia Institute of Geophysics of I. Javakhishvili Tbilisi State University, Tbilisi, Georgia
[2]A. Janelidze Geological Institute of I. Javakhishvili Tbilisi State University, Tbilisi, Georgia
avtandilamiranashvili@gmail.com

ABSTRACT

The article presents the results of an analysis of radar measurements of precipitation intensity preceding a series of small landslides in the Akhaldaba region (a suburb of Tbilisi, Georgia) on June 13-14, 2015. Specifically, the following results were obtained. The time course of the cumulative precipitation in the zone of maximum cloud radar reflectivity from 20:49 hour to 23:58 hour on June 13, 2015, has the form of a fifth-degree polynomial. The cumulative precipitation by 23:58 hour was 402.8 mm. The time course of the cumulative number of small landslides from 22:30 hour on June 13, 2015, to 01:00 hour on June 14, 2015, has the form of a third-degree polynomial. The number of landslides by 01:00 hour was 98.
The dependence of the cumulative landslide sum on the cumulative precipitation with a one-hour lead time is obtained, which has the form of a third-degree polynomial. A rapid increase in the number of landslides is observed with increasing accumulated precipitation (with a one-hour lead time).
This study once again demonstrates that radar measurements of precipitation intensity can be an effective tool for studying the role of precipitation in landslide occurrence, as well as for short-term forecasting of their activation, especially in areas where ground-based precipitation measurements are unavailable.

Key words: *atmospheric precipitation, radar observations, landslides.*

Introduction

The activation of landslide and mudflow processes is often associated with precipitation patterns on various time scales (from minutes to several years) [1,2]. In Georgia, a modern database of these processes [3-5], as well as precipitation data, has been created and is being improved based on ground-based [6-18], satellite [19-21], and radar [22-25] observations.

Using these databases, the relationships between landslides and mudflows and precipitation on various time scales (from hours to climate scales) and territories (landslide location, regions of Georgia, territory of Georgia [10,11,14-18,20,23-25]) have been studied in recent years, including using machine learning methods [26].

In particular, in the works [23,24] data on the radar characteristics of a rain cloud that caused a landslide in Akhaldaba and a catastrophic flood in Tbilisi on June 13-14, 2015 are presented. The temporal variability of the maximum radar reflectivity of the cloud, precipitation intensity, etc. was studied. It is noteworthy that the cloud did not move much and was over the zone where the landslide descended for more than 5 hours. The consequences of this landslide are well known - the closure of the Vere River, the accumulation of water, the breaking of an artificial dam and the catastrophic flood in Tbilisi.

In the next work [25] results of the analysis of radar measurements of precipitation intensity preceding the landslide in the vicinity of Akhaldaba (a suburb of Tbilisi, Georgia) on June 13, 2015 from 21.00 to 23.97 h are presented. In particular, the following results are obtained. Time-series of precipitation intensity under zone with the maximum radar reflectivity of the cloud has the form of a fifth power of polynomial. Time series of areas of precipitation of different intensity under the cloud were obtained and their statistical characteristics were studied. Dependence of the average intensity of precipitation under the cloud on the effective radius from the zone with the maximum radar reflectivity is obtained.

Statistical characteristics of precipitation intensity over the center of the landslide top is presented. Sum of precipitation under zone with the maximum radar reflectivity of the cloud and over the center of the landslide top on 13 June 2015 from 21.00 to 23.97 h and before landslide from 21.00 to 22.45 h is assessed.

This work is a continuation of previous studies [23-25]. Below the results of a more detailed analysis of the relationship between intense rainfall and the formation of landslides in Akhaldaba on June 13-14, 2015 are presented.

Study Area, Materials and Methods

Study Area – landslide (LS) zone in Akhaldaba (a suburb of Tbilisi, Georgia, Fig. 1).

Fig. 1 illustrates the current state of the main landslide in Akhaldaba with the reconstructed road. It should be noted that following flash floods in the region on June 14, 2014, a landslide on the Vera River near the village of Akhaldaba damaged several sections of roads in the area. The area directly affected by the landslide was approximately 537065 square meters, with 1110 meters of roadway buried or damaged by the landslide [25].

According to data of the Georgian Environment Agency in addition to the largest landslide (Fig. 1), up to 98 small landslides were recorded in the Akhaldaba zone.

Fig. 1. Largest LS Center below the road (after road reconstruction), Lat 41.676421° N, Lon 44.677314° E.

Fig. 2-4 provide information on the number and location of small landslides at different time intervals.

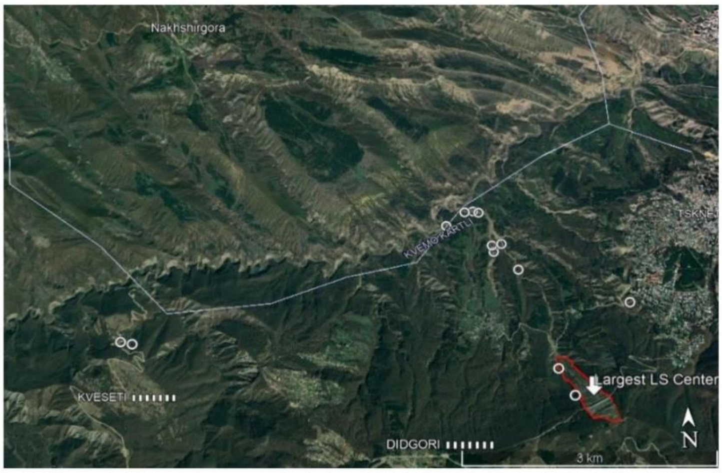

Fig. 2. LS 13.06.2015, 22:30 hour (13 LS locations).

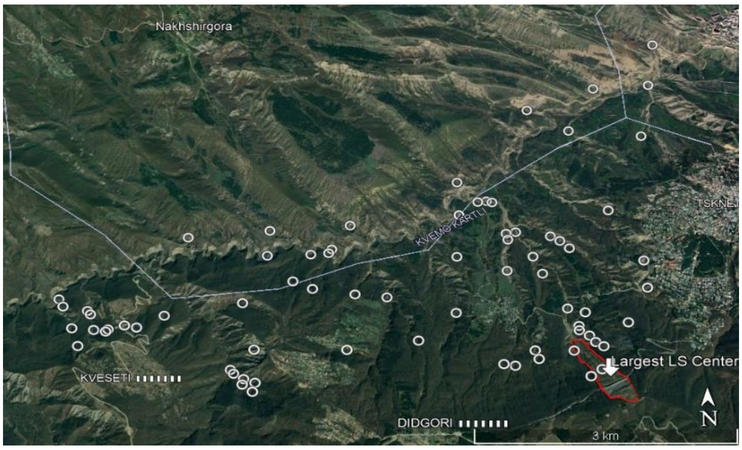

Fig. 3. LS 13.06.2015, 23:00-23:45 hour (73 LS locations).

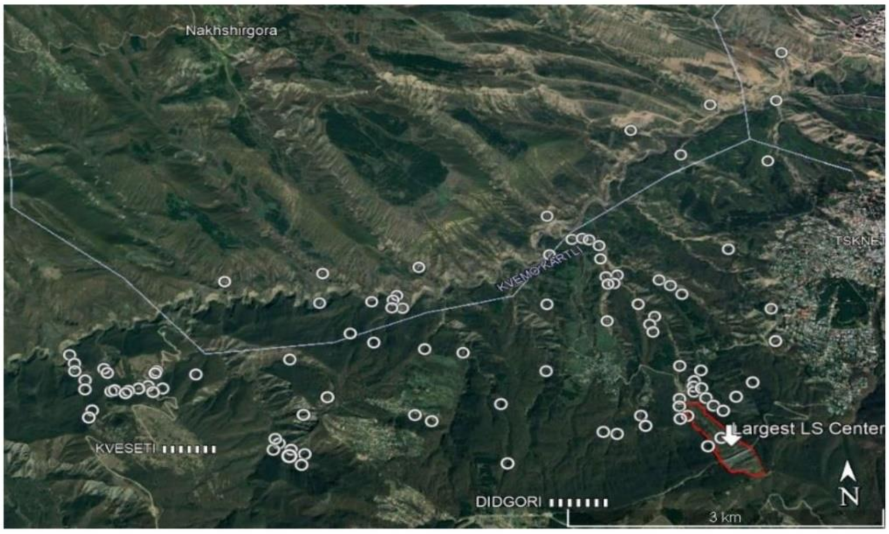

Fig. 4. LS 14.06.2015, 00:30-01:00 hour (98 LS locations).

Precipitation intensity was measured using meteorological radar "METEOR 735 CDP 10 - Doppler Weather Radar". Radar is established in the village Chotori of the Signagi municipality of Kakheti region of Georgia [35,36]. In this work radar product MPPI (dBz) is used [27-29]. Example of this radar product on Fig. 5 is presented.

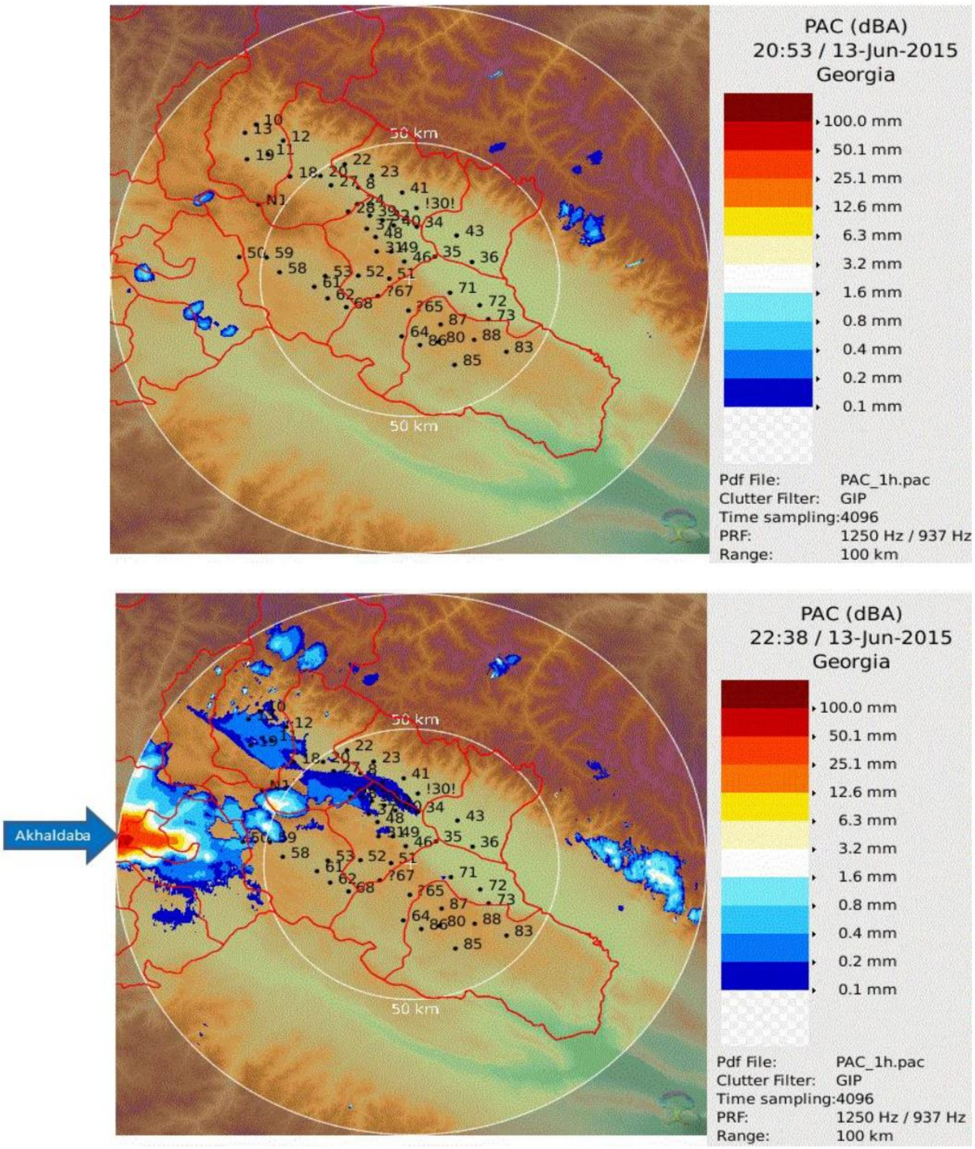

Fig. 5. Radar images of hourly precipitation sums in eastern Georgia in 20.53 and 22.38 hours on June 13, 2015.

In the proposed work the analysis of data is carried out with the use of the standard statistical analysis methods [30].

Results

Results in Fig. 6-8 are presented.

In Fig. 6 time course of the cumulative max precipitation sums in the zone of max cloud radar reflectivity from 20:49 to 23:58 hour on June 13, 2015, having the form of a fifth-degree polynomial, is presented. Accumulated max precipitation sum to 23:58 hour on June 13, 2015 was 402.8 mm.

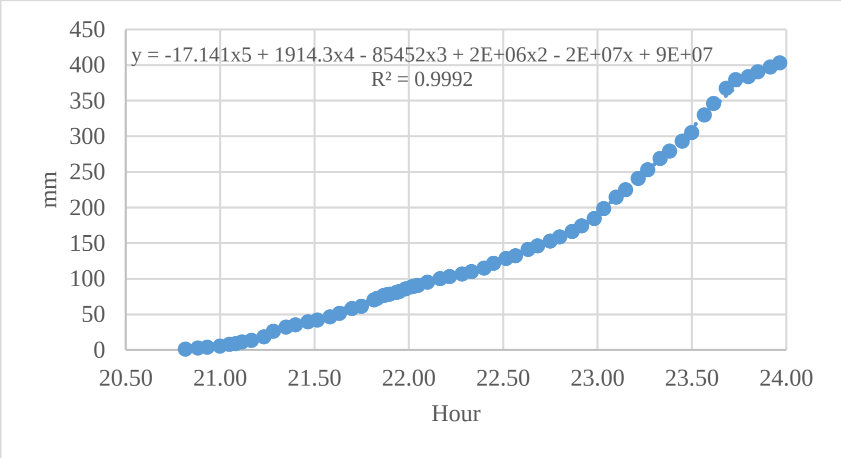

Fig. 6. Time course of the cumulative maximum precipitation sums from 20:49 to 23:58 hour on June 13, 2015.

In Fig. 7 time course of the cumulative number of landslides from 22:30 hour on June 13 to 01:00 hour on June 14, 2015, having the form of a third-degree polynomial, is presented. Accumulated number of landslides to 01:00 hour on June 14, 2015 was 98.

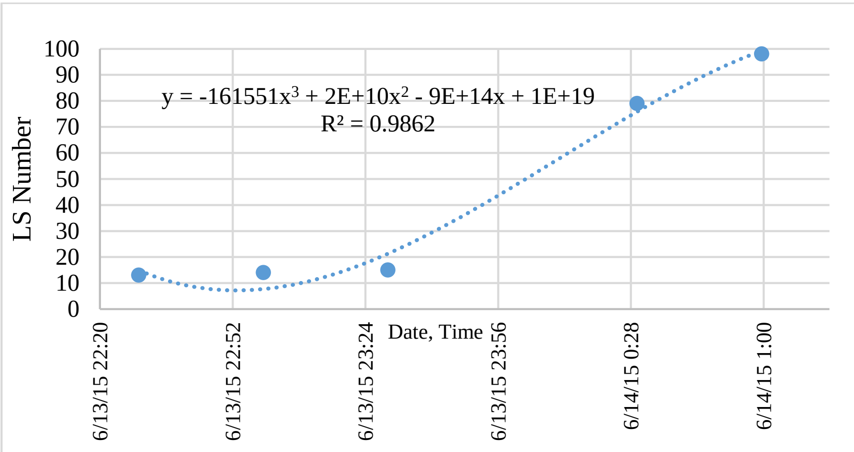

Fig. 7. Time course of the cumulative number of landslides from 22:30 hour on June 13 to 01:00 hour on June 14, 2015.

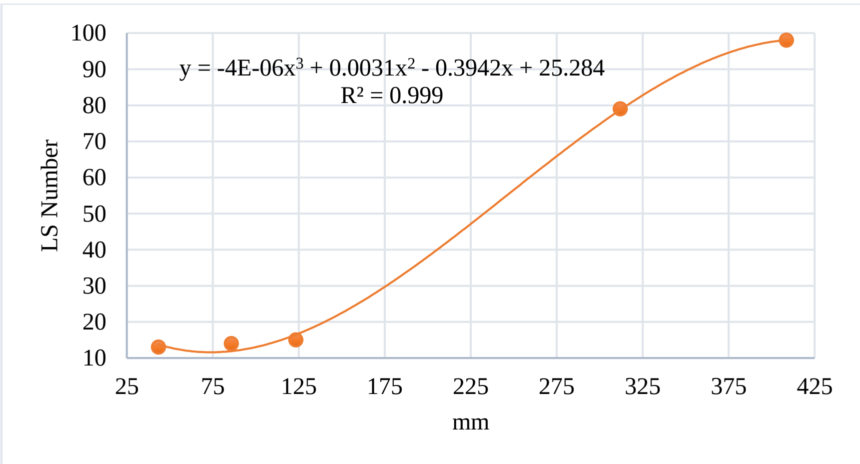

Fig. 8. The relationship between the cumulative number of landslides and the cumulative maximum precipitation amount with a one-hour lead time on June 13-14, 2015.

Finally, Fig. 8 present the relationship between the cumulative number of landslides and the cumulative maximum precipitation amount with a one-hour lead time on June 13-14, 2015. This relationship has the form of a third-degree polynomial. Fig. 8 clearly demonstrates the rapid increase in the number of landslides as the accumulated amount of precipitation increases with the indicated lead time (one hour).

Conclusion

This study further demonstrated that radar measurements of rainfall intensity can be an effective tool for studying the role of rainfall in landslide occurrence and for short-term prediction of landslide activation, especially in areas where ground-based rainfall measurements are not available.

In the future, we plan to further explore this area (comparison of ground-based, radar, and satellite precipitation data, the use of machine learning methods for integrated short-term landslide prediction based on these data, etc.).

Acknowledgments

This work was supported by Shota Rustaveli National Science Foundation of Georgia (SRNSFG), Grant number FR-23-5466, "Machine Learning Approach to the Landslide Activation Prediction in Georgia".

References

[1] Segoni S., Piciullo L., Gariano S.L. A Review of the Recent Literature on Rainfall Thresholds for Landslide Occurrence. Landslides, vol. 15, pp. 1483–1501, 2018. DOI 10.1007/s10346-018-0966-4.

[2] Gonzalez F.C.G., Cavacanti M.D.C.R., Nahas Ribeiro W., Mendonça M.B., Haddad A.N. A systematic review on rainfall thresholds for landslides occurrence. Heliyon, 10, 2024, https://doi.org/10.1016/j.heliyon.2023.e23247

[3] Fourth National Communication of Georgia Under the United Nations Framework Convention on Climate Change. Chapter 4.9 Geological Hazards in Georgia, Tbilisi, 2021, pp. 278-286.

[4] Varazanashvili O., Gaprindashvili G., Elizbarashvili E., Basilashvili, Ts., Amiranashvili A., Fuchs S. The First Natural Hazard Event Database for the Republic of Georgia (GeNHs). Catalog, 2023, 270 p. https://openscience.ge/server/api/core/bitstreams/12d32a4e-11dc-4b5c-8878-7c1bf091039d/content; DOI: 10.13140/RG.2.2.12474.57286

[5] Geological bulletins. 2015-2025, (in Georgian). https://nea.gov.ge/c/Departments/Geology

[6] Amiranashvili A.G. Special Features of Changeability of Daily Sum of Precipitation in Tbilisi in 1957-2006. Journal of the Georgian Geophysical Society, Issue B. Physics of Atmosphere, Ocean and Space Plasma, v.18B, Tbilisi, 2015, pp.81-91.

[7] Sakartvelos sametsniero-gamoqenebiti klimaturi tsnobari. Gamomtsemloba "Universali", ISBN 978-9941-26-798-7, Tbilisi, 2020, 307 gv.

[8] Amiranashvili A., Chelidze T., Svanadze D., Tsamalashvili T., Tvauri G. On the Representativeness of Data from Meteorological Stations in Georgia for Annual and Semi-Annual Sum of Atmospheric Precipitation Around of These Stations. International Scientific Conference „Natural Disasters in the 21st Century: Monitoring, Prevention, Mitigation". Proceedings, ISBN 978-9941-491-52-8, Tbilisi, Georgia, December 20-22, 2021. Publish House of Iv. Javakhishvili Tbilisi State University, Tbilisi, 2021, pp. 79 - 83. http://openlibrary.ge/bitstream/123456789/9566/1/20_Conf_ND_2021.pdf

[9] Kartvelishvili L., Tatishvili M., Amiranashvili A.,Megrelidze L., Kutaladze N. Weather, Climate and their Change Regularities for the Conditions of Georgia. Monograph, Publishing House "UNIVERSAL", Tbilisi 2023, 406 p., https://doi.org/10.52340/mng.9789941334658

[10] Amiranashvili A., Chelidze T., Svanadze D., Tsamalashvili T., Tvauri G. Study of the Relationship Between the Mean Annual Sum of Atmospheric Precipitation and Re-Activated and New Mudflow Cases in Georgia. Journal of the Georgian Geophysical Society, e-ISSN: 2667-9973, p-ISSN: 1512-1127, Physics of Solid Earth, Atmosphere, Ocean and Space Plasma, v. 26(1), 2023, pp. 19–29.

[11] Amiranashvili A., Brocca L., Chelidze T., Svanadze D., Tsamalashvili T., Varamashvili N. Analysis of the precipitation regime that triggered the landslide in Nergeeti (Imereti, Georgia) on February 7, 2024. Int. Sc. Conf. "Complex Geophysical Monitoring in Georgia: History, Modern Problems, Promoting Sustainable Development of the Country", Proceedings, ISBN 978-9941-36-272-9, Publish house of Iv. Javakhishvili Tbilisi State University, Tbilisi, Georgia, October 17-19, 2024, pp. 155 – 158. http://dspace.gela.org.ge/bitstream/123456789/10619/1/39_MM-180.pdf

[12] Amiranashvili A., Chelidze T., Svanadze D., Tsamalashvili T., Varamashvili N. About the Representativeness of Data from Meteorological Stations in Georgia for Monthly Sum of Atmospheric Precipitation Around of These Stations. Journal of the Georgian Geophysical Society, e-ISSN: 2667-9973, p-ISSN: 1512-1127, Physics of Solid Earth, Atmosphere, Ocean and Space Plasma, v. 27(1), 2024, pp. 52–57. https://ggs.openjournals.ge/index.php/GGS/article/view/7983

[13] Amiranashvili A.G., Brocca L., Chelidze T.L., Svanadze D.T., Tsamalashvili T.N., Varamashvili N.D. Statistical Analysis of Annual and Semi-Annual Sum of Atmospheric Precipitation Data for 59 Municipalities (11 Regions) of Georgia with Landslide Hazard Zones from 2015 to 2024. Journal of the Georgian Geophysical Society, e-ISSN: 2667-9973, p-ISSN: 1512-1127 Physics of Solid Earth, Atmosphere, Ocean and Space Plasma, v.28(1), 2025, pp. 50 - 63. https://ggs.openjournals.ge/index.php/GGS/article/view/9249

[14] Amiranashvili A., Brocca L., Chelidze T., Kiria T., Svanadze D., Tsamalashvili T., Varamashvili N. Statistical Analysis of the Relationship Between Monthly and Cumulative Multi-Month Sums of Precipitation with the Number of Landslides in the Regions of Georgia. Transactions of Mikheil Nodia Institute of Geophysics, ISSN 1512-1135, vol. LXXVIII, Publish House of Ivane Javakhishvili Tbilisi State University, Tbilisi, 2025, pp. 49-66. http://dspace.gela.org.ge/bitstream/123456789/10809/1/7_Tr_IG_78_2025.pdf

[15] Amiranashvili A., Brocca L., Chelidze T., Svanadze D., Tsamalashvili T., Varamashvili N. Statistical Analysis of the Number of Damaging Landslides in Municipalities and Regions of Georgia and their Relationship with Atmospheric Precipitation in 2015-2024. Reliability: Theory and Applications, ISSN 1932-2321, Volume 20, Special Issue No. 9 (87), November 2025, pp. 255-264. https://doi.org/10.24412/1932-2321-2025-987-255-264

[16] Amiranashvili A., Brocca L., Chelidze T., Kiria T., Svanadze D., Tsamalashvili T., Varamashvili N. Intra-Annual Distribution of Landslide Recurrence in Georgia and its Relationship with Monthly and Cumulative Multi-Month Sums of Precipitation. Journal of the Georgian Geophysical Society, e-ISSN: 2667-9973, p-ISSN: 1512-1127, Physics of Solid Earth, Atmosphere, Ocean and Space Plasma, v.28(2), 2025, pp. 25-30. https://ggs.openjournals.ge/index.php/GGS/article/view/10453

[17] Amiranashvili A., Brocca L., Chelidze T., Kiria T., Svanadze D., Tsamalashvili T., Varamashvili N. Assessment of the Relationship Between Daily and Total Multi-Day Precipitation Sums and Landslide Activation in the Regions of Georgia. Journal of the Georgian Geophysical Society, e-ISSN: 2667-9973, p-ISSN: 1512-1127, Physics of Solid Earth, Atmosphere, Ocean and Space Plasma, v.29(1), 2026, pp. 27-49.

[18] Amiranashvili A., Brocca L., Chelidze T., Kiria T., Svanadze D., Tsamalashvili T., Varamashvili N. Peculiarities of Intra-Annual Distribution of Landslide Recurrence in Adjara and Guria Regions (Western Georgia) and in Eastern Georgia and their Relationship with Monthly Sums of Precipitation. Journal of the Georgian Geophysical Society, e-ISSN: 2667-9973, p-ISSN: 1512-1127, Physics of Solid Earth, Atmosphere, Ocean and Space Plasma, v.29(1), 2026, pp. 60-68.

[19] Amiranashvili A., Chelidze T., Svanadze D., Tsamalashvili T., Tvauri G. Comparison of Data from Ground-Based and Satellite Measurements of the Monthly Sum of Atmospheric Precipitation on the Example of Tbilisi City in 2001-2020. Int. Conf. of Young Scientists "Modern Problems of Earth Sciences". Proceedings, ISBN 978-9941-36-044-2, Publish House of Iv. Javakhishvili Tbilisi State University, Tbilisi, November 21-22, 2022, pp. 154-158. http://openlibrary.ge/bitstream/123456789/10251/1/37_YSC_2022.pdf

[20] Chelidze T., Amiranashvili A., Svanadze D., Tsamalashvili T., Tvauri G. Terrestrial and Satellite-Based Assessment of Rainfall Triggered Landslides Activity in Georgia, Caucasus. Bull. Georg. Nat. Acad. Sci., vol. 17, no. 2, 71-77, 2023, http://science.org.ge/bnas/vol-17-2.html

[21] Amiranashvili A., Chelidze T., Svanadze D., Tsamalashvili T., Varamashvili N. Comparison of Satellite and Ground-Based Data on Semi-Annual and Annual Sum of Atmospheric Precipitation for 26 Points in Georgia in 2001-2020. Int. Sc. Conf. "Complex Geophysical Monitoring in Georgia: History, Modern Problems, Promoting Sustainable Development of the Country", Proceedings, ISBN 978-9941-36-272-9, Publish House of Iv. Javakhishvili Tbilisi State University, Tbilisi, Georgia, October 17-19, 2024, pp. 159 – 163. http://www.openlibrary.ge/bitstream/123456789/10618/1/40_MM-180.pdf

[22] Banetashvili V., Gelovani G., Grebentsova A., Javakhishvili N., Iobadze K., Mitin M., Saginashvili N., Samkharadze I., Khurtsidze G., Tsereteli A., Tskhvediashvili G., Chkhaidze B. Some Examples of Strong Precipitation in Eastern Georgia According to the Data of Radar Surveillance of 2015. Trans.of Mikheil Nodia Institute of Geophysics, ISSN 1512-1135, v. 66, Tbilisi, 2016, pp. 75-83, (in Russian).

[23] Amiranashvili A., Kereselidze Z., Mitin M., Khvedelidze I., Chikhladze V. Alarming Factors of the Microclimate of the Vere River Valley and their Influence on the Floods Intensity. Trans. of Mikheil Nodia Institute of Geophysics, ISSN 1512-1135, v. 69, Tbilisi, 2018, pp. 204-218, (in Georgian).

[24] Mitin M., Khvedelidze I. Radar Characteristics of Rain Cloud wich Caused Landslide into Akhaldaba and Catastrophic Flood in Tbilisi on June 13-14, 2015. Int. Sc. Conf. „Natural Disasters in Georgia: Monitoring, Prevention, Mitigation", Proc., ISBN 978-9941-13-899-7, pp. 167-171, Tbilisi, Georgia, December 12-14, 2019

[25] Amiranashvili A., Chelidze T., Svanadze D., Tsamalashvili T., Tvauri G. Abnormal Precipitation before the Landslide in Akhaldaba (A Suburb of Tbilisi, Georgia) on June 13, 2015 according to Radar Measurements. Journal of the Georgian Geophysical Society, e-ISSN: 2667-9973, p-ISSN: 1512-1127, Physics of Solid Earth, Atmosphere, Ocean and Space Plasma, v. 26(1), 2023, pp. 30–41.

[26] Chelidze T., Kiria T., Amiranashvili A., Svanadze D., Tsamalashvili T., Varamashvili N. Landslide Hazard Maps of Georgia Using Machine Learning Approach. Bulletin of the National Academy of Sciences of Georgia, ISSN: 0132 - 1447, vol. 20(194), no. 2, 2026, pp. 23-29. http://science.org.ge/bnas/t20-n2/03_Chelidze_Geophysics.pdf

[27] Amiranashvili A., Chikhladze V., Dzodzuashvili U., Ghlonti N., Sauri I., Telia Sh., Tsintsadze T. Weather Modification in Georgia: Past, Present, Prospects for Development. International Scientific Conference "Natural Disasters in Georgia: Monitoring, Prevention, Mitigation". Proceedings, ISBN 978-9941-13-899-7, Publish House of Iv. Javakhishvili Tbilisi State University, December 12-14, Tbilisi, 2019, pp. 216-222, http://dspace.gela.org.ge/handle/123456789/8613

[28] Selex ES GmbH · Gematronik Weather Radar Systems. Rainbow®5 User Guide, 464 p., www. gematronik.com

[29] Avlokhashvili Kh., Banetashvili V., Gelovani G., Javakhishvili N., Kaishauri M., Mitin M., Samkharadze I., Tskhvediashvili G., Chargazia Kh., Khurtsidze G. Products of Meteorological Radar «METEOR 735CDP10». Trans. of Mikheil Nodia Institute of Geophysics, ISSN 1512-1135, Tb., 2016, vol. 66, pp. 60-65, (in Russian).

[30] Hinkle D. E., Wiersma W., Jurs S. G. Applied Statistics for the Behavioral Sciences. Boston, MA, Houghton Mifflin Company, ISBN: 0618124055; 9780618124053, 2003, 756 p.

ახალდაბაში (თბილისის გარეუბანი, საქართველო) მეწყრული პროცესების რეტროსპექტული ანალიზი, 2015 წლის 13-14 ივნისი

ა. ამირანაშვილი, თ. ჭელიძე, თ. ქირია,
დ. სვანაძე , თ. წამალაშვილი, ნ. ვარამაშვილი

რეზიუმე

სტატიაში წარმოდგენილია 2015 წლის 13-14 ივნისს ახალდაბის რაიონში (თბილისის გარეუბანი, საქართველო) მომხდარი მცირე მეწყერების სერიამდე ნალექების ინტენსივობის რადიოლოკაციური გაზომვების ანალიზის შედეგები. კერძოდ, მიღებული იქნა შემდეგი შედეგები. 2015 წლის 13 ივნისის 20:49 საათიდან 23:58 საათამდე ღრუბლის მაქსიმალური რადიოლოკაციური არეკვლის ზონაში კუმულაციური ნალექების დროითი სვლა მეხუთე ხარისხის პოლინომის ფორმას ატარებს. 23:58 საათისთვის კუმულაციური ნალექების რაოდენობა 402.8 მმ-ს შეადგენდა. მცირე მეწყერების დაგროვილი რაოდენობის დროითი სვლა 2015 წლის 13 ივნისის 22:30 საათიდან 2015 წლის 14 ივნისის 01:00 საათამდე მესამე ხარისხის პოლინომის ფორმას ატარებს. 1:00 საათისთვის მეწყერების რაოდენობა 98 იყო.
მიღებულია მეწყერების დაგროვილი ჯამის დამოკიდებულება დაგროვილი ნალექების რაოდენობაზე ერთსაათიანი წინსწრები დროით, რომელსაც მესამე ხარისხის პოლინომის ფორმა აქვს. მეწყერების რაოდენობის სწრაფი ზრდა შეინიშნება დაგროვილი ნალექების ზრდასთან ერთად (ერთსაათიანი წინსწრები დროით).
ეს კვლევა კიდევ ერთხელ აჩვენებს, რომ ნალექების ინტენსივობის რადიოლოკაციური გაზომვები შეიძლება ეფექტური ინსტრუმენტი იყოს მეწყერების წარმოქმნაში ნალექების როლის შესასწავლად, ასევე მათი გააქტიურების მოკლევადიანი პროგნოზირებისთვის, განსაკუთრებით იმ ადგილებში, სადაც მიწისზედა ნალექების გაზომვები არ არის ხელმისაწვდომი.

საკვანძო სიტყვები: ატმოსფერული ნალექები, რადიოლოკაციური დაკვირვებები, მეწყერები.

Ретроспективный анализ оползневых процессов в Ахалдабе (пригород Тбилиси, Грузия) 13-14 июня 2015 года

А. Амиранашвили, Т. Челидзе, Т. Кириа,
Д. Сванадзе , Т. Цамалашвили, Н. Варамашвили

Резюме

Представлены результаты анализа радиолокационных измерений интенсивности осадков, предшествующих серии небольших оползней в районе Ахалдаба (пригород Тбилиси, Грузия) 13-14 июня 2015 г. В частности, получены следующие результаты. Временной ход накопленной суммы осадков в зоне максимальной радиолокационной отражаемости облака с 20:49 по 23:58

час 13 июня 2015 имеет вид полинома пятой степени. Накопленная сумма осадков к 23:58 час состаляла 402.8 мм. Временной ход накопленной суммы количества небольших оползней с 22:30 час 13 июня 2015 по 01:00 час 14 июня 2015 имеет вид полинома третьей степени. Количество оползней к 01:00 час час состаляло 98.
Получена зависимость накопленной суммы оползней от накопленной суммы осадков с опережением в один час, имеющий вид полинома третьей степени. Отмечается быстрое увеличение количества оползней с ростом накопленной суммы осадков (с опережением в один час).
Данное исследование еще раз продемонстрировало, что радиолокационные измерения интенсивности осадков могут быть эффективным инструментом для изучения роли осадков в возникновении оползней, а также для краткосрочного прогнозирования их активиации, особенно в районах, где наземные измерения осадков недоступны.

Ключевые слова: атмосферные осадки, радиолокационные наблюдения, оползни.

Journal of the Georgian Geophysical Society, e-ISSN: 2667-9973, p-ISSN: 1512-1127
Physics of Solid Earth, Atmosphere, Ocean and Space Plasma, v. 29(1), 2026, pp. 60 - 68

Peculiarities of Intra-Annual Distribution of Landslide Recurrence in Adjara and Guria Regions (Western Georgia) and in Eastern Georgia and their Relationship with Monthly Sums of Precipitation

[1]Avtandil G. Amiranashvili, [2]Luca Brocca, [1]Tamaz L. Chelidze,
[1]Tengiz V. Kiria, [1] David T. Svanadze, [3] Tamar N. Tsamalashvili,
[1] Nodar D. Varamashvili

[1]M. Nodia Institute of Geophysics of I. Javakhishvili Tbilisi State University, Tbilisi, Georgia
[2]Research Institute for Geo-Hydrological Protection, Perugia, Italy
[3]A. Janelidze Geological Institute of I. Javakhishvili Tbilisi State University, Tbilisi, Georgia
avtandilamiranashvili@gmail.com

ABSTRACT

Correlation and regression relationships between the intra-annual distribution (%) of the relative number of landslides and the relative precipitation amounts in the month of the landslide occurrence were studied for the regions of Adjara and Guria (Georgia), and Eastern Georgia. Specifically, it was found that the intra-annual distribution of landslides across the studied territories of Georgia is quite uneven. The highest relative number of landslides in Adjara and Guria occurs in October (18.7%), and the lowest in August (3.4%). The highest relative number of landslides in Eastern Georgia occurs in June (12.4%), and the lowest in July (6.4%). In Adjara and Guria in the linear approximation, correlation coefficient R between intra-annual distribution of the recurrence of landslides and mean sum of precipitation during the month of their activation is moderate (R=0.62), and in the case of approximation by a third-degree polynomial - index of correlation R' is high (R'=0.80). In Eastern Georgia between specified parameters mostly linear correlation is observed (R=0.60, moderate correlation). The level of nonlinear relationships does not go beyond moderate correlation.

Key words: *natural disasters, landslides, precipitation, correlation and regression analysis.*

Introduction

Landslides are a type of natural disaster that often cause significant environmental damage, lead to significant human casualties, and are widespread in many countries worldwide [1–4], including Georgia [5–13]. Landslide activation, along with many natural and anthropogenic factors, is also caused by prolonged, intense, or extreme precipitation [14-25]. Landslides have a seasonal pattern, which is often associated with seasonal variations in precipitation [26–30].

For example, in study [27] investigates the relationship between landslides and annual precipitation as well as selected monthly landslide distributions and their connection with weather anomalies in southern Lower Saxony, northern Hesse and the surroundings. Data about 394 landslide events between 1901 and 2016 was used. It was received that landslide distributions are correlated with precipitation records of a synthetic precipitation series as a representative for the study area. The annual landslide distribution shows an overall increasing number of events with alternating periods of low and high landslide activity. Correlation with the annual precipitation predominantly reveals a more frequent occurrence of landslides in humid years. The monthly landslide distribution between 1901 and 2016 shows a first accumulation of events in winter months (January–March: 31%) and a second one in summer months (June–August: 32%). In general, this monthly landslide distribution follows the annual course of precipitation. Particular monthly landslide distributions are apparent for periods of increased landslide activity which coincide with exceptional long-term winter and summer precipitation trends. In these periods the monthly distributions widely follow the annual precipitation courses. Overall, the results show that the precipitation is basically suitable for an explanation for the occurrence of landslide events. Whereas the annual precipitation is only partially meaningful for the annual landslide activity, the influence of exceptional seasonal precipitation is reflected in the monthly landslide distributions. The authors believe that the results provide a promising basis for more detailed analyses of the relationship between landslides and the precipitation in the study area [27].

In work [30] the correlation and regression relationship between the intra-annual distribution (%) of the number of landslides (LS) and the precipitation sums in the month when the landslide occurred and the accumulated sums for the month and 1...11 months before the landslide, P(1)…P(12), respectively, were studied. In particular, it was found that the intra annual distribution of landslides across the territory of Georgia is rather uneven. The highest number of landslides occurs in July and September (11.7% and 11.0%, respectively), while the lowest occur in January and November (5.3% and 5.6%, respectively). A moderate correlation is observed between the intra-annual distribution of LS with the intra-annual distributions of P(9)…(12). For the pairs LS – P(1) and LS – P(8), the correlation is low. For the remaining cases, the correlation is negligible. Linear regression equations between the parameters under study are presented.

This work is a continuation of the study [30]. Below are the results of analysis of peculiarities of intra-annual distribution of landslide recurrence in Adjara and Guria regions (Georgia) and in Eastern Georgia and their relationship with monthly sums of precipitation.

Study area, material and methods

Study area: Adjara and Guria regions (Georgia) and Eastern Georgia.

Data on the number of landslides (LS) with a known month of their activation were taken from the catalog [9] (Table 1). Adjara, Guria. Period of observation: 1968,2008-2010,2012-2022, Total LS Number – 145. Eastern Georgia. Period of observation: 1968,1973-1976,1983,1984,1988,1989,2001,2002,2004-2007,2011-2015,2017-2022, Total LS Number – 183. Table 1 also provides data on the number of landslides per year in different months (LS Numb/Year).

The data from the National Environmental Agency on monthly precipitation from 10 meteorological stations in Adjara and Guria, as well as from 27 meteorological stations in Eastern Georgia were used (Table 2). List of meteorological stations, their coordinates and locations in [24] are presented. Table 2 data on mean sum of precipitation during the months of landslides activation in Adjara, Guria and Eastern Georgia are presented.

In the proposed work the analysis of data is carried out with the use of the standard statistical analysis methods [31]. The following designations will be used below: R^2 – coefficient of determination; R – coefficient of linear correlation; R' - index of correlation for nonlinear equations.

The degree of correlation was determined in accordance with [31]: very high correlation ($0.9 \le R \le 1.0$); high correlation ($0.7 \le R < 0.9$); moderate correlation ($0.5 \le R < 0.7$); low correlation ($0.3 \le R < 0.5$); negligible correlation ($0 \le R < 0.3$).

Table 1. Data on landslides numbers in Adjara, Guria and Eastern Georgia by months according to [9].

Region	Adjara, Guria			Eastern Georgia		
Parameter	LS Number	Number of years	LS Numb/Year	LS Number	Number of years	LS Numb/Year
Jan	3	2	1.5	8	5	1.6
Feb	5	3	1.667	8	4	2
Mar	12	4	3	16	8	2
Apr	19	8	2.375	24	12	2
May	12	5	2.4	24	12	2
Jun	24	7	3.429	35	12	2.917
Jul	9	6	1.5	9	6	1.5
Aug	4	4	1	16	9	1.778
Sep	27	9	3	17	9	1.889
Oct	22	4	5.5	13	6	2.167
Nov	3	2	1.5	7	4	1.75
Dec	5	2	2.5	6	3	2
Jan-Dec	145		29.371	183		23.601

Table 2. Data on mean sum of precipitation during the months of landslides activation in Adjara, Guria and Eastern Georgia.

Parameter	Mean sum of precipitation during the months of LS activation, mm	
Region	Adjara, Guria	Eastern Georgia
Jan	186.2	25.3
Feb	128.6	36.6
Mar	157.1	80.8
Apr	67.5	78.3
May	58.6	122.3
Jun	93.7	117.8
Jul	150.5	59.6
Aug	109.8	54.9
Sep	352.3	65.8
Oct	389.1	46.6
Nov	130.7	47.4
Dec	214.4	49.9
Jan-Dec	2038.53	785.24

Results and discussion

Results in Table 3 and Fig. 1-4 are presented.

In Table 3 statistical characteristics of intra-annual distribution of landslides numbers in year and mean sum of precipitation during the months of landslides activation in Adjara, Guria and Eastern Georgia (data from Tables 1 and 2) are presented.

Table 3. Statistical characteristics of intra-annual distribution of landslides numbers in year and mean sum of precipitation during the months of landslides activation in Adjara, Guria and Eastern Georgia

Parameter	LS Numb/Year		Mean sum of precipitation during the months of LS activation, mm	
Region	Adjara, Guria	Eastern Georgia	Adjara, Guria	Eastern Georgia
Max	5.5	2.92	389.1	122.3
Min	1.0	1.5	58.6	25.3
Average	2.45	1.97	169.9	65.4
St Dev	1.22	0.36	104.1	29.9

Fig. 1 and 2 shows the intra-annual distribution of the recurrence of landslides and sum of precipitation during the month of their activation in Adjara, Guria and Eastern Georgia, normalized by their sum values (Table 3).

Values of LS Numb/Year and their normalized values change as follows (Tables 1, 3, Fig. 1,2). Adjara, Guria: from 1.0 (or 3.4 %) in August to 5.5 (or 18.7 %) in October with average value – 2.45; Eastern Georgia: from 1.5 (or 6.4 %) in July to 2.92 (or 12.4 %) in June with average value – 1.97.

Mean sum of precipitation during the months of LS activation and their normalized values change as follows (Tables 2, 3, Fig. 1,2). Adjara, Guria: from 58.6 mm (or 2.9 %) in May to 389.1 mm (or 19.1 %) in October with average value – 169.9 mm; Eastern Georgia: from 25.3 mm (or 3.2 %) in January to 122.3 mm (or 15.6 %) in May with average value – 65.4 mm.

As follows from Fig. 1 and 2 in general, despite the heterogeneity of the initial data (Tables 1 and 2), the intra-annual distribution of landslide recurrences in the studied regions of Georgia is to a certain extent synchronous with the intra-annual distribution of precipitation recurrences.

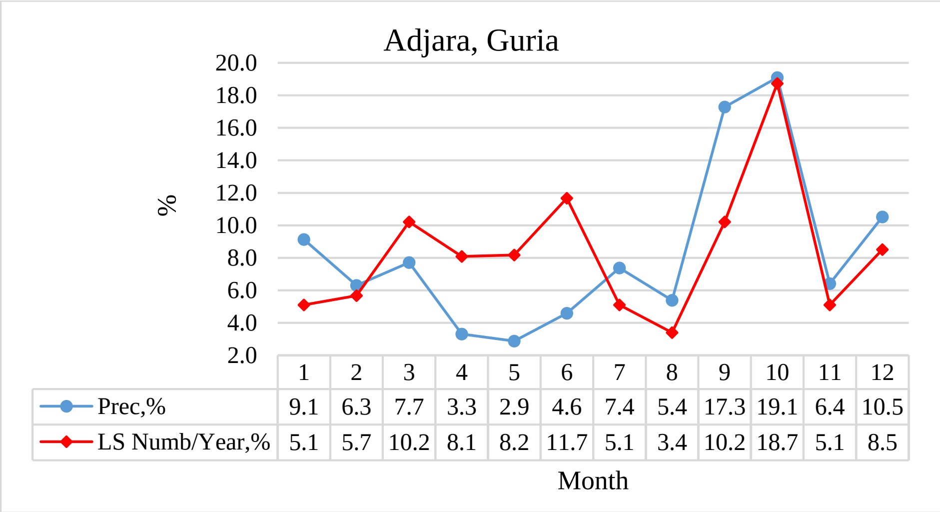

Fig. 1. Intra-annual distribution of the recurrence of landslides and sum of precipitation during the month of their activation in Adjara and Guria, normed on their average values.

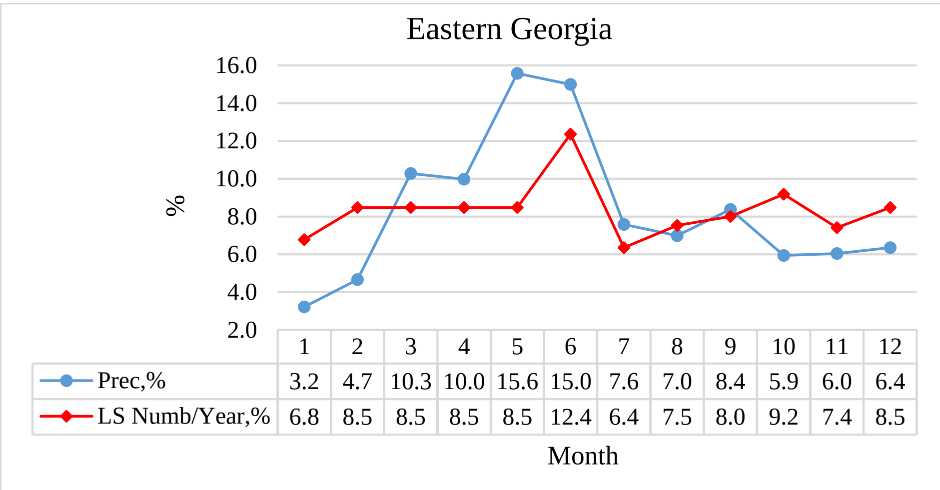

Fig. 2. Intra-annual distribution of the recurrence of landslides and sum of precipitation during the month of their activation in Eastern Georgia, normed on their average values.

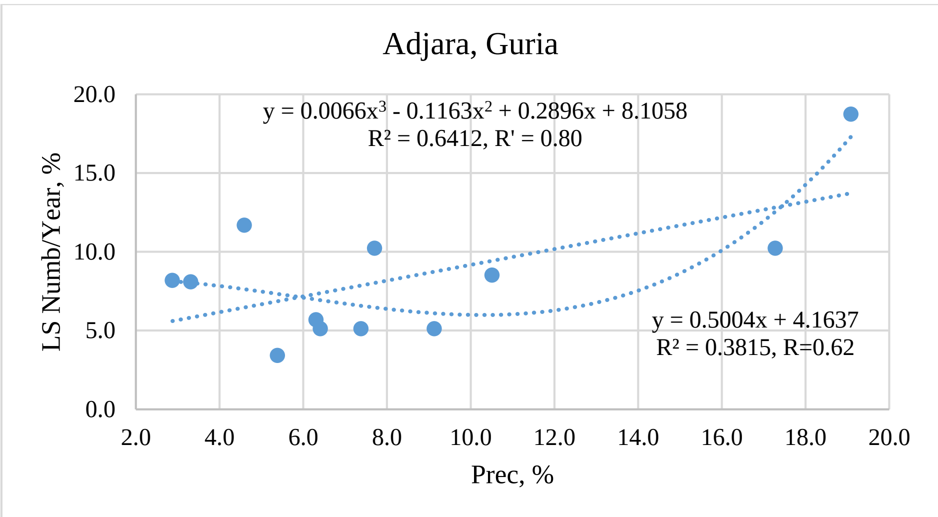

Fig. 3. Connection between intra-annual distribution of the recurrence of landslides and mean sum of precipitation during the month of their activation in Adjara and Guria.

At the same time, in Adjara and Guria (Fig. 3) in the linear approximation, correlation between intra-annual distribution of the recurrence of landslides and mean sum of precipitation during the month of their activation is moderate (R=0.62), and in the case of approximation by a third-degree polynomial - high (R'=0.80).

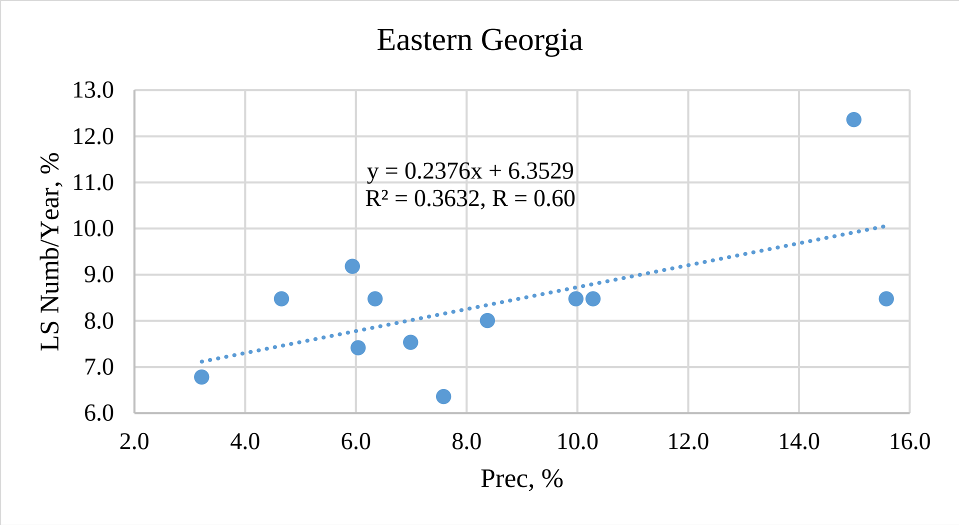

Fig. 4. Connection between intra-annual distribution of the recurrence of landslides and mean sum of precipitation during the month of their activation in Eastern Georgia.

In Eastern Georgia (Fig. 4) between specified parameters mostly linear correlation is observed (R=0.60, moderate correlation). The level of nonlinear relationships does not go beyond moderate correlation.

Our earlier study [30] showed that for Georgia as a whole the value of the linear correlation coefficient between the intra-annual distributions of landslides number and mean sum of precipitation during the month of their activation is 0.42 (low correlation), which is below the same value for Adjara, Guria (R=0.62, moderate correlation, Fig. 3) and for Eastern Georgia (R=0.60, moderate correlation, Fig. 4).

Note, that according to [32] mean monthly sum precipitation in Adjara, Guria and Eastern Georgia in 1961-1990 are respectively equal 155.7 and 61.3 mm. Comparison of these data with the data in Table 3 shows that mean monthly sum precipitation during the months of LS activation more than their average long-term values on 9.1 % in Adjara, Guria and on 6.9 % in Eastern Georgia.

Conclusion

In the future, as new data accumulates, we plan to refine the results obtained in this study. We also plan to conduct research assessing the role of various factors (including precipitation) in landslide activation in different seasons using artificial intelligence methods in both steady-state and dynamic modes.

Acknowledgments

This work was supported by Shota Rustaveli National Science Foundation of Georgia (SRNSFG), Grant number FR-23-5466, “Machine Learning Approach to the Landslide Activation Prediction in Georgia”.

References

[1] Froude M., Petley D. Global fatal landslide occurrence from 2004 to 2016. Nat. Hazards Earth Syst. Sci., 18, 2018, pp. 2161–2181.

[2] Li H., Samsudin N. A. A Systematic Review of Landslide Research in Urban Planning Worldwide. Nat Hazards, 121, 2025, pp. 6391–6411. https://doi.org/10.1007/s11069-024-07064-4

[3] Alcántara-Ayala I. Landslides in a Changing World. Landslides, 2025. https://doi.org/10.1007/s10346-024-02451-1

[4] Fidan S., Tanyaş H., Akbaş A., Lombardo L., Petley D.N., Görüm T. Understanding fatal landslides at global scales: a summary of topographic, climatic, and anthropogenic perspectives. Nat Hazards 120, 2024, pp. 6437–6455. https://doi.org/10.1007/s11069-024-06487-3

[5] Varazanashvili O., Tsereteli N., Amiranashvili A., Tsereteli E., Elizbarashvili E., Dolidze J., Qaldani L., Saluqvadze M., Adamia Sh., Arevadze N., Gventcadze A. Vulnerability, hazards and multiple risk assessment for Georgia. Natural Hazards, Vol. 64, Number 3, 2012, pp. 2021-2056. DOI: 10.1007/s11069-012-0374-3, http://www.springerlink.com/content/9311p18582143662/fulltext.pdf.

[6] Gaprindashvili G., Van Westen C.J. Generation of a national landslide hazard and risk map for the country of Georgia. Natural Hazards, 80(1), January 2016. DOI: 10.1007/s11069-015-1958-5

[7] Gaprindashvili, M., Tsereteli, E., Gaprindashvili, G., Kurtsikidze, O. Landslide and mudflow hazard assessment in Georgia. In: Bonali, F.L., Pasquaré Mariotto, F., Tsereteli, N. (eds) Building Knowledge for Geohazard Assessment and Management in the Caucasus and other Orogenic Regions. NATO Science for Peace and Security Series C: Environmental Security. Springer, Dordrecht, 2021. https://doi.org/10.1007/978-94-024-2046-3_14

[8] Fourth National Communication of Georgia Under the United Nations Framework Convention on Climate Change. Chapter 4.9 Geological Hazards in Georgia, Tbilisi, 2021, pp. 278-286.

[9] Varazanashvili O., Gaprindashvili G., Elizbarashvili E., Basilashvili, Ts., Amiranashvili A., Fuchs S. The First Natural Hazard Event Database for the Republic of Georgia (GeNHs). Catalog, 2023, 270 p. http://dspace.gela.org.ge/handle/123456789/10369; DOI: 10.13140/RG.2.2.12474.57286

[10] Geological bulletins. 2016-2025, (in Georgian). https://nea.gov.ge/c/Departments/Geology

[11] Amiranashvili A., Elizbarashvili E., Gaprindashvili G., Varazanashvili O., Fuchs S. Statistical analysis of parameterized landslide data in Georgia from 1900 to 2022. Reliability: Theory and Applications, ISSN 1932-2321, Special Issue № 6 (81), Part-2, Vol. 19, 2024, pp. 812 - 818. https://doi.org/10.24412/1932-2321-2024-681-812-818

[12] Amiranashvili A., Brocca L., Chelidze T., Svanadze D., Tsamalashvili T., Varamashvili N. Statistical analysis of the annual number of registered landslides and mudflows in Georgia in 1995-2024. 1st International Scientific Conference "Modern problems in Geophysics". Proceedings, ISBN 978-9941-36-434-1, ISSN 3088-4349, Tbilisi, Georgia, November 6-8, 2025. Publish House of Iv. Javakhishvili Tbilisi State University, Tbilisi, 2025, pp. 35-38. http://dspace.gela.org.ge/bitstream/123456789/10789/1/9_Conf_MPG_2025.pdf

[13] Amiranashvili A., Brocca L., Chelidze T., Svanadze D., Tsamalashvili T., Varamashvili N. Variability of the Annual Number of Registered Landslides and Mudflows in Georgia in 1995-2024 and their Expected Change up to 2030. Transactions of Mikheil Nodia Institute of Geophysics, ISSN 1512-1135, vol. LXXVIII, Publish House of Ivane Javakhishvili Tbilisi State University, Tbilisi, 2025, pp. 67-74.

[14] Segoni S., Piciullo L., Gariano S.L. A Review of the Recent Literature on Rainfall Thresholds for Landslide Occurrence. Landslides, 15, 2018, pp. 1483–1501, DOI: 10.1007/s10346-018-0966-4.

[15] Amiranashvili A., Chelidze T., Svanadze D., Tsamalashvili T., Tvauri G. Abnormal precipitation before the landslide in Akhaldaba (A Suburb of Tbilisi, Georgia) on June 13, 2015 according to radar measurements. Journal of the Georgian Geophysical Society, e-ISSN: 2667-9973, p-ISSN: 1512-1127, Physics of Solid Earth, Atmosphere, Ocean and Space Plasma, v. 26(1), 2023, pp. 30–41.

[16] Amiranashvili A., Chelidze T., Kiria T., Svanadze D., Tsamalashvili T., Varamashvili N. Retrospective Analysis of Landslides Processes in Akhaldaba (A Suburb of Tbilisi, Georgia) on June 13-14, 2015. Journal of the Georgian Geophysical Society, e-ISSN: 2667-9973, p-ISSN: 1512-1127, Physics of Solid Earth, Atmosphere, Ocean and Space Plasma, v.29(1), 2026, pp. 50-59.

[17] Amiranashvili A., Brocca L., Chelidze T., Svanadze D., Tsamalashvili T., Varamashvili N. Analysis of the precipitation regime that triggered the landslide in Nergeeti (Imereti, Georgia) on February 7, 2024. Int. Sc. Conf. "Complex Geophysical Monitoring in Georgia: History, Modern Problems, Promoting Sustainable Development of the Country", Proceedings, ISBN 978-9941-36-272-9, Publish house of Iv. Javakhishvili Tbilisi State University, Tbilisi, Georgia, October 17-19, 2024, pp. 155 – 158. http://dspace.gela.org.ge/bitstream/123456789/10619/1/39_MM-180.pdf

[18] Beglarashvili N., Elizbarashvili I., Jamrishvili N., Janelidze I., Pipia M., Tavidashvili Kh. Analysis of heavy precipitation in the Adigeni and Chokhatauri municipaliities on July 21, 2025 based on satellite measurements. 1st International Scientific Conference "Modern problems in Geophysics". Proceedings, ISBN 978-9941-36-434-1, ISSN 3088-4349, Tbilisi, Georgia, November 6-8, 2025. Publish House of Iv. Javakhishvili Tbilisi State University, Tbilisi, 2025, pp. 125-128.

[19] Chelidze T., Amiranashvili A., Svanadze D., Tsamalashvili T., Tvauri G. Terrestrial and satellite-based assessment of rainfall triggered landslides activity in Georgia, Caucasus. Bull. Georg. Nat. Acad. Sci., vol. 17, no. 2, 71-77, 2023, http://science.org.ge/bnas/vol-17-2.html

[20] Chelidze, T., Tsamalashvili, T., Fandoeva, M. Mass-movement stationary hazard maps of Georgia including precipitation triggering effect: fuzzy logic approach. Bull. Georg. Nat. Acad. Sci., vol. 16, no. 2, 56-63, 2022, http://science.org.ge/bnas/t16-n2/07_Chelidze_Geophysics.pdf

[21] Amiranashvili A., Chelidze T., Svanadze D., Tsamalashvili T., Tvauri G. Some results of a study of the relationship between the mean annual sum of atmospheric precipitation and re-activated and new landslide cases in Georgia taking into account of climate change. Journal of the Georgian Geophysical Society, e-ISSN: 2667-9973, p-ISSN: 1512-1127, Physics of Solid Earth, Atmosphere, Ocean and Space Plasma, v. 25(2), 2022, pp. 38–48. https://openjournals.ge/index.php/GGS/article/view/5959, DOI: https://doi.org/10.48614/ggs2520225959

[22] Amiranashvili A., Chelidze T., Svanadze D., Tsamalashvili T., Tvauri G. Study of the relationship between the mean annual sum of atmospheric precipitation and re-activated and new mudflow cases in Georgia. Journal of the Georgian Geophysical Society, e-ISSN: 2667-9973, p-ISSN: 1512-1127, Physics of Solid Earth, Atmosphere, Ocean and Space Plasma, v. 26(1), 2023, pp. 19–29. https://ggs.openjournals.ge/index.php/GGS/article/view/6958;
DOI: https://doi.org/10.48614/ggs2620236958

[23] Amiranashvili A., Brocca L., Chelidze T., Svanadze D., Tsamalashvili T., Varamashvili N. Statistical analysis of the number of damaging landslides in municipalities and regions of Georgia and their relationship with atmospheric precipitation in 2015-2024. Reliability: Theory and Applications, ISSN 1932-2321, Special Issue No. 9 (87), Volume 20, November 2025, pp. 255-264.

[24] Amiranashvili A., Brocca L., Chelidze T., Kiria T., Svanadze D., Tsamalashvili T., Varamashvili N. Statistical Analysis of the Relationship Between Monthly and Cumulative Multi-Month Sums of Precipitation with the Number of Landslides in the Regions of Georgia. Transactions of Mikheil Nodia Institute of Geophysics, ISSN 1512-1135, vol. LXXVIII, Publish House of Ivane Javakhishvili Tbilisi State University, Tbilisi, 2025, pp. 49-66.

[25] Amiranashvili A., Brocca L., Chelidze T., Kiria T., Svanadze D., Tsamalashvili T., Varamashvili N. Assessment of the Relationship Between Daily and Total Multi-Day Precipitation Sums and Landslide Activation in the Regions of Georgia. Journal of the Georgian Geophysical Society, e-ISSN: 2667-9973, p-ISSN: 1512-1127, Physics of Solid Earth, Atmosphere, Ocean and Space Plasma, v.29(1), 2026, pp. 27-49.

[26] Kirschbaum D., Stanley T., Zhou Y. Spatial and temporal analysis of a global landslide catalog. Geomorphology, 249, 2015, pp. 4–15. https:// doi.org/10.1016/j.geomorph.2015.03.016

[27] Rupp S., Wohlers A., Damm B. Long-term relationship between landslide occurrences and precipitation in southern Lower Saxony and northern Hesse. Zeitschrift für Geomorphologie, 61(4), 2018, pp.327-338.

[28] Luna L. V., Korup O. Seasonal landslide activity lags annual precipitation pattern in the Pacific Northwest. Geophysical Research Letters, 49, 2022, e2022GL098506. https://doi. org/10.1029/2022GL098506

[29] Dandridge C., Stanley T.A., Kirschbaum D.B., Lakshmi V. Spatial and Temporal Analysis of Global Landslide Reporting Using a Decade of the Global Landslide Catalog. Sustainability 15, 2023, 3323. https://doi.org/10.3390/su15043323
[30] Amiranashvili A., Brocca L., Chelidze T., Kiria T., Svanadze D., Tsamalashvili T., Varamashvili N. Intra-Annual Distribution of Landslide Recurrence in Georgia and its Relationship with Monthly and Cumulative Multi-Month Sums of Precipitation. Journal of the Georgian Geophysical Society, e-ISSN: 2667-9973, p-ISSN: 1512-1127, Physics of Solid Earth, Atmosphere, Ocean and Space Plasma, v.28(2), 2025, pp. 25-30. https://ggs.openjournals.ge/index.php/GGS/article/view/10453
[31] Hinkle D. E., Wiersma W., Jurs S. G. Applied statistics for the behavioral sciences. Boston, MA, Houghton Mifflin Company, ISBN: 0618124055; 9780618124053, 2003, 756 p.
[32] Sakartvelos sametsniero-gamoqenebiti klimaturi tsnobari. Gamomtsemloba "Universali", ISBN 978-9941-26-798-7, Tbilisi, 2020, 307 gv.

მეწყრის განმეორების შიდა წლიური განაწილების თავისებურებები აჭარისა და გურიის რეგიონებში (დასავლეთ საქართველო) და აღმოსავლეთ საქართველოში და მათი კავშირი ყოველთვიურ ნალექების რაოდენობასთან

ა. ამირანაშვილი, ლ. ბროკა, თ. ჭელიძე, თ. ქირია,
დ. სვანაძე , თ. წამალაშვილი, ნ. ვარამაშვილი

რეზიუმე

აჭარის, გურიისა და აღმოსავლეთ საქართველოს რეგიონებისთვის შესწავლილი იქნა მეწყერების ფარდობითი რაოდენობის შიდაწლიურ განაწილებასა (%) და მეწყრული თვის განმავლობაში მოსული ნალექების ფარდობით რაოდენობას შორის კორელაციური და რეგრესიული კავშირები. კერძოდ, დადგინდა, რომ საქართველოს შესწავლილ ტერიტორიებზე მეწყერების წლიური განაწილება საკმაოდ არათანაბარია. აჭარასა და გურიაში მეწყერების ყველაზე მაღალი ფარდობითი რაოდენობა ოქტომბერში (18.7%), ხოლო ყველაზე დაბალი - აგვისტოში (3.4%) ფიქსირდება. აღმოსავლეთ საქართველოში მეწყერების ყველაზე მაღალი ფარდობითი რაოდენობა ივნისში (12.4%), ხოლო ყველაზე დაბალი - ივლისში (6.4%) ფიქსირდება. აჭარასა და გურიაში, მეწყერის განმეორებადობის წლიური განაწილებისა და მათი გააქტიურების თვის საშუალო ნალექებს შორის კორელაციის კოეფიციენტი R ზომიერია (R=0.62) წრფივი მიახლოებით, ხოლო მესამე ხარისხის პოლინომური მიახლოებით კორელაციის ინდექსი R' მაღალია (R'=0.80). აღმოსავლეთ საქართველოში ამ პარამეტრებს შორის უპირატესად წრფივი კორელაცია შეინიშნება (R=0.60, ზომიერი კორელაცია). არაწრფივი დამოკიდებულებების დონე არ აღემატება ზომიერ კორელაციას.

საკვანძო სიტყვები: სტიქიური უბედურება, მეწყერი, ნალექი, კორელაციური და რეგრესიული ანალიზი.

Особенности внутригодового распределения частоты оползней в регионах Аджария и Гурия (Западная Грузия) и в Восточной Грузии и их связь с месячными суммами осадков

А. Амиранашвили, Л. Брокка, Т. Челидзе, Т. Кириа, Д. Сванадзе, Т. Цамалашвили, Н. Варамашвили

Резюме

Для регионов Аджарии и Гурии (Грузия) и Восточной Грузии были изучены корреляционные и регрессионные зависимости между внутригодовым распределением (%) относительного числа оползней и относительным количеством осадков в месяце возникновения оползня. В частности, было установлено, что внутригодовое распределение оползней на исследуемых территориях Грузии довольно неравномерно. Наибольшее относительное число оползней в Аджарии и Гурии приходится на октябрь (18.7%), а наименьшее — на август (3.4%). Наибольшее относительное число оползней в Восточной Грузии приходится на июнь (12.4%), а наименьшее — на июль (6.4%). В Аджарии и Гурии при линейной аппроксимации коэффициент корреляции R между внутригодовым распределением повторяемости оползней и средней суммой осадков за месяц их активации является умеренным (R=0,62), а в случае аппроксимации полиномом третьей степени – индекс корреляции R' высок (R'=0,80). В Восточной Грузии между указанными параметрами в основном наблюдается линейная корреляция (R=0.60, умеренная корреляция). Уровень нелинейных зависимостей не выходит за рамки умеренной корреляции.

Ключевые слова: стихийные бедствия, оползни, атмосферные осадки, корреляционный и регрессионный анализ.

Journal of the Georgian Geophysical Society, e-ISSN: 2667-9973, p-ISSN: 1512-1127
Physics of Solid Earth, Atmosphere, Ocean and Space Plasma, v. 29(1), 2026, pp. 69 - 73

Comparing Satellite and Weather Station Wind Speed Data: A Case Study of Telavi city (Kakheti, Georgia)

[1]Mariam K. Modrekelidze, [1]Lamzira D. Laghidze, [2] Giorgi O. Ghambashidze

[1]Ivane Javakhishvili Tbilisi State University
[2]Agricultural University of Georgia

Mariam.modrekelidze643@ens.tsu.edu.ge

ABSTRACT

In modern times, the use of satellite-derived information is becoming increasingly vital in both the operations of meteorological services and scientific research. This information plays a crucial role in evaluating air temperature, precipitation, drought monitoring, food security, and weather-related issues, as well as in making data-driven decisions. Studying ongoing processes via artificial satellites provides the opportunity to obtain unique data within a short timeframe.
This study assesses the potential risk of making incorrect decisions when utilizing satellite-derived meteorological data, using the case of Telavi (in particular, wind speed).

Key Words: *climate change, Kakheti, air temperature, wind speed, satellite data.*

Introduction

Satellite data plays a crucial role in assessing climate risks by providing accurate and timely information on environmental conditions. This data facilitates the monitoring of changes, forecasting of extreme weather events, and evaluation of climate change impacts across various regions. The primary advantage of using satellite data lies in its ability to cover vast territories, offer high-resolution satellite imagery to users, and provide near real-time updates, making it an essential tool for effective climate risk management. Since the early 1980s, polar-orbiting and geostationary satellites have been providing various types of data, including:

- Land surface temperature;
- Precipitation;
- Air temperature;
- Spatial distribution of drought intensity;
- Vegetation characteristics, their condition, etc. [1]

Study area, Materials and Methods

This paper compares the wind speed data of Telavi, one of Georgia's municipalities, with satellite-derived information spanning the years 2000-2016. TerraClimate data (derived from NASA's Terra satellite MODIS sensor) is utilized for this data comparison. Within the territory of Georgia, the combined application of satellite information and GIS methods allows for a more precise comparison and evaluation of the consistency between the country's meteorological stations and satellite data. Ultimately, this obtained satellite information can be utilized for forecasting purposes [https://www.climatologylab.org/terraclimate.html].

Modern meteorological stations integrate multiple sensors to provide a comprehensive view of environmental conditions. As for meteorological satellites, they are used to observe Earth's atmospheric conditions from space, providing essential data for weather forecasting, climate change research, and environmental monitoring. Theoretically, satellites can monitor the environment at any point on Earth, at any time. Instead of directly measuring air temperature, they capture information across various wavelengths—such as infrared radiation from the Earth's surface—and then perform calculations to determine the temperature.

Terra is a NASA scientific research satellite. It investigates the connections between Earth's atmosphere, land, snow, ice, and ocean to better understand Earth's climate and climate change [https://terra.nasa.gov/]. MODIS stands for Moderate Resolution Imaging Spectroradiometer. It features numerous data products capable of measuring temperature, precipitation, land surface temperature, drought, phenology, and more.

Results

Wind speed data in Georgia is recorded by meteorological stations and observation posts across the country [2-13]. However, there are locations where meteorological stations are not installed due to various reasons. Consequently, satellite-derived information serves as an alternative option for measuring and verifying **wind speed**, capable of supplementing traditional methods. In Georgia, studying atmospheric processes using artificial satellites provides an opportunity to obtain unique data within a short timeframe; therefore, it is crucial to utilize all available information that enables more accurate and reliable forecasts of weather and natural disasters.

An integrated approach provides a large-scale, consistent, and continuous picture of the atmospheric processes occurring on the Earth's surface. Regular observations ensure a continuous flow of data. Furthermore, long-term satellite series allow for the comprehensive study of climate trends.

Table 1. Telavi Wind Speed Regression Statistics, Terraclimate and Telavi meteorological in 2000-2016 years

Parameter	Multiple R	R Square	Adjusted R Square	Standard Error	Number of observations
Value	0.445335	0.198323	0.194355	0.229063	204 month

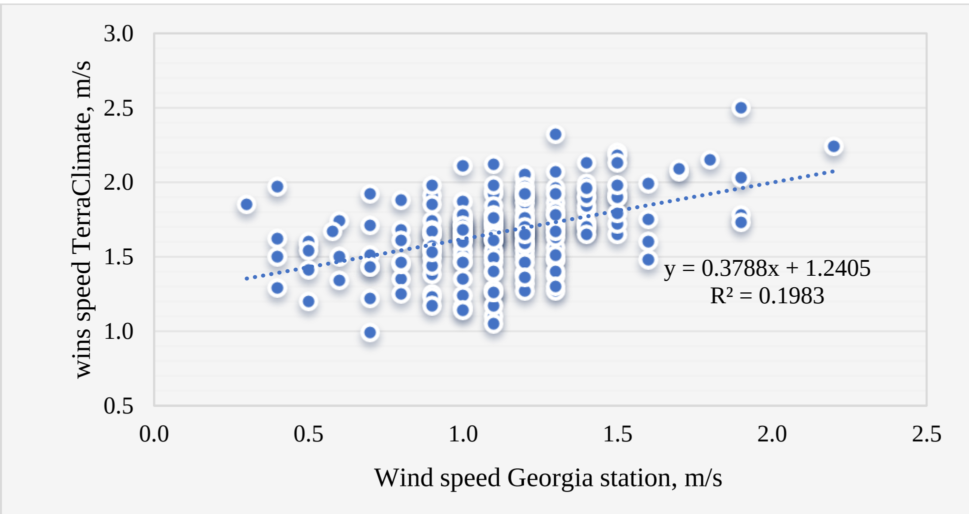

Fig. 1. Regression Statistics, Comparing Satellite and Weather Station Wind Speed Data: A Case Study of Telavi (2000-2016).

Validation of the monthly wind speed data from 2000-2016 reveals a moderate to low positive linear correlation [14] (R=0.445, Table 1, Fig. 1) between satellite estimations and ground-based station observations. The analysis yielded a Mean Bias Error (MBE) of +0.54 m/s and Root Mean Square Error (RMSE) of 0.615 m/s. The low correlation coefficient (R=0.445) can be primarily attributed to the spatial scale mismatch. While the satellite dataset represents a grid-averaged wind speed over a broad area, the ground station captures localized point, measurements heavily influenced by microtopography, surface roughness and local obstacles. Nevertheless, the low RMSE and small systematic positive Bias demonstrate that the overall magnitude of deviation remains within an acceptable range. Consequently, applying the linear regression correction allows for effective bias adjustment, making the satellite product a viable alternative for regional wind resource assessment where station data is absent.

Conclusion

Based on the provided regression analysis tables, we can conclude that there is a positive linear relationship between the TerraClimate data and the data from Georgian meteorological stations.

Wind is the most variable meteorological parameter. The spatial resolution of the TerraClimate is approximately 4 km. Although it can't provide accurate daily values, it can reflect seasonal trends or the general dynamics of windy periods. When ground-based observations are unavailable, satellite data serves as the sole source, despite its inherent errors. The average Bias for entire 17-year period (2000-2016) is 0.54. This indicates that the satellite overestimated wind speed by an average of 0.54 m/s compared to the measurements from Georgian stations.

Predicting global changes with high accuracy is essential for making prudent decisions related to environmental protection issues.

References

[1] Sivakumar M.V.K., Roy P.S., Harmsen K. Satellite Remote Sensing and GIS Applications in Agricultural Meteorology, Switzerald, 2004.

[2] Amiranashvili A.G., Chikhladze V.A., Gvasalia G.D., Loladze D.A. Statistical Characteristics of the Daily Max of Wind Speed in Kakheti in 2017-2019. Journal of the Georgian Geophysical Society, ISSN: 1512-1127, Physics of Solid Earth, Atmosphere, Ocean and Space Plasma, v. 23(1), 2020, pp. 73-86. DOI: https://doi.org/10.48614/ggs2320202655

[3] Amiranashvili A., Chikhladze V., Gvasalia G., Loladze D. Statistical Characteristics of the Daily Max of Wind Speed in Kakheti in the Days with and without Hail Processes in 2017-2019. Int. Sc. Conf. „Modern Problems of Ecology", Proc., ISSN 1512-1976, v. 7, Tbilisi-Telavi, Georgia, 26-28 September, 2020, pp. 197-201. http://www.dspace.gela.org.ge/bitstream/123456789/8808/1/Eco_2020_3.32.pdf

[4]Beglarashvili N., Chikhladze V., Janelidze I., Pipia M., Tsintsadze T. Strong Wind on the Territory of Georgia in 2014-2018. International Scientific Conference „Natural Disasters in the 21st Century: Monitoring, Prevention, Mitigation". Proceedings, ISBN 978-9941-491-52-8, Tbilisi, Georgia, December 20-22, 2021. Publish House of Iv. Javakhishvili Tbilisi State University, Tbilisi, 2021, pp. 19 - 22.

[5] Amiranashvili A., Jamrishvili N., Janelidze I., Pipia M., Tavidashvili Kh. Statistical Analysis of the Daily Wind Speed in Tbilisi in 1971-2016. Int. Conf. of Young Scientists "Modern Problems of Earth Sciences". Proceedings, ISBN 978-9941-36-044-2, Publish House of Iv. Javakhishvili Tbilisi State University, Tbilisi, November 21-22, 2022, pp. 159-163. http://openlibrary.ge/handle/123456789/10250

[6] Beglarashvili N., Pipia M., Jamrishvili N., Janelidze I. Some Results of the Analysis of Number of Days with Strong Wind in Various Regions of Georgia in 2019-2022. Georgian Geographical Journal, E-ISSN: 2667-9701, Vol.3 (2), 2023, 5 p. DOI: https://doi.org/10.52340/ggj.2023.03.02.05

[7] Beglarashvili N., Jamrishvili N., Janelidze I., Pipia M., Tavidashvili Kh., Tsintsadze T. Some Results of Statistical Analysis of the Daily Wind Speed in Tbilisi in 1971-2020. Int. Sc. Conf. "Geophysical Processes in the Earth and its Envelopes". Proceedings, ISBN 978-9941-36-147-0, Publish House of Iv. Javakhishvili Tbilisi State University, November 16-17, 2023, pp. 151-155. http://www.openlibrary.ge/handle/123456789/10423

[8] Elizbarashvili E., Varazanashvili O., Lagidze L., Pipia M., Chikhladze V. About Strong Winds in Kakheti Region. Int. Sc. Conf. "Geophysical Processes in the Earth and its Envelopes". Proceedings, ISBN 978-

9941-36-147-0, Publish House of Iv. Javakhishvili Tbilisi State University, November 16-17, 2023, pp. 156-160, (in Georgian). http://www.openlibrary.ge/handle/123456789/10424
[9] Kartvelishvili L., Tatishvili M., Amiranashvili A., Megrelidze L., Kutaladze N. Weather, Climate and their Change Regularities for the Conditions of Georgia. Monograph, Publishing House “UNIVERSAL”, ISBN: 978-9941-33-465-8, Tbilisi 2023, 406 p., https://doi.org/10.52340/mng.9789941334658
[10] Elizbarashvili E.Sh., Varazanashvili O.Sh., Amiranashvili A.G., Fuchs F., Basilashvili Ts.Z. Statistical Characteristics of Hurricane Winds over Georgia for the Period 1961–2022. European Geographical Studies, E-ISSN: 2413-7197, 10(1), 2023, pp. 8-18, DOI: 10.13187/egs.2023.1.8, https://egs.cherkasgu.press
[11] Amiranashvili A., Elizbarashvili E., Gaprindashvili G., Varazanashvili O., Fuchs S. Assessment of the Long-Term Risk of Dangerous Hurricanes on the Territory of Georgia Using Data from 1961 to 2022. "Reliability: Theory and Applications", ISSN 1932-2321, Special Issue № 6 (81), Part-2, Vol. 19, 2024, pp. 508 - 514. https://doi.org/10.24412/1932-2321-2024-681-508-514
[12] Aliyev V., Amiranashvili A., Pipia M., Varamashvili N. Wind Conditions at the Heydar Aliyev Baku and Shota Rustaveli Tbilisi International Airports in 2015–2024. Theory and Applications, ISSN 1932-2321, Volume 20, Special Issue No. 9 (87), November 2025, pp. 651-659. https://doi.org/10.24412/1932-2321-2025-987-651-659
[13] Elizbarashvili E.S., Varazanashvili O.S., Amiranashvili A.G., Pipia M.G. Long-term Trends in the Frequency and Intensity of Hurricane Winds over the Territory of Georgia in 1961–2022. Russ. Meteorol. Hydrol. 50, 2025, pp. 1061–1067. https://doi.org/10.3103/S1068373925120076
[14] Hinkle D. E., Wiersma W., Jurs S. G. Applied Statistics for the Behavioral Sciences. Boston, MA, Houghton Mifflin Company, ISBN: 0618124055; 9780618124053, 2003, 756 p.

ქარის სიჩქარის თანამგზავრული და მიწისზედა მეტეოროლოგიური მონაცემების შედარებითი ანალიზი ქ. თელავის მაგალითზე (კახეთი, საქართველო)

მ.მოდრეკელიძე., ლ.ლაღიძე., გ.ღამბაშიძე

რეზიუმე

თანამედროვე პირობებში, მეტეოროლოგიური სამსახურების საქმიანობაში და სამეცნიერო-კვლევით მუშაობაში, თანამგზავრებიდან მიღებული ინფორმაციის გამოყენებას სულ უფრო მეტი მნიშვნელობა ენიჭება. ეს ინფორმაცია მნიშვნელოვან როლს ასრულებს ჰაერის ტემპერატურის, ნალექებისა, გვალვის მონიტორინგის, სასურსათო უსაფრთხოების და ამინდთან დაკავშირებულ საკითხების შეფასებასა და მონაცემებზე დაფუძნებული გადაწყვეტილებების მიღებაში. მიმდინარე პროცესების ხელოვნური თანამგზავრების საშუალებით შესწავლა, მოკლე დროში უნიკალური ინფორმაციის მიღების შესაძლებლობას იძლევა.
მოცემული კვლევა ეხება თანამგზავრებიდან მიღებული მეტეოროლოგიური მონაცემების გამოყენებისას, არასწორი გადაწყვეტილებების პოტენციური რისკის შეფასებას თელავის მაგალითზე (კერძოდ, ქარის სიჩქარე).

საკვანძო სიტყვები: კლიმატის ცვლილება, კახეთი, ჰაერის ტემპერატურქარის, ქარის სიჩქარე, სატელიტური მონაცემები.

Сравнение спутниковых данных и данных метеостанции о скорости ветра: пример г. Телави (Кахети, Грузия)

М. Модрекелидзе, Л. Лагидзе, Г. Гамбашидзе

Резюме

В современную эпоху использование информации, полученной со спутников, приобретает все большее значение как в работе метеорологических служб, так и в научных исследованиях. Эта информация играет решающую роль в оценке температуры воздуха, осадков, мониторинге засухи, обеспечении продовольственной безопасности и решении погодных проблем, а также в принятии решений на основе данных. Изучение текущих процессов с помощью искусственных спутников предоставляет возможность получения уникальных данных в короткие сроки.
В данном исследовании на примере Телави оценивается потенциальный риск принятия неверных решений при использовании метеорологических данных, полученных со спутников (в частности, скорости ветра).

Ключевые слова: изменение климата, Кахетия, температура воздуха, скорость ветра, спутниковые данные.

Journal of the Georgian Geophysical Society, e-ISSN: 2667-9973, p-ISSN: 1512-1127
Physics of Solid Earth, Atmosphere, Ocean and Space Plasma, v.29 (1), 2026, pp. 74 – 84

Machine Learning and Hybrid Approaches in Weather and Climate

[1,2]Marika R. Tatishvili, [1,2] Ana M. Palavandishvili

[1] Institute of Hydrometeorology of Georgian Technical University, Tbilisi, Georgia
[2]Vakhushti Bagrationi Institute of Geography of the Ivane Javakhishvili Tbilisi State University, Tbilisi, Georgia

ABSTRACT

Climate change is one of the most significant global challenges that need to be managed Understanding of the natural environment is increasingly important to respond to the climate change negative impacts and anthropogenic pressures on finite natural resources, and their impacts on water, energy and food security, infrastructure, human health, natural hazards. The paper reviewed ML application in weather and acclimate, its further development and activities and achievements of ECMWF in creating and app]lying of ML/AI methods. This is also a major interdisciplinary challenge involving almost all scientific fields Artificial intelligence and machine learning (AI/ML) applications have recently widely expanded in all fields. ML can enhance our computations by adding components or replacing some parts of the process. This is what is called the 'hybrid' approach. Instead, ML can also fully replace the whole model, at a much lower computing cost. In addition, AI/ML opens some avenues in other activities we are involved in, such as flood forecasts, fire danger forecasts, monitoring of observations, managing the supercomputer, or enhancing user experience.

***Key words**: Big Data, Machin Learning, Neural Network, CEMS (Climate and Environmental Monitoring from Space, ECMWF's Artificial Intelligence Forecasting System (AIFS),Hybrid approach*

1. Introduction

Climate change is one of the most significant global challenges that need to be managed. To resolve any of the climate change related challenges, "it is essential to elicit and integrate knowledge across a range of systems, informing the design of solutions that take into account the complex and uncertain nature of the individual systems and their interrelationships" [20]. Many studies and researches are devoted to this problem [1-10]. The trends in data science and information technology supports the integration of various disciplines and research outcomes to represent a socio-environmental system holistically inform policy and decision-making processes, which can be referred as climate computing. Understanding of the natural environment is increasingly important to respond to the climate change negative impacts and anthropogenic pressures on finite natural resources, and their impacts on water, energy and food security, infrastructure, human health, natural hazards. This is also a major interdisciplinary challenge involving almost all scientific fields

In 2013, the UK government announced large-scale investment in Big Data infrastructure for science, particularly in the environmental sector starting funding for a program called CEMS (Climate and Environmental Monitoring from Space) [3,5,20,23]. This allowed for the creation of larger databases to cope with the upcoming Big Data revolution and to allow research partner organizations to work with more data and produce more results. With a specific focus on climate change and planetary monitoring, CEMS storage removed the need to download enormous data sets while reducing the cost of access. Along with Cloud data, this is now the standard globally for some of the world's top research institutes.

Environmental data comes from a wide variety of sources and this is increasingly rapidly with new innovations in data capture:

1. Large volumes of data are collected via remote sensing, typically from satellite sensing or aircraft-borne sensing devices, including an increasing use of drones. This includes passive sensing, such as photography or infrared imagery, and active sensing, e.g., RADAR/LIDAR. The increasing availability of open satellite data is a major trend in earth and environmental sciences. For example, the EU Copernicus program and the associated Sentinel missions, or NASA's Earth Observing System satellites, LandSat archive are regularly mined for data for a variety of applications

2. Other data are collected via earth monitoring systems, which consist of a range of sensor technologies measuring various physical entities. Namely weather stations and monitoring systems
3. Model output is also a significant generator of environmental data with results from previous model runs often stored for subsequent analysis

Machine Learning

Artificial intelligence and machine learning (AI/ML) applications have recently widely expanded in all fields. ML uses a lot of data to produce results, and ECMWF is all about data: to use a lot of data – tens of millions of weather observations per day – and we create a lot of data by producing weather analyses and forecasts at high resolution (Fig.1).

Traditionally, the physics-based methods are used for our computations in the Integrated Forecasting System (IFS). This is the case for numerical weather prediction (NWP), reanalysis of past weather, and atmospheric composition. All computations require large computing power to produce high-quality predictions, based on the accurate description of physical processes.

ML can enhance our computations by adding components or replacing some parts of the process. This is what we call the 'hybrid' approach. Instead, ML can also fully replace the whole model, at a much lower computing cost. In addition, AI/ML opens some avenues in other activities we are involved in, such as flood forecasts, fire danger forecasts, monitoring of observations, managing the supercomputer, or enhancing user experience.

Fig.1. Machine learning is well suited to weather forecasting due to the vast amounts of data that are used to determine the best possible initial conditions and to produce global forecasts [22].

Machine learning (ML) is the use of statistical algorithms that can learn from data and generalize to unseen data without explicit instructions. It is a sub-class of artificial intelligence (AI), which is the capability of computer systems to perform tasks typically associated with human intelligence. Many of the statistical methods that have been used for decades in Earth sciences can be counted into the wider class of ML. Examples are multi-dimensional linear regression, or dimensionality reduction via principal components. Even deep learning – the use of neural networks to perform ML – was already applied at ECMWF for the emulation of the radiation scheme more than two decades ago [1,22]. It may therefore surprise that many claims that we have seen an ML "revolution" during the last couple of years. What happened? Beyond the domain of Earth system science, AI and ML have seen an enormous rise that was mainly fueled by:

• A massive increase in computational power with computer hardware customized towards the needs of deep learning, and deep learning being the ideal application for state-of-the-art supercomputers that excel for simple arithmetic and linear algebra.

• The exponential increase of data in many domains – including weather and climate – and the ability of deep learning to learn systems of arbitrary complexity if enough data and compute capacity are available.

• The availability of software libraries such as TensorFlow and PyTorch that allow a user to create complex deep learning architectures with very minimal Python code.

• The massive amount of experience that was collected on how to design efficient deep learning methods with new neural network architectures and training procedures being invented, including convolutional neural networks, recurrent neural networks, generative adversarial networks, attention and transformers, and diffusion networks

It became more obvious around 2018 that the developments in general machine learning would also impact data assimilation and Earth system modelling. Early success stories across ECMWF's workflow included the use of neural networks for SMOS soil moisture data assimilation for the land surface [21,22] and the use of neural networks for bias correction learned within the 4D-Var data assimilation framework [21. Deep learning has been used successfully for the emulation of the gravity wave drag parametrization schemes [22], and the deep learning emulators could be used to generate tangent linear and adjoint model code for 4D-Var data assimilation. Furthermore, decision trees have been used for the post-processing of ensemble predictions for precipitation, and there have been plenty of links and similarities between data assimilation and deep learning. As ECMWF hosts more than one exabyte of weather and climate data, there were plenty of possible application areas for versatile, scalable tools that allow the extraction of complex information from data – such as deep learning. The potential applications were distributed across all parts of the numerical weather prediction (NWP) pipeline, from observation processing [22 to data assimilation, to the forecast model and the post-processing and dissemination of the forecasts. These included methods to improve our understanding of the Earth system such as unsupervised learning and causal discovery, uncertainty quantification, and AI powered visualization; methods to speed-up conventional models such as emulators for parametrization 3 schemes including with low numerical precision, the optimization of the high performance computing (HPC) and data workflow, and data compression; methods to improve the models such as bias correction tools, tools for quality control of observations, feature detection algorithms, and the learning of model components from observations; and methods that linked different datasets to weather and climate datasets that have interesting applications for health, energy, transport and pollution applications, as well as for extremes such as wildfires or flooding.

Machine learning scientists and Earth Science domain scientists often follow a different philosophy. The former tends to solve data science problems that optimize for specific goal functions (e.g. the reduction of Root Mean Square Error of precipitation at 48-hour lead time), while the latter aim to improve and validate models with physical understanding and checks for physical consistency (e.g. conservation laws or process feedbacks). Domain scientists are sometimes defensive regarding the establishment of machine learning as they consider the new capabilities as a threat rather than as an extension of their toolbox. This makes communication and collaboration difficult, but it also represents a barrier for the uptake of machine learning solutions by domain scientists who do not trust black box approaches that do not offer physical understanding. This is in particular the case as many of the machine learning architectures that are currently applied have been developed for other domains such as image recognition and do not allow for the introduction of domain knowledge into solution design. There is a risk that solutions for specific applications will be developed in parallel with no synergies between domain scientists on the one side and machine learning scientists on the other.

The hybrid approach

Machine learning can be used to better estimate some components of NWP, and to estimate model error. This is true for the process of establishing the best possible starting conditions of forecasts, called data assimilation, but also for forecasts themselves.

Aspects of the Earth system, such as sea ice, snow, soil and vegetation, are hard to model from pure physics, so in practice, the modelling can be quite empirical. In such cases, there is great potential to let the observations increasingly define the models. It is more likely to achieve the best results by carefully combining known physics with empirical and ML components, rather than throwing away physical models entirely.

There are also some predictable model errors which we can estimate and remove from data assimilation and subsequent forecasts using ML. Weather and climate reanalysis can benefit from ML, too. For example [22], for ECMWF's next reanalysis, ERA6, an ML model error correction method developed for the period from 2006 (Fig.2), which is rich in satellite observations, will be applied to earlier, data-sparse periods.

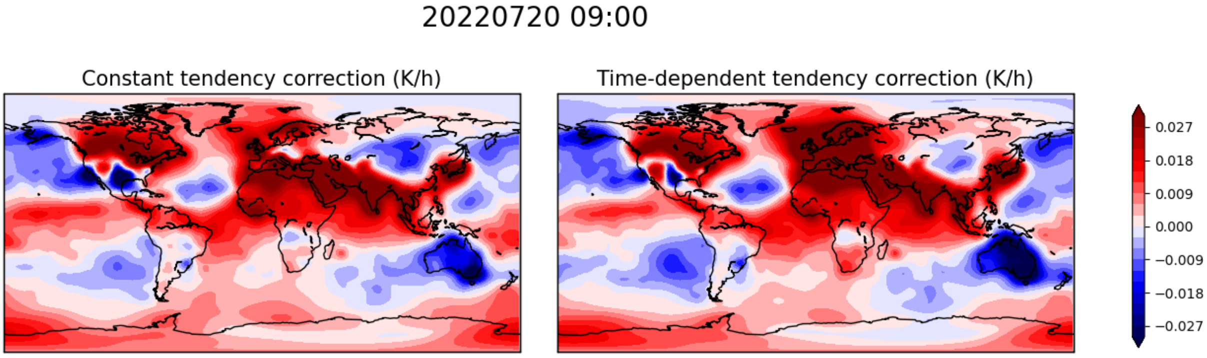

Fig.2. The variable corrections of near-surface temperature tendencies per hour, established by machine learning, that are going to be applied in the data assimilation system from 2025, compared to constant tendency corrections. The constant tendency correction includes small changes for every 12-hour assimilation window. (Time series courtesy of Patrick Laloyaux, ECMWF).

ECMWF made tremendous progress in the last 18 months or so in building such a system, called the Artificial Intelligence Forecasting System (AIFS). This is the result of decisions by our Member States on investments, the motivation and dedication of our staff, and collaborative efforts with partners. The AIFS uses Copernicus climate reanalysis and weather analysis for training, and it relies on IFS initial conditions, so it is not entirely divorced from traditional techniques. But it makes forecasts just on the basis of ML.

This year, *ECMWF* has lowered the grid spacing of the AIFS from 100 to 28 km, and it will go down further. This compares with a grid spacing of currently 9 km for the IFS., *ECMWF* has also built a first AIFS ensemble system, in which a number of slightly different forecasts are made for each time in the future to scan the possible scenarios and thus enable the estimation of uncertainty. These forecasts have been added to our chart's web page, and they are available as open data.

ECMWF is looking at sub-seasonal timescales, up to 46 days ahead, and at the addition of various Earth system components. There are also plans for AIFS forecasts of hydrology and atmospheric composition., *ECMWF* is collaborating in an ECMWF ML pilot project with Member and Co-operating States, taking part in a EUMETNET AI initiative. This will help us to compare different approaches, at different timescales and resolutions. The collaboration with our Member and Co-operating States is also key to the development of a platform called **Anemoi,** which will enable users to build their own ML models (Fig.3).

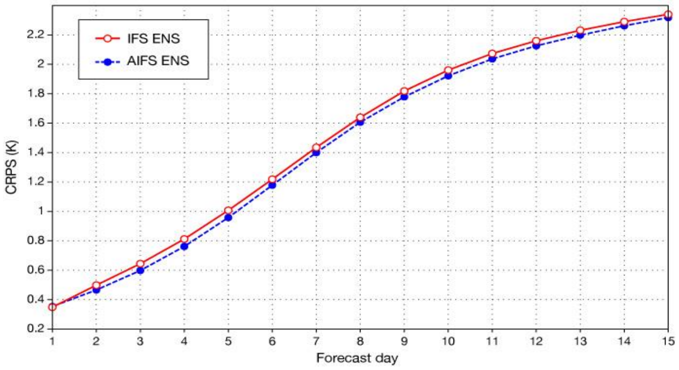

Fig.3. The continuous ranked probability score (CRPS – lower is better) measures the quality of ensemble forecasts. Here we show it for 850 hPa temperature, with results for the IFS ensemble (IFS ENS – red) and for the experimental AIFS ensemble (AIFS ENS – blue). Scores are aggregated over the northern hemisphere extratropics and approximately a five-month period.

Over the last year, *ECMWF* has started a radically new approach to weather prediction: the production of weather forecasts directly from observations. Physics-based data assimilation relies on some assumptions, such as a perfect knowledge of model and observation errors, and of the link between the model and observations. The new approach tries to circumvent these aspects of conventional data assimilation.

It means that observations do not need to be mapped to a fine grid of unmeasured parameters. It also opens up the possibility of exploiting the information content of exciting new observations. This AI-Direct Observation Prediction (AI-DOP) project involves a neural network trained to predict future observations from long historical records of past observations (Fig.4.) [22].

In this new approach, we effectively use observations to forecast future states of the atmosphere learned directly from the observations themselves. First results are very promising, but this approach is still experimental.

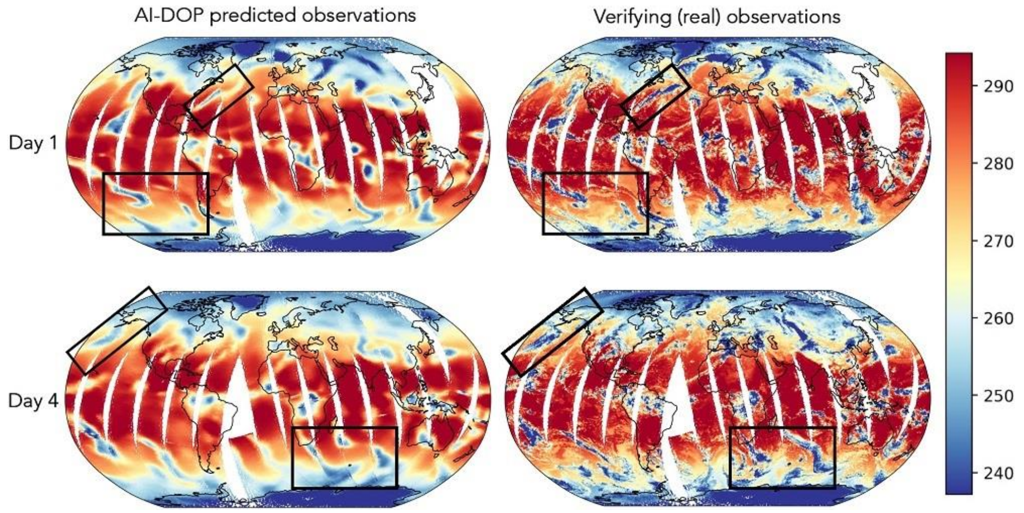

Fig.4. An example of forecasting future observations with AI-DOP. We show infrared window channel brightness temperatures (in Kelvin), measured by the Infrared Atmospheric Sounding Interferometer (IASI), predicted one and four days ahead. The left column shows the predicted values and the right column real radiances measured one and four days later. This channel is very sensitive to atmospheric cloud structures, and we can see that AI-DOP produces very plausible forecasts of the evolution of the large-scale weather patterns, although they are rather smoothed with the current low-resolution experimental system. The rectangles highlight some of the more conspicuous weather patterns that are predicted well.

ML in NWP and climate services

While some of the applications from Machine Learning in Earth system sciences are conceptually close to the use of machine learning methods in other domains (such as the detection of tropical cyclones in model output which can be formulated as an image recognition task), many will require customized machine learning solutions. Physical fields, for example, are often stored on unstructured grids on the sphere which do not allow for a simple application of convolutions in space or time which are a core element of many machine learning approaches. While the vertical dimension of atmosphere models is structured, the physical fields still show very different dynamics close to the surface and at the model top, which will, again, make it difficult to apply standard convolution approaches [1, 23]. Furthermore, physical fields need to follow physical constraints such as conservation laws or a limit to positive values

The training of machine learning tools requires data. As the complexity of machine learning tools can be increased arbitrarily, the only limits for the accuracy of machine learning methods are the amount of data that is available for training and the limits of the computational and data handling infrastructure. More data allow more sophisticated machine learning solutions to be designed. Machine learning users will therefore show a different and more greedy data access pattern when compared to conventional users, towards larger and more selective data access (e.g. retrieving a single field over a specific area of the globe for a long period of time). This generates a significant challenge for data centers such as ECMWF as data production and use is already growing fast for the conventional workflow.

When compared to conventional methods in NWP and climate services, machine learning requires a different set of tools regarding both software and hardware. Most Earth system models are still based on Fortran code and are typically run on CPU-based supercomputing hardware. On the other hand, machine learning tools are typically based on Python code and Python libraries as well as Jupiter notebooks and are trained and used most efficiently on GPU hardware. Most of the computational cost for supervised learning is generated by the training of the machine learning tool, while the application of the tool (the "inference") is typically very cost efficient. As part of the code refactorization to improve portability, models are now being rewritten into domain-specific languages and in some cases also Python or Julia code [22], including the Finite Volume version of the ECMWF Integrated Forecasting System (IFS-FVM). However, it will still take a couple of years until these developments reach a large fraction of domain scientists.

Earthkit

ECMWF has also developed Earthkit, a modular Python ecosystem that provides consistent tools for retrieving, manipulating and analyzing Earth system data. Earthkit builds on the principles used in ECMWF's operations, ensuring that users preparing AI training datasets benefit from the same reliability and transparency that underpin ECMWF's daily forecasts (Fig.5.) [22].

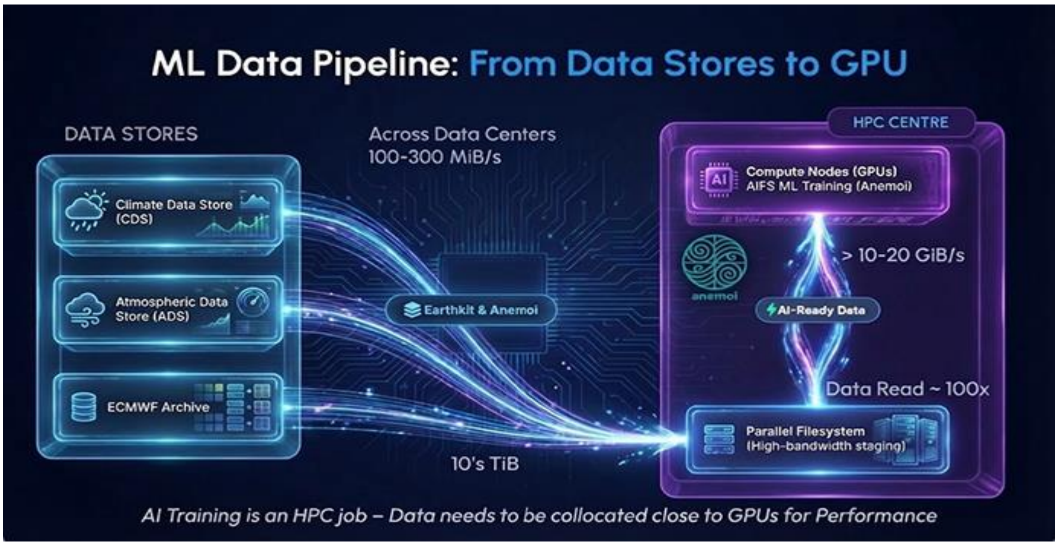

Fig.5. Machine learning pipelines: optimal performance relies on placing large datasets close to Graphics Processing Units (GPUs) within HPC environments, ensuring efficient machine learning workflows.

Anemoi: a shared European framework for AI weather prediction

While datasets and processing tools are essential, the rapid progress in AI weather forecasting across Europe is also due to shared software frameworks that support collaboration.

A major reason Europe has advanced so quickly in AI-based weather and climate prediction is the emergence of Anemoi, a jointly developed, open-source framework created by ECMWF together with several national meteorological services. Anemoi provides a coherent, shared foundation that supports the full lifecycle of developing machine learning models, from data preparation to model training, inference and operational use.

At its core, **Anemoi** offers three essential capabilities (Fig.6):

- AI-ready datasets: production, cataloguing and distribution of more than 150 curated training datasets derived from ERA5, operational ECMWF data, satellite and in situ observations, and Member State archives. These datasets are prepared using domain expertise and deployed across multiple HPC systems across Europe.
- Training and ML operations: tools for large-scale, distributed model training, experiment tracking and workflow reproducibility, enabling consistent development across institutions and HPC environments, including the world-class EuroHPC supercomputers.
- Inference and applications: components that support scalable model execution for weather and climate applications across both timescales and spatial scales. Examples include nowcasting, limited-area ML models, ECMWF's own Artificial Intelligence Forecasting System (AIFS) and the AI Earth system components and climate emulator developed within the Destination Earth initiative of the European Commission.

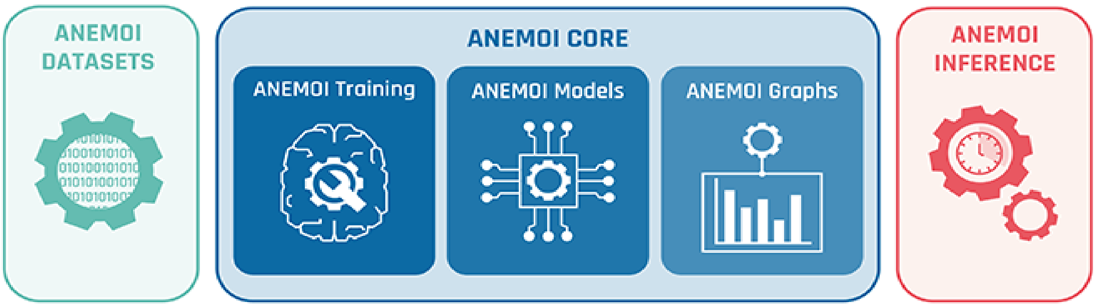

Fig.6. Overview of the Anemoi pipeline, from datasets through core components – training, models, and graphs – to inference [22].

By providing an end-to-end, operationally aligned framework, Anemoi enables ECMWF and its Member States to build, operationalize and improve AI models in a consistent way. This shared framework ensures the rapid progress in AI prediction, while ensuring transparency, scientific robustness and a clear pathway from research to operational implementation."

In 2025, **Anemoi** received two major international recognitions. It was awarded the Technology Achievement Award by the European Meteorological Society (EMS) for its collaborative approach to machine learning, and also the 2025 HPC wire Readers' and Editors' Choice Award for "Best Use of AI Methods for Augmenting HPC Applications".

AIFS: operationalizing AI models

ECMWF's Artificial Intelligence Forecasting System (AIFS), which is operationally run daily since 2025, demonstrates how machine learning models can be integrated into a rigorous operational environment. Running the AIFS alongside the Integrated Forecasting System (IFS) allows ECMWF and its Member States to:

- evaluate AI forecasts with established verification methods,
- analyze strengths and limitations under diverse conditions, and
- explore the complementarity of physics and machine learning forecasting approaches.

This side-by-side exploration ensures that emerging AI methods can be assessed transparently and responsibly, in line with ECMWF's commitment to scientific trust, quality, and reliability (Fig.7).

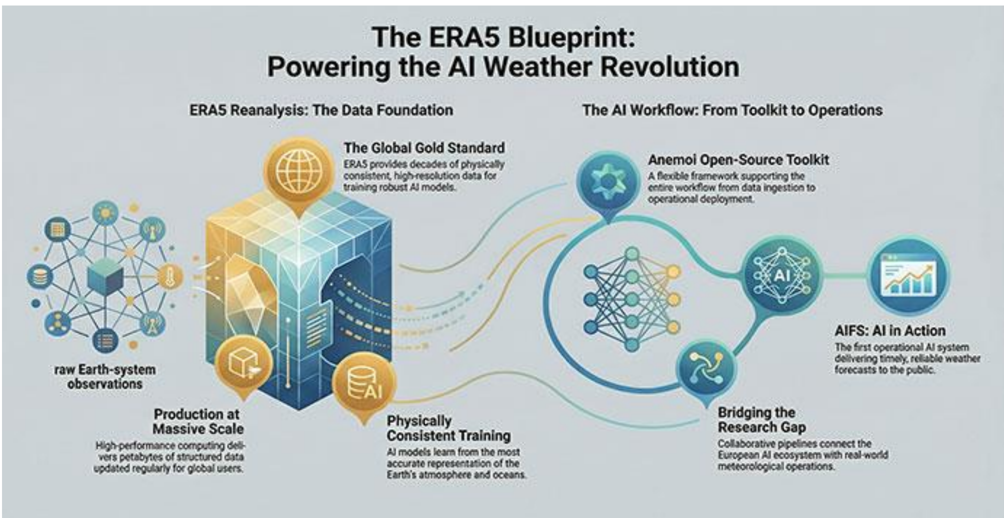

Fig.7. The ERA5 Blueprint illustrates the journey from raw Earth observations to next-generation AI weather forecasts. Credit: generated by Notebook [22].

Interest in AI-enabled forecasting is growing, with ECMWF, national meteorological services, research institutes and private actors exploring applications from post-processing and downscaling to nowcasting and regional and global prediction. One example is the recent operationalization of AICON by the German Meteorological Service (DWD) utilizing **Anemoi.**

Building on shared foundations such as ERA5, Earthkit and Anemoi allows ECMWF and its Member States to develop these methods in a consistent way, supporting joint approaches to model development and evaluation.

This collective momentum is one of Europe's strengths, helping establish a coherent and scientifically robust pathway for AI-enabled weather prediction, strengthening the capacity of the European meteorological infrastructure.

These digital representations combine EO data with advanced modelling frameworks to simulate environmental processes and explore future, "what if", scenarios. Using high-performance computing, machine learning, and satellite data, the digital twins of Destination Earth (DestinE) combine Earth Observation data with numerical models and AI techniques to simulate the behavior of the Earth system and explore possible future scenarios [21].

The **WEkEO** DIAS provides **Earth Observation datasets** coming from many different services (and allows all users to **download data for free**.

Another question about the future of ML for Earth system modelling is whether the domain will follow the developments of large language models (LLMs) towards larger and more generic ML tools that can then be used for multiple application areas – so-called foundation models. LLMs are trained to fill in gaps in huge amounts of text, rather than for a specific task such as the translation from language A to language B. The resulting tools can be used for diverse tasks beyond their training objective, along this line, it may be possible that a foundation model trained from various Earth system datasets and with a huge latent space with many billions of trainable parameters may perform better in certain tasks when compared with a task-specific model. To explore foundation models for weather and climate applications, ECMWF and a number of Member States have started the Weather Generator EU Horizon project that will build such a foundation model and serve as an additional digital twin for **Destination Earth** [21].

The Weather Generator will serve as foundation model for weather and climate applications. It will be able to digest datasets from various sources, including observations, local and global analysis products, and local and global models, and will be useful for many different application domains in weather and climate science. The input and output of the Weather Generator can be local or global, at a resolution between 100 m and 100 km, and can be in the past, present and future. Figure 8: Showing the evolution of 24-hour rainfall forecasts on 16 April 2024 over the grid box including Dubai. The model climate is about zero precipitation, with a maximum of less than 25 mm based on 1,800 forecasts (marked by the black triangle). Experimental versions of AIFS Single (blue dots) and AIFS Ensemble (green box and whisker) models both predicted precipitation values well-outside the model climatology and values in line with the IFS ensemble (blue box and whisker). All systems underestimated the observed value (purple hourglass). Data is obviously a key ingredient in accurate forecasting using physics-based approaches. We view that the role of data will grow even larger with the rise of data-driven forecasting. Curating large, calibrated datasets will be vital to feed these models. Direct incorporation of surface observations into model training and inference will increase the value of sharing these datasets. Novel data sources, e.g. cameras measuring visibility, could be directly included in model pipelines.

Conclusion

Big Data and Artificial Intelligence greatly enhance weather forecast and climate assessment as in spatial-temporal scale as accuracy. The Machine Learning methods are successfully used in prediction of dangerous hydrometeorological events, such as drought [23], flooding, frost, etc. These methods became more and more accurate due to Earth Observing Satellite data and computing facilities. The best way to achieve more accuracy is enhancement of those ML models by learning them physical lows. These includes microphysical processes, thermodynamics and also quantum electrodynamics, due to cosmic weather events [14]. Hybrid approach together with space weather prediction will be able to handle weather forecasting gaps and difficulties.

Acknowledgement: The study was conducted by financial support of Shota Rustaveli Science Foundation **Grant #FR 25-16-929**

References

[1] Kartvelishvili, L., Tatishvili, M., Amiranashvili, A., Megrelidze, L., Kutaladze, N. Weather, Climate and their Change Regularities for the Conditions of Georgia. Monograph, Publishing House "UNIVERSAL", Tbilisi, 2023.

[2] Tatishvili M., Elizbarashvili E., Meskhia R., Elizbarashvili Sh. Natural hydrometeorological disasters, their causes and prevention measures. The Macrotheme Review. A multidisciplinary journal of global macro trends, 148-154, A Macrotheme Capital Management, LLC Academic Publication, Volume 2, Issue 1, Winter 2013 (January). ISSN 1848-4735, France

[3] Tatishvili M.R., Palavandishvili A.M., Tsitsagi M.B., Suknidze N.E. The Use of Structured Data for Drought Evaluation in Georgia. Journal of Georgian Geophysical Society, 2*5*(1), 2022. https://doi.org/10.48614/ggs2520224806

[4] Amiranashvili A.G., Kartvelishvili L.G., Kutaladze N.B., Megrelidze L.D., Tatishvili M.R. Changeability of the Meteorological Parameters Associated with Holiday Climate Index in Different Mountainous Regions of Georgia in 1956-2015. Journal of Georgian Geophysical Society, 24(2), 2021. https://doi.org/10.48614/ggs2420213326

[5] Tatishvili M., Palavandishvili A., Tsitsagi M., Suknidze N. The Big Data for Drought Monitoring in Georgia. In: Geibel, R.C., Machavariani, S. (eds) Chances and Challenges of Digital Management. ISPC 2022. Springer Proceedings in Business and Economics. Springer, Cham., 2023. https://doi.org/10.1007/978-3-031-45601-5_13

[6] Amiranashvili A., Kartvelishvili L., Kutaladze N., Megrelidze L., Tatishvili M. Variability of the Mean Max Annual Air Temperature in 39 Locations of Georgia in 1956-2015. International Scientific Conference "Geophysical Processes in the Earth and its Envelopes" Proceedings, ISBN 978-9941-36-147-0, Tbilisi, Georgia, 2023.

[7] Tsitsagi M., Gulashvili Z., Bolashvili N., Tatishvili M., Suknidze N. Relationship Between Normalised Difference Vegetation Index, Precipitation and Drought Indices (Case of Kakheti, Georgia). International Multidisciplinary Scientific GeoConference: SGEM**;** Sofia, Vol. 22, Iss. 4.1, 2022. DOI:10.5593/sgem2022/4.1/s19.46 mber 16-17, 2023

[8] Tatishvili M.R., Megrelidze L.D., Palavandishvili A.M. Study of the Mean and Extreme Values, Intensity and Recurrence Variability of Meteorological Elements Based on the 1956-2015 Observation Data. Journal of Georgian Geophysical Society, 24(2), 2021. https://doi.org/10.48614/ggs2420213325

[9] Aliyev V., Amiranashvili A., Kartvelishvili L., Matzarakis A., Tatishvili M. Comparative Analysis of the Variability of Daily Minimum, Maximum and Mean Air Temperature in Baku and Tbilisi in 2005-2024. International Journal of Sustainability and Risk Control, 1(2), 2025, pp. 63-70.

[10] Aliyev V., Amiranashvili A., Kartvelishvili L., Matzarakis A., Tatishvili, M. Variability of Monthly Average Values of Daily Minimum, Maximum and Mean Air Temperature in Baku and Tbilisi in 2005-2024. Int. Journal of Sustainability and Rick Control, e-ISSN, 3104-8358, v/ 1, N 2(2), 2025, pp. 63-70.

[11] Tatishvili, M.R., Palavandishvili A.M. Atmospheric Periodic Oscillations. Journal of Georgian Geophysical Society, 26(1), 2023. https://doi.org/10.60131/ggs.1.2023.6961

[12] Kutaladze N., Mikuchadze G., Tatishvili, M. Verification of WRF simulated accumulated precipitation. The Journal of Nature Studies - Annals of Agrarian Science, 19(1), 2021. Retrieved from https://journals.org.ge/index.php/aans/article/view/258

[13] Tatishvili M., Bolashvili N., Karalashvili T., Suknidze, N. Impact of Atmosphere Perturbation and Microcirculation on Tbilisi Thermal Regime. Georgian Geographical Journal, *5*(3), 2025, pp. 34–42. https://doi.org/10.52340/ggj.2025.05.03.05

[14] Tatishvili M. Energy Transformation in Clouds According Quantum Principles. International Scientific Journal. Journal of Environmental Science. ISBN- 13: 978-1499721980; ISBN -10: 1499721986, v.3, Vienna, Austria, 2014, pp. 7-9.

[15] Tatishvili M., Palavandishvili A. Impact of Short-Term Geomagnetic Activity on Weather and Climate Formation in Georgian Region. Journal of the Georgian Geophysical Society, Physics of Solid Earth, Atmosphere, Ocean and Space Plasma, v. 23(2), 2020, ISSN: 1512-1127 DOI: https://doi.org/10.48614/ggs2320202730

[16] Tatishvili M., Mkurnalidze I., Samkharadze I., Tsintsadze N. Impact of solar coronal mass ejections (CME) on formation of Earth climate and weather pattern. ADEO MEDIA/International Scientific Journal. Journal of Environmental Science, vol. 7, issue 1, 2018, pp. 1-5. ISBN -13:978-1721539185. http://www.scientific-journal.com/journals.html
[17] Tatishvili M., Bolashvili N., Palavandishvili A. Impact of short-term geomagnetic activity on meteorological parameters variability on the middle latituge region. Georgian Geographical Journal, Volume 2, 2022. https://doi.org/10.52340/ggj.2022.756_2022
[18] Tatishvili M. Developing Weather Forecasting System in Georgia. MOJ Eco Environ Sci 2(7): 00046, 2017. DOI: 10.15406/mojes.2017.02.00046
[19] Tatishvili M., Khvedelidze Z., Demetrashvili D. On some weather forecasting models in Georgia. Journal of the Georgian Geophysical Society, Physics of Solid Earth, Atmosphere, Ocean and Space Plasma, v. 23(2), 2020, ISSN: 1512-1127.
[20] Tatishvili M., Bolashvili N., Elbakidze Kh., Tsitsagi M., Palavandishvili A. Modern Methods and Big Data to Study Dangerous Hydrometeorological Events. RT&A, Special Issue No. 9 (87), Volume 20, November 2025.
[21] Hoffmann J., Bauer P., Sandu I., Wedi N., Geenen T., Thiemert D. Destination Earth – A digital twin in support of climate services. https://doi.org/10.1016/j.cliser.2023.100394Get rights and content.
[22] Roadmap for machine learning activities at ECMWF Technical Memorandum No. 878 http://www.ecmwf.int/en/publications
[23] Palavandishvili A. Supervised Machine Learning in Drought Evaluation. Georgian Geographical Journal, 4(2), 2024, pp. 30–37. https://doi.org/10.52340/ggj.2024.04.02.04

მანქანური სწავლება და ჰიბრიდული მიდგომები ამინდსა და კლიმატში

მ. ტატიშვილი, ა. ფალავანდიშვილი

რეზიუმე

კლიმატის ცვლილება ერთ-ერთი უმნიშვნელოვანესი გლობალური გამოწვევაა, რომლის მართვაც აუცილებელია. ბუნებრივი გარემოს გაგება სულ უფრო მნიშვნელოვანი ხდება კლიმატის ცვლილების ნეგატიურ ზემოქმედებასა და ანთროპოგენურ ზეწოლაზე რეაგირებისთვის, ასევე მათ წყალზე, ენერგეტიკულ და სასურსათო უსაფრთხოებაზე, ინფრასტრუქტურაზე, ადამიანის ჯანმრთელობასა და ბუნებრივ საფრთხეებზე. ნაშრომში განხილულია მანქანური სწავლების გამოყენება ამინდსა და კლიმატში, მისი შემდგომი განვითარება და ECMWF-ის საქმიანობა და მიღწევები მანქანური სწავლების/ხელოვნური ინტელექტის მეთოდების შექმნაში და გამოყენებაში. ეს ასევე მნიშვნელოვანი ინტერდისციპლინარული გამოწვევაა, რომელიც მოიცავს თითქმის ყველა სამეცნიერო სფეროს. ხელოვნური ინტელექტისა და მანქანური სწავლების (AI/ML) აპლიკაციები ბოლო დროს ფართოდ გავრცელდა ყველა სფეროში. მანქანურ სწავლებას შეუძლია გააუმჯობესოს გამოთვლები კომპონენტების დამატებით ან პროცესის ზოგიერთი ნაწილის ჩანაცვლებით. ეს არის ის, რასაც „ჰიბრიდულ“მიდგომას უწოდებენ. სამაგიეროდ, მანქანურ სწავლებას (ML) ასევე შეუძლია მთლიანად ჩაანაცვლოს მთელი მოდელი გაცილებით დაბალი გამოთვლითი ხარჯებით. გარდა ამისა, ხელოვნური ინტელექტი/მანქანური სწავლება (AI/ML) ხსნის გარკვეულ გზებს სხვა პროცესებში, როგორიცაა წყალდიდობის პროგნოზირება, ხანძრის საფრთხის პროგნოზირება, დაკვირვებების მონიტორინგი, სუპერკომპიუტერის მართვა ან მომხმარებლის გამოცდილების გაუმჯობესება.

საკვანძო სიტყვები: დიდი მონაცემები, მანქანური სწავლება, ნეირონული ქსელი, CEMS (კლიმატისა და გარემოს მონიტორინგი კოსმოსიდან), ECMWF-ის ხელოვნური ინტელექტის პროგნოზირების სისტემა (AIFS), ჰიბრიდული მიდგომა.

Машинное обучение и гибридные подходы в погоде и климате

М. Татишвили, А. Палавандишвили

Резюме

Изменение климата является одной из наиболее значительных глобальных проблем, требующих решения. Понимание природной среды приобретает все большее значение для реагирования на негативные последствия изменения климата и антропогенное давление на ограниченные природные ресурсы, а также на их влияние на водную, энергетическую и продовольственную безопасность, инфраструктуру, здоровье человека и стихийные бедствия. В статье рассмотрено применение машинного обучения в погоде и климате, его дальнейшее развитие, а также деятельность и достижения Европейского центра изучения погоды и климата (ECMWF) в создании и применении методов машинного обучения/искусственного интеллекта (ИИ). Это также важная междисциплинарная задача, затрагивающая почти все научные области. Применение искусственного интеллекта и машинного обучения (ИИ/МО) в последнее время широко распространилось во всех областях. Машинное обучение может улучшить наши вычисления, добавляя компоненты или заменяя некоторые части процесса. Это называется «гибридным» подходом. Кроме того, машинное обучение может полностью заменить всю модель, при этом значительно снизив вычислительные затраты. Помимо этого, ИИ/машинное обучение открывает новые возможности в других областях нашей деятельности, таких как прогнозирование наводнений, прогнозирование пожарной опасности, мониторинг наблюдений, управление суперкомпьютером или улучшение пользовательского опыта.

Ключевые слова: Большие данные, машинное обучение, нейронные сети, CEMS (мониторинг климата и окружающей среды из космоса), система прогнозирования на основе искусственного интеллекта ECMWF (AIFS), гибридный подход.

Journal of the Georgian Geophysical Society, e-ISSN: 2667-9973, p-ISSN: 1512-1127
Physics of Solid Earth, Atmosphere, Ocean and Space Plasma, v. 29(1), 2026, pp. 85 - 89

Studying Forbush Effect in Geomagnetic Field of Earth

Mariam R. Aslamazishvili, Oleg A. Kharshiladze,
Aleksandre P. Ghurchumelia, Giorgi I. Takadze

M. Nodia Institute of Geophysics of the I. Javakhishvili Tbilisi State University, Georgia
e-mail: mariam.aslamazishvili722@ens.tsu.edu.ge

ABSTRACT

The report discusses the dynamics of charged particle motion in a non-uniform magnetic field. Specifically, we examine the possible trajectories of cosmic rays in Earth's dipole magnetic field. The study demonstrates the potential chaotic dynamics of cosmic rays using the Lyapunov exponent and Fourier spectrum. Additionally, it presents modeling of Van Allen belt formation and analyzes the influence of cosmic ray energy on the geometry of these belts. Furthermore, an analysis was conducted on the impact of the May 10, 2024, magnetic storm on cosmic ray detection on Earth. As is known, during such storms, the Forbush effect is observed, which manifests as a decrease in the intensity of detected cosmic rays. Relevant laboratory records are provided, utilizing data from the Tbilisi Cosmic Ray Laboratory. The study also investigates the dependence of the Forbush effect's depth on the magnitude of geomagnetic field disturbances.

Key words: *Forbush effect, non-uniform magnetic field, cosmic rays*

Introduction

A non-uniform magnetic field is a field whose magnetic induction varies from point to point in space. An example of such field is the Earth's magnetic field, which in the first approximation can be considered as a dipole magnetic field. The field lines emerge from northern magnetic pole and enter the southern magnetic pole. In the case of a uniform magnetic field, the equation of motion can be solved analytically, but for a non-uniform magnetic field we must use numerical methods. The magnetic field produced by a magnetic dipole is known from the formula [1] [4]:

$$\vec{B} = \frac{\mu_0}{4\pi r^3}[3(\vec{m}\cdot\hat{r})\hat{r} - \vec{m}] \qquad (1)$$

$\vec{B}$ — magnetic field (T)

$\vec{m}$— magnetic dipole moment(for earth: $8.0 * 10^{22}$ ($A*m^2$))

$\hat{r}$— unit vector from dipole moment center to point in space

r — distance from dipole center(m)

μ_0— magnetic constant($1.256 *10^{-6}$ N/A^2)

Our goal is to investigate the trajectory of a particle moving in non-uniform magnetic field.Using the Lorenz force, we write the corresponding equation of motion and solve the system of differential equations using the Runge-Kutta numerical method(ODE-45):

$$\frac{d^2\vec{r}}{dt^2} = \frac{q}{m}\frac{\mu_0}{4\pi r^3}\frac{d\vec{r}}{dt} \times [3(\vec{m}\cdot\hat{r})\hat{r} - \vec{m}] \quad (2)$$

As charged particles we consider cosmic rays, which allows us to investigate and qualitatively evaluate the Forbush effect.

Results and disscusion

We obtained various trajectories for the motion of charged particles. The plots show coordinate system scaled by the Earth's radius. In this work, we chose alpha particles (He^{2+}) to model cosmic rays, since they constitute approximately 10% of the cosmic-ray flux. Alpha particles have charge q=2e and mass $m=4m_p$.

Additionally, the Lyapunov exponent was calculated for each trajectory to characterize the degree of chaotic behavior (Fig.1, Fig.2, Fig.3)

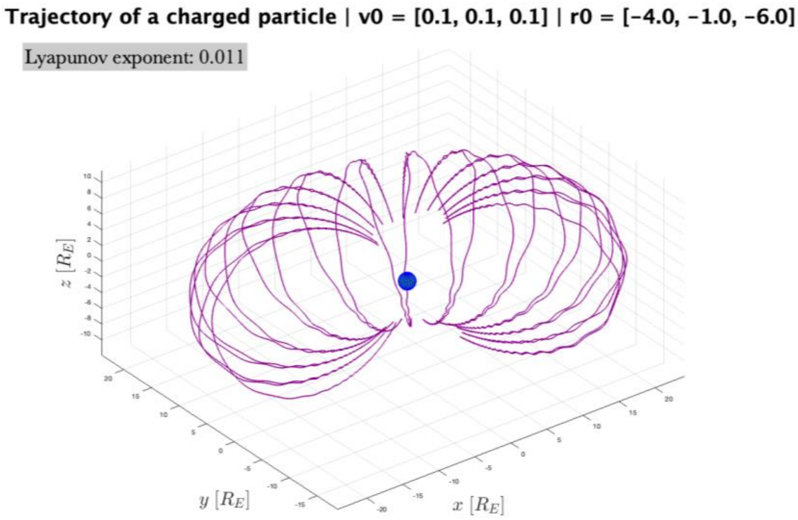

Fig. 1

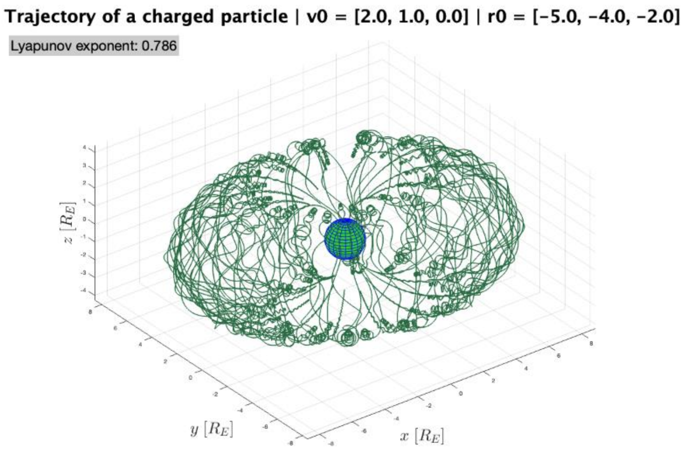

Fig. 2

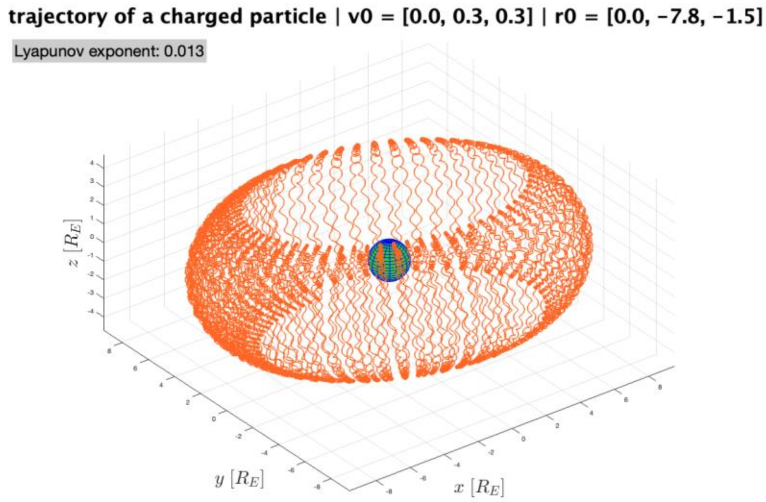

Fig. 3

Using this model, it is also possible to explain the Forbush effect. The Forbush effect is the reduction in cosmic-ray intensity observed on Earth during geomagnetic storms, caused by magnetic disturbances generated by solar eruptions.

In the model, we compare two cases: one with the normal geomagnetic field, and one with an enhanced field due to solar disturbances. The modeled particle moves in the Earth's dipole magnetic field under normal contidions (fig.5) and under enhanced field conditions (fig.4). When the magnetic field is doubled, the particle's trajectory changes significantly, it moves away from Earth and can no longer reach the same location.

This demonstrates that a strong magnetic field, such as that occurring during a Forbush event, hinders the arrival of cosmic rays at Earth- and this is precisely the Forbush effect.

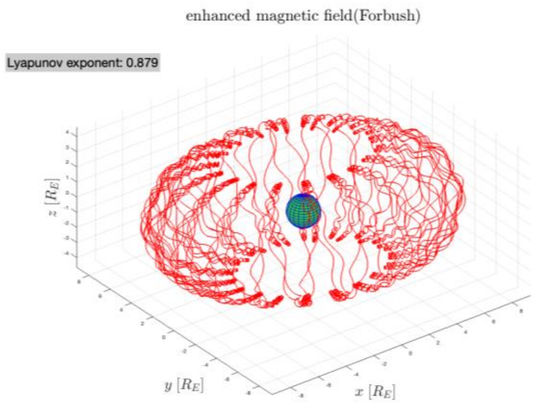

Fig. 4

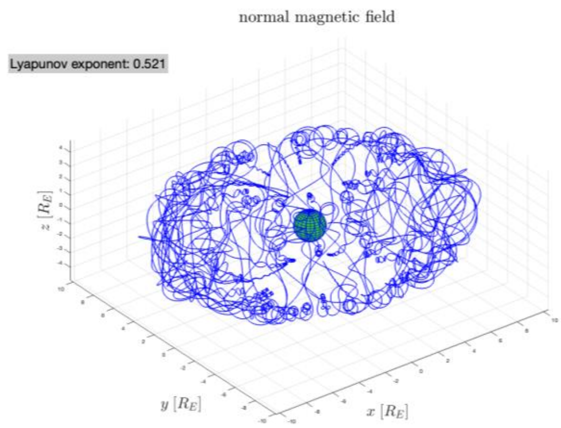

Fig. 5

We also used data from the Tbilisi Cosmic Ray Laboratory [5] to analyze the geomagnetic storm that occured between may 10-13, 2024. As can be seen in the yellow-highlighted region (fig.6), a sharp decrease in cosmic-ray intensity is recorded during the geomagnetic storm, which corresponds exactly to the forbush effect.

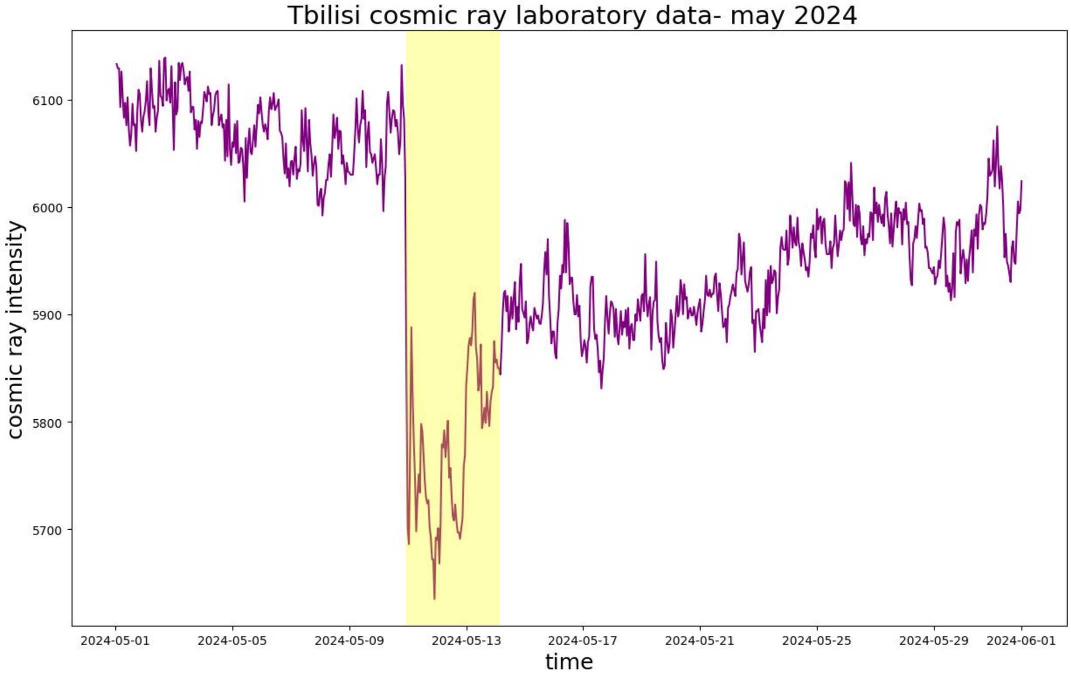

Fig. 6

Conclusion

In this work, we modeled the motion of charged particles in the Earth's non-uniform magnetic field and analyzed the impact of geomagnetic disturbances on their trajectories. Using alpha particles (He^{2+}) to represent cosmic rays, our simulations demonstrated that under normal geomagnetic conditions, charged particles can reach the Earth, whereas under enhanced magnetic field conditions such as those caused by solar eruptions, the trajectories are significantly altered, preventing particles from reaching the same locations.
The results clearly illustrate the physical mechanism behind the Forbush effect: strong geomagnetic fields generated during solar events reduce the flux of cosmic rays arriving at Earth. This modeling is supported by observational data from the Tbilisi Cosmic Ray Laboratory, which recorded a sharp decrease in cosmic-ray intensity during the geomagnetic storm of May 10-13, 2024.
Overall, this study highlights how numerical simulations of particle motion in the Earth's magnetosphere can effectively reproduce observed cosmic-ray modulation events, providing a valuable tool for understanding space weather effects on the near-Earth environment. The approach also allows for quantitative analysis of chaotic particle dynamics and can be extended to study other magnetospheric phenomena, such as the formation and structure of the Van Allen radiation belts.

References

[1] Pikelner S. Physics of Interstellar Space, 1962, 230 p.
[2] Artsimovich L., Lukyanov S. Motion of charged particles in electric and magnetic fields, ISBN-10. 0714715964, ISBN-13. 978-0714715964, 1981, 224 p.

[3] Tsulukidze L. K., Kharshiladze O. A., Ghurchumelia A. P., Sorriso-Valvo L., Elbakidze K. Z., Matiashvili, T. G. Coherent Analysis of Intense Geomagnetic Disturbances Using Dusheti Observatory Data and the DST Index. Journals of Georgian Geophysical Society, 27(2), 2024.
[4] García-Farieta J. E., Hurtado A. Simulation of charged particles in Earth's magnetosphere: An approach to the Van Allen belts. 2024.
[5] https://cosmicrays.epizy.com/index.php?opt=home&i=1

დედამიწის გეომაგნიტურ ველში ფორბუშის ეფექტის შესწავლა

მ. ასლამაზიშვილი, ო. ხარშილაძე, ა. ღურჭუმელია, გ. თაყაძე

რეზიუმე

მოხსენებაში განხილულია დამუხტული ნაწილაკების მოძრაობის დინამიკა არაერთგვაროვან მაგნიტურ ველში. კერძოდ, ვიხილავთ კოსმოსური სხივების შესაძლო ტრაექტორიებს დედამიწის დიპოლურ მაგნიტურ ველში. ნაშრომში ნაჩვენებია კოსმოსური სხივების შესაძლო ქაოსური დინამიკა ლიაპუნოვის მაჩვენებლისა და ფურიე სპექტრის საშუალებით. ასევე წარმოდგენილია ვან-ალენის სარტყლების ფორმირების მოდელირება და განხილულია კოსმოსური სხივების ენერგიის გავლენა ამ სარტყლების გეომეტრიაზე. ასევე ჩატარდა 2024 წლის 10 მაისის მაგნიტური ქარიშხლის გავლენის ანალიზი დედამიწის კოსმოსური სხივების დეტექტირებაზე. როგორც ცნობილია, ასეთი ქარიშხლების პერიოდში შეიმჩნევა ფორბუშის ეფექტი, რაც მდგომარეობს დედამიწაზე დეტექტირებული კოსმოსური სხივების ინტენსივობის შემცირებაში. მოყვანილი გვაქვს შესაბამისი ლაბორატორიული ჩანაწერები, სადაც გამოყენებულია თბილისის კოსმოსური სხივების ლაბორატორიის მონაცემები. გამოკვლეულია ფორბუშის ეფექტის სიღრმის დამოკიდებულება გეომაგნიტური ველის შეშფოთების სიდიდეზე.

საკვანძო სიტყვები: ფორბუშის ეფექტი, არაერთგვაროვანი მაგნიტური ველი, კოსმოსური სხივები

Изучение эффекта Форбуша в геомагнитном поле Земли

М. Асламазишвили, О. Харшиладзе, А. Гурчумелия, Г. Такадзе

Резюме

В работе рассматривается динамика движения заряженных частиц в неоднородном магнитном поле. В частности, изучаются возможные траектории космических лучей в дипольном магнитном поле Земли. В работе показана возможная хаотическая динамика космических лучей с использованием показателя Ляпунова и анализа Фурье. Также представлено моделирование формирования поясов Ван Аллена и обсуждается влияние энергии космических лучей на геометрию этих поясов. Кроме того, проведен анализ влияния магнитной бури 10 мая 2024 года на регистрацию космических лучей на Земле. Как известно, в периоды таких бурь наблюдается эффект Форбуша, заключающийся в уменьшении интенсивности космических лучей, зарегистрированных на Земле. Приведены соответствующие лабораторные записи, использующие данные Тбилисской лаборатории космических лучей. Исследуется зависимость глубины эффекта Форбуша от величины возмущения геомагнитного поля.

Ключевые слова: эффект Форбуша, неоднородное магнитное поле, космические лучи

Journal of the Georgian Geophysical Society, e-ISSN: 2667-9973, p-ISSN: 1512-1127
Physics of Solid Earth, Atmosphere, Ocean and Space Plasma, v.29 (1), 2026, pp. 90 – 97

27-Day Variations in Cosmic Rays During the Ascending and Descending Phase of the 24th Solar Activity Cycle

[1,2]George K. Vanishvili, [1]Teimuraz S. Bakradze, [1]Eteri M. Alania, [1]Tereza G. Erkomaishvili, [1]Vitali G. Kavlashvili, [2]Mariam G. Gugunashvili, [2]Omar E. Khajishvili

[1]M. Nodia Institute of Geophysics, Tbilisi State University, Tbilisi
[2]Sokhumi State University, Tbilisi
e-mail: g.vanishvili@sou.edu.ge

ABSTRACT

Based on the study of the 27-day variations of the neutron component of cosmic rays at two stations of the Global Cosmic Ray Network (Moscow and Yakutsk) and the Tbilisi Cosmophysical Observatory in the ascending and descending phases of the 24th cycle of solar activity, it has been established that the 27-day variation profile describes a quasi-sinusoidal curve. The deviation from the sinusoidal curve is determined by the change in the number, coordinates and power of sunspots (2.2 in the ascending phase and 81.8 in the descending phase) in a given phase of solar activity.

Key Words: *Cosmic ray 27- day variations, Solar Cycle, Bartels Rotation Number, Carrington Rotation Number, Solar Activity ascending & descending phase, World -Wide Network of cosmic ray neutron monitors, quasisinusiudal curve.*

1. Introduction

The article discusses the daily data of the intensity of the neutron component of cosmic rays, corrected for the effect of atmospheric pressure, registered by the Tbilisi CosmoPhysical Complex and two stations of the World Network of Cosmic Rays, Moscow and Yakutsk, and studies the 27-day variations of the neutron component of cosmic rays, in the case of the ascending and descending phases of the 24th cycle of solar activity.

2. Materials and Methods,

The last completed 24-day solar cycle began in December 2008, with a mini-mum corrected sunspot number of 2.2 [1] and ended in December 2019. Activity was minimal until early 2010. [2] [3]. Activity reached its maximum in April 2014 with a 23 months smoothed sunspot numbers of 81.8 [4]
To study the 27-day variations of cosmic rays, the starting points of the Carrington rotation were chosen as the reference point in time.

Based on the acquisition, processing and analysis of daily data on the intensity of cosmic rays registered by the Tbilisi Cosmophysical Observatory and neutron monitors of two stations of the World Network of Cosmic Rays, Moscow and Yakutsk, verified at atmospheric pressure, the solar activity was studied during the ascending and descending phases of the last completed 24 cycles. The ascending phase of the 24-cycle solar activity was located in the time interval from December 17, 2008 to December 02, 2012, The descending phase of the 24-cycle solar activity was located in the time interval from April 7, 2014 to December 10, 2019.

a. For the stations of the World Wide Web, Moscow and Yakutsk

Accordingly, to study the 27-day variations of cosmic rays, 53 Carrington rotations corresponding to 53 rotations of the Sun around its own axis of rotation, in the ascending phase of the 24th cycle of solar activity, were considered separately, Similarly, 76 Carrington rotations corresponding to 76 rotations of the Sun around its own axis of rotation, in the descending phase of the 24th cycle of solar activity, were also considered separately. Thus, the 27-day variations in the intensity of the neutron component of cosmic rays registered by the World Cosmic Ray Network are described by 53 separate Carrington rotations during the ascending phase of the 24th solar cycle, and by 76 separate Carrington rotations during the descending phase of the 24th solar cycle.

b. For the Tbilisi Cosmo Physical Complex

The 27-day variations of the neutron component of cosmic rays registered by the Tbilisi Cosmo-physical Observatory, since December 2009, are described by 41 separately taken Carrington rotations, during the ascending phase of the 24-th cycle of solar activity, and by 76 separately taken Carrington rotations during the descending phase of the 24-th cycle of solar activity. The data of the Cosmic Rays Laboratory are posted at the newly created web address: http://cosmicrays.tbilisi.com/

2. Methods for detecting recurring and non-periodic dependencies:

epoch superposition method

Small effects of influence can be detected using a special method of averaging data values, which was originally used in the study of geomagnetic variations [5] and which is known as the method of superposition of epochs, or the Kri method. Suppose that n events have been observed, during which the effect of a certain influence on cosmic rays should be studied. For the beginning of each of these events, we record the numerical values of the cosmic ray intensity in the corresponding cells of the horizontal rows forming a vertical column. And we assign such a vertical column the corresponding number at the beginning of the count. The corresponding values for moments after zero time are recorded in the vertical columns with the next ordinal number. Thus, we fill in a total of 27 columns in order to detect a 27-day cycle. And we calculate the average of the values recorded in the horizontal rows within each column [5-20].

Solar rotation is the rotation of the Sun around its axis.

The Sun is not a solid body, but rather consists of a gaseous plasma, and rotates with different periods at different latitudes. The solar rotation period is 25.67 days at the equator and increases with latitude, reaching 33.40 days at 75 degrees latitude [5]. The source of this differential rotation is an ongoing area of research in solar astronomy.[5]

Carrington rotation

The Carrington rotation is a system for comparing the positions of the Sun over a period of time, allowing the tracking of sunspot groups or the reappearance of flares at a later time. Since the rotation of the Sun varies with latitude, depth, and time, any such system is necessarily arbitrary and makes comparisons only meaningful over moderate periods. For the purposes of the

Carrington rotations, the solar rotation is taken to be 27.2753 days (see below). Under this scheme, each rotation of the Sun is assigned a unique number, called the Carrington rotation number, starting on November 9, 1853.

To study the 27-day variations in cosmic rays, the letters of the beginning of the Carrington rotation were chosen as the reference point in time.

The starting date for using the World Wide Web of Cosmic Rays data for the ascending phase of the 24^{-th} cycle of solar activity was December 17, 2008, which corresponds to the beginning of the 2078^{-th} Carrington rotation, and the final date for using the World Wide Web of Cosmic Rays data was December 02, 2012, which corresponds to the end of the 2131st Carrington rotation.

Thus, a total of CR2131 – CR 2078 = 53 Carrington rotations (CR) were considered for studying the ascending phase of the 24-th cycle of solar activity.

The starting date for using the World Wide Web of Cosmic Rays data in the descending phase of the 24-th cycle of solar activity was April 7, 2014, corresponding to the beginning of the Carrington rotation CR 2149, and the final date for using the World Wide Web of Cosmic Rays data was December 2, 2019, corresponding to the end of the Carrington rotation 2225. Thus, a total of CR 2225 – CR 2149 = 76 Carrington rotations (CR) were considered to study the descending phase of the 24-th cycle of solar activity.

3. Results

a)

Results for two stations of the World Wide Web, Moscow and Yakutsk

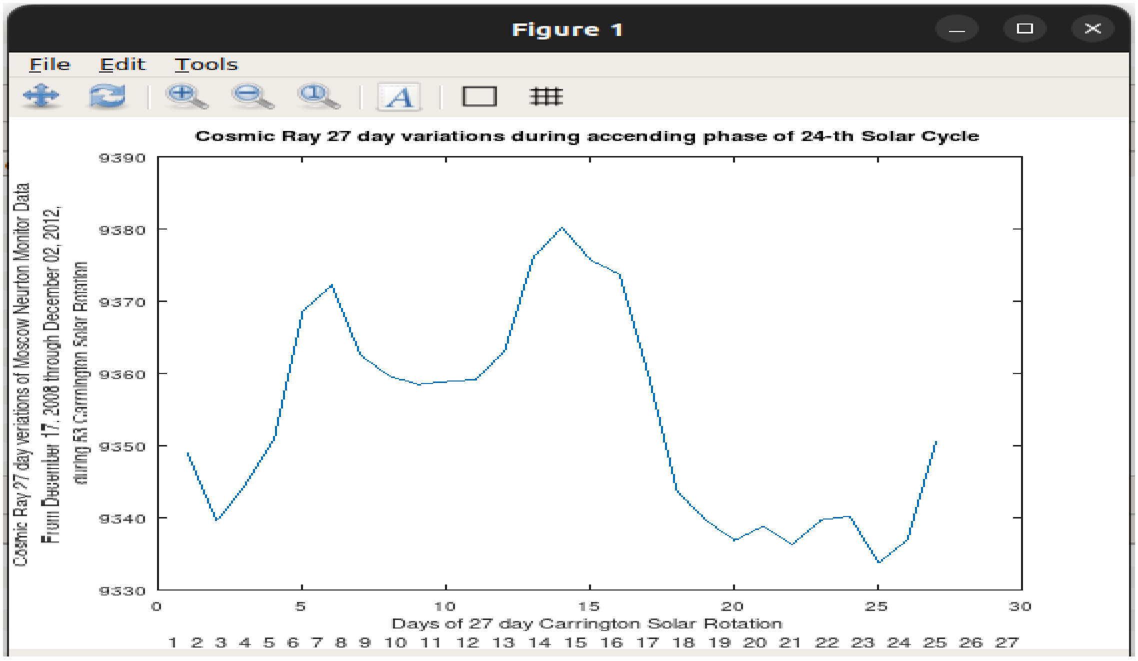

Fig. 1. Solar Activity Ascending phase, Moscow

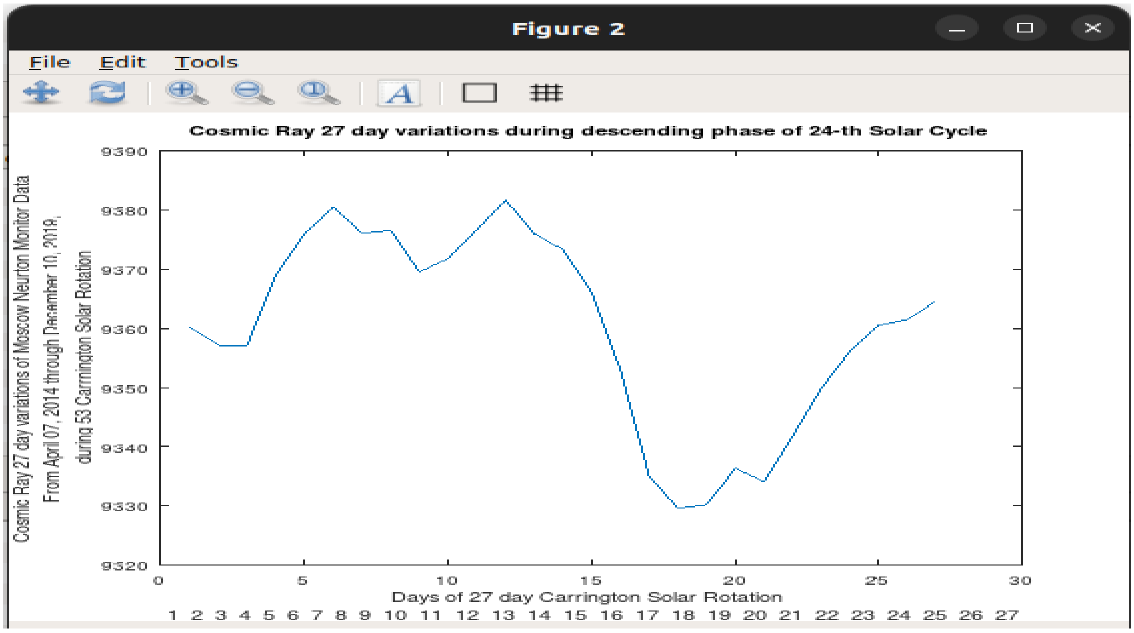

Fig. 2. Solar Activity Descending phase, Moscow

F

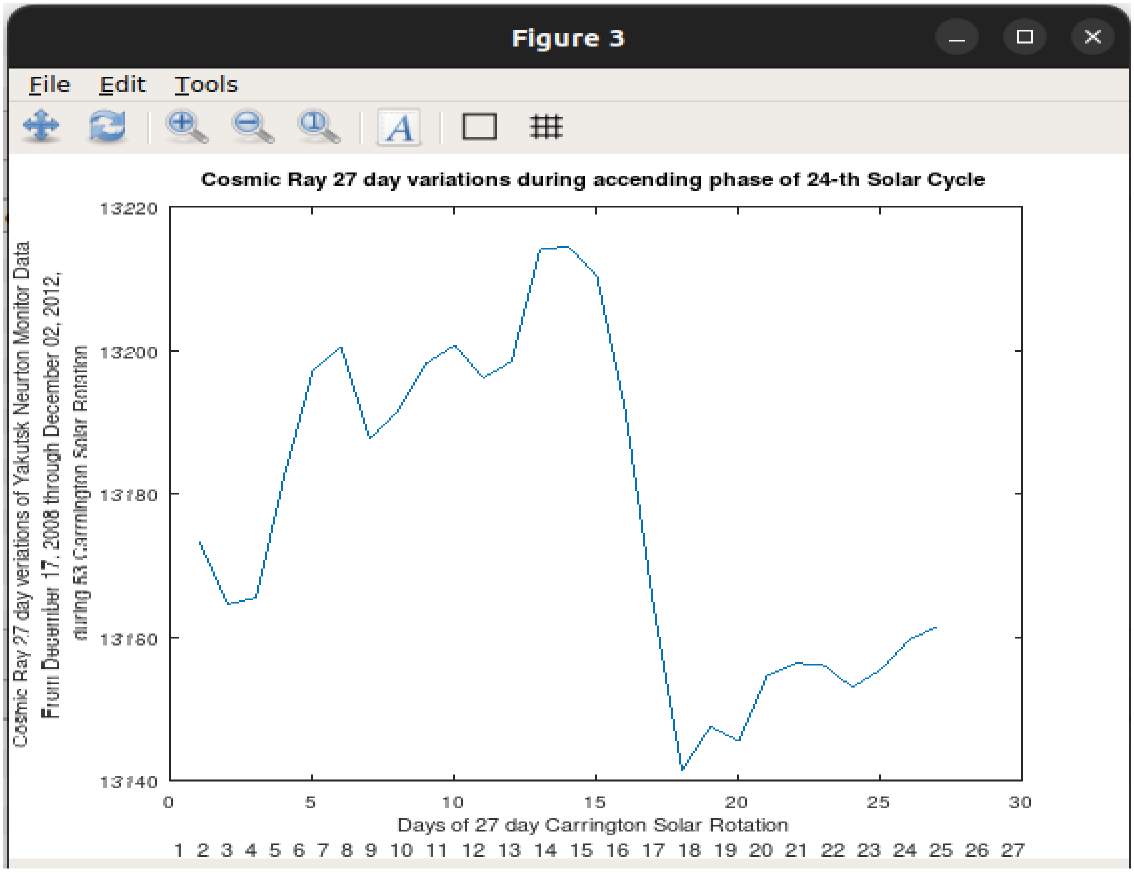

3. Solar Activity Ascending phase, Yakutsk.

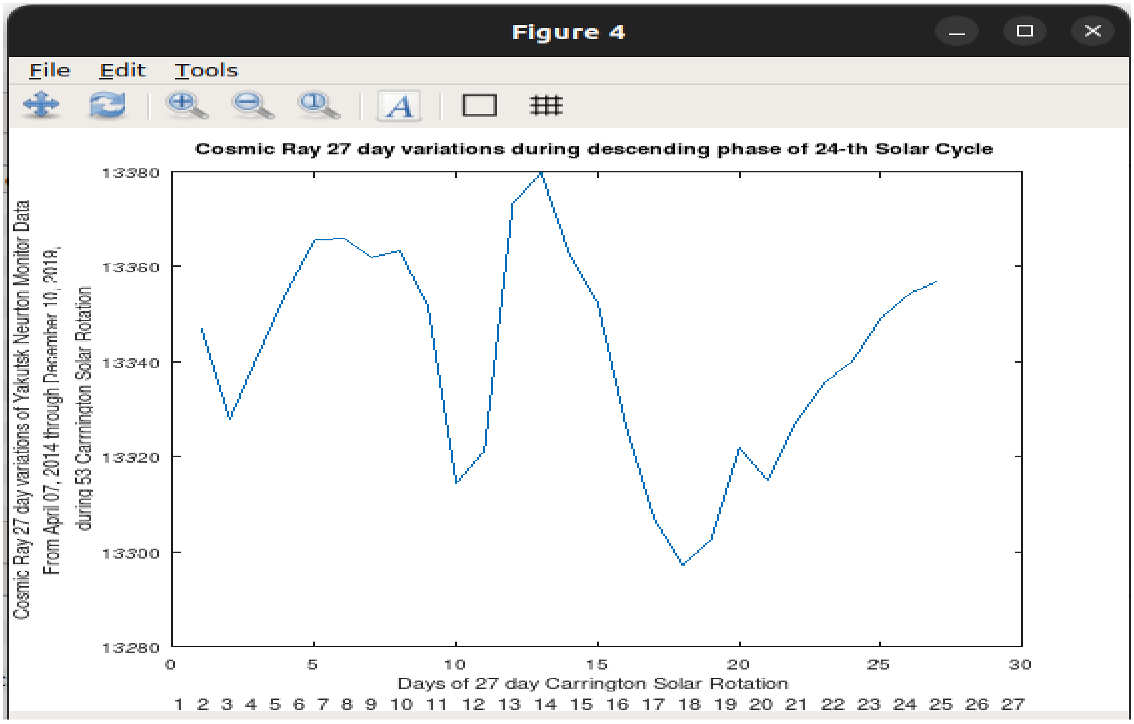

Fig. 4. Solar Activity Descending phase, Yakutsk.

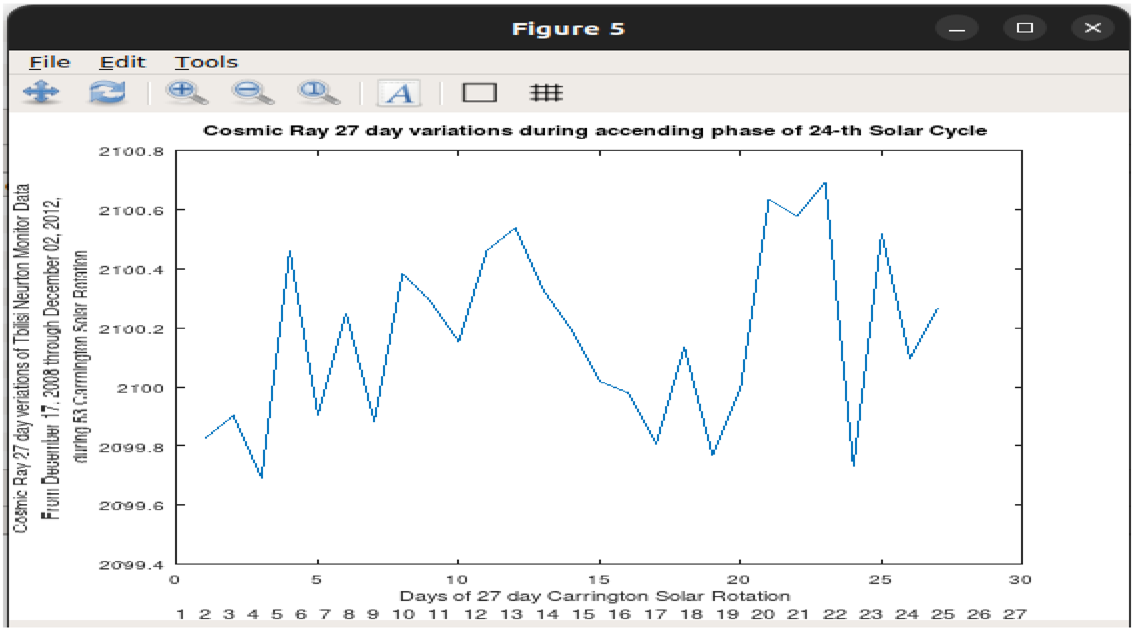

Fig. 5. Solar Activity Ascending phase, Tbilisi.

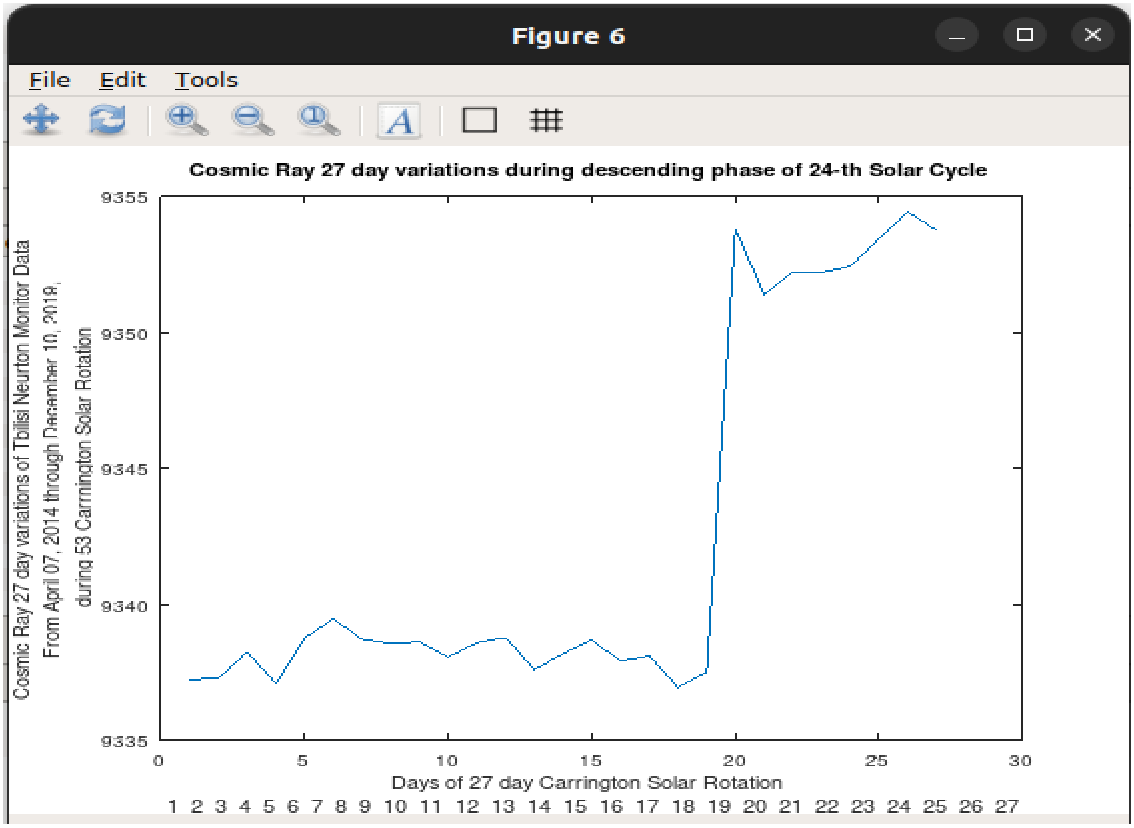

Fig. 6. Descending phase, Tbilisi

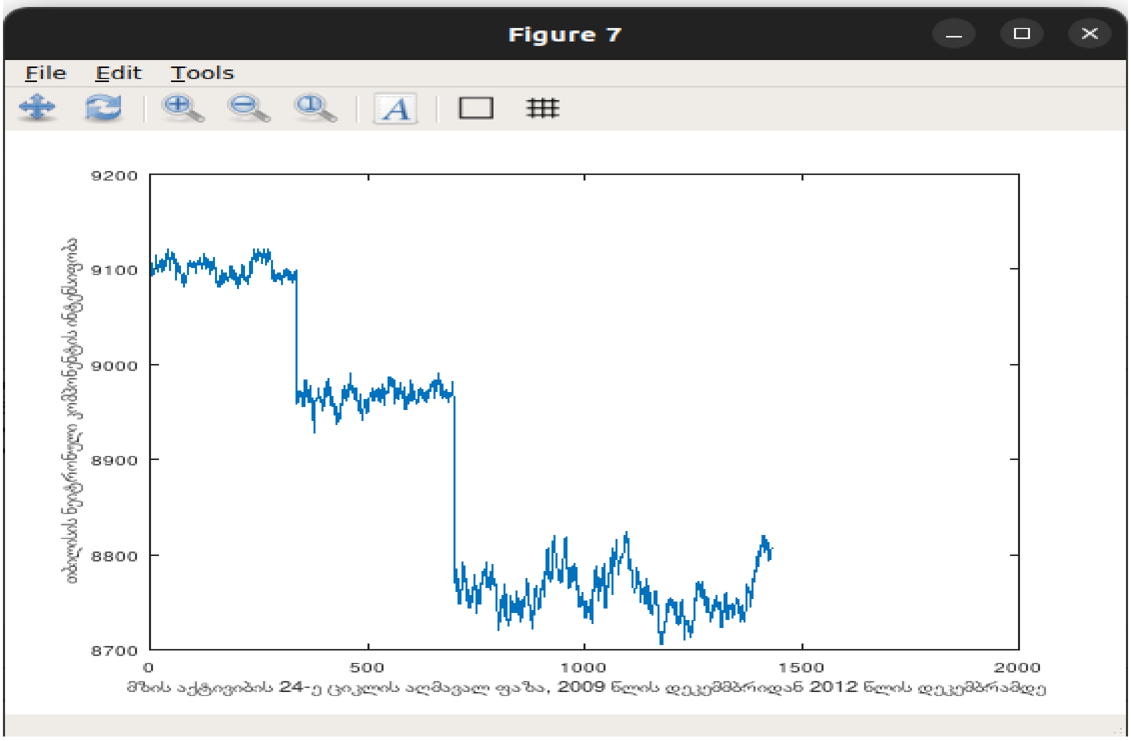

Fig. 7. Tbilisi Neutron Monitor intensity change during the ascending phase of the 24-cycle solar activity, from 2009 to 2012

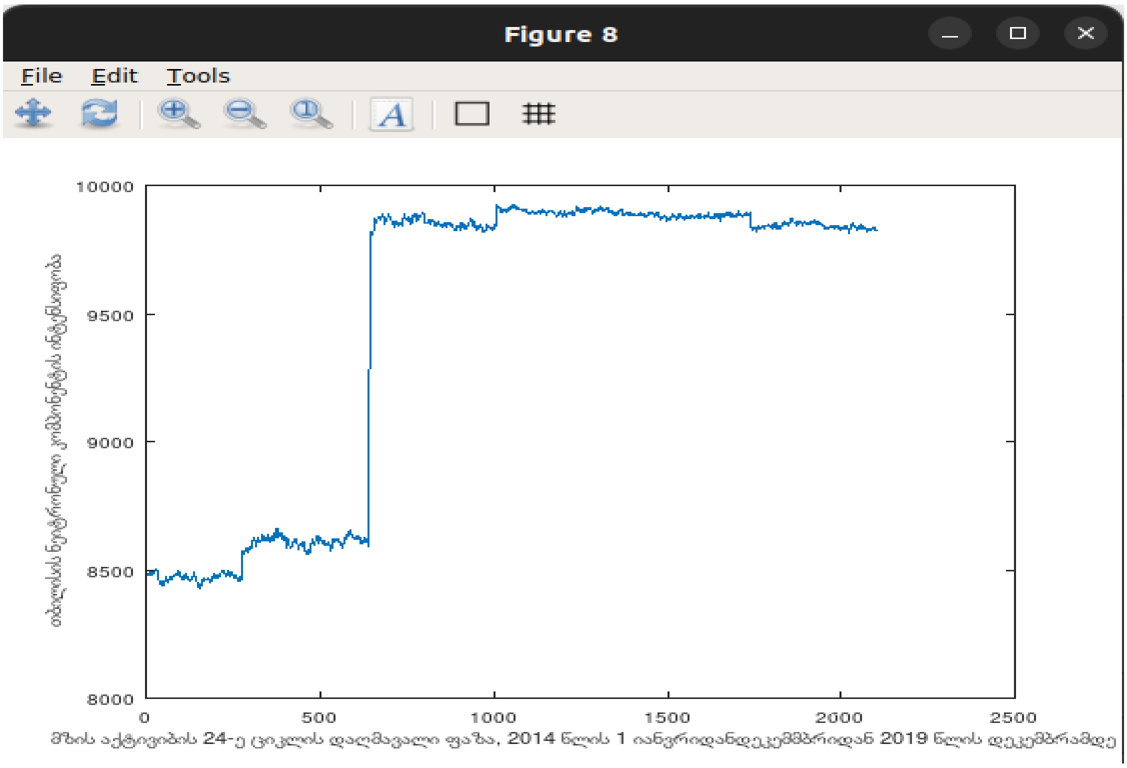

Fig. 8. Tbilisi Neutron Monitor intensity change during the declining phase of the 24-cycle solar activity, from 2014 to 2019.

4. Discussion

The 27-day variations of the Neutron Monitor of the World Wide Web (Moscow and Yakutsk) show that the 27-day variation profile describes a quasi-sinusoidal curve (Fig. 1, Fig. 2, Fig. 3, Fig. 4). The difference between the quasi-sinusoidal profiles in the rising and falling phases should be caused by different sunspots in the rising and falling phases. The 27-day variation profile of the Tbilisi Neutron Monitor does not describe a quasisinusoidal curve (Fig. 5, Fig. 6), which can be explained by the variation pro- file of the hourly intensity data of the Tbilisi Neutron Monitor (Fig. 7, Fig. 8).

5. Conclusion

The 27-day variation profile of the neutron component of cosmic rays is described by a quasi-sinusoidal curve, and the deviation from the sinusoidal curve is caused by the coordinates and strength of sunspots.

References

[1] https://link.springer.com/article/10.1023/A:1014296529097

[2] https://www.sidc.be/SILSO/node/52

[3] http://www.spacetoday.org/SolSys/Sun/Sunspots.html

[4] https://www.weather.gov/news/201509-solar-cycle

[5] Дорман Л.И. Вариации Космических Лучей. “Государственное издательство Технико-Теоретической Литературы”, М., 1957.

[6] Дорман Л.И. Вариации Космических Лучей и Исследование Космоса. “Издательство Академии Наук СССР”, М., 1963.

[7] Дорман Л.И. Вариации Галактических Космических Лучей. “Издательство Московского Университета” М., 1975.

[8] Дорман Л.И. Экспериментальные и Теоретические Основы Астрофизики Космических Лучей. “Наука”, М., 1975.

[9] Наскидашвили Б. Д., Шаташвили Л. Х. Квазипериодические вариации интенсивности космических лучей. Мецниереба, Тбилиси, 1981.

[10] Наскидашвили Б. Д., Рогава О. Г., Шаташвили Л. Х. Квазипериодические вариации космических лучей и солнечро-земные связи. Мецниереба, Тбилиси, 1991.

[11] Gil A., Alania M.V. α-ω Effect and peculiarities of the 27-day variations of the galactic cosmic rays intensity, solar wind and solar activity. Advances in Space Research, Volume 52, Issue 5, 2013, pp. 951-956.

[12] Gil A., Alania M.V. Theoretical and Experimental Studies of the Rigidity Spectrum of the 27 Day variations of galactic Cosmic Ray Intensity in Diferent Epochs of Solar Activity. Solar Physics, Vol. 283, Issue 2, April 2013, pp. 565–577.

[13] Modzelewska R., Alania M.V., The 27-Day Cosmic ray Variations During Solar Minimum 23/24, Solar Physics, April 2013, doi:10.1007/s11207-13-0261-4

[14] Gil A., Alania M.V. Cycling changes in the amplitudes of the 27-day variation of the galactic cosmic rays intensity. Solar Physics, vol 278, 2, 2012, pp. 447-455. DOI: 10.1007/s11207-012- 9944-5

[15] Alania M.V., Wawrzynczak A., Energy dependence of the rigidity spectrum of Forbush decrease of galactic cosmic ray intensity. Advances in Space Research, Volume 50, Issue 6, September, 2012, pp. 725–730. doi:10.1016/j.asr.2011.09.027,

[16] Modzelewska R., Alania M.V. Dependence of the 27-day variation of cosmic rays on the global magnetic field of the Sun. J. Adv. Space Res.,Volume 50, Issue 6, September, 2012, pp. 716–724, doi:10.1016/j.asr.2011.07.022

[17] Wawrzynczak A., Modzelewska R., Alania M. V. Three dimensional model of the interplanetary magnetic field and 27-day variation of the galactic cosmic ray intensity. Astrophys. Space Sci. Trans., 7, 2011, pp. 351-354. doi:10.5194/astra-7-351-2011

[18] Gil A., Modzelewska R., Alania M.V. 27 - day variations of the galactic cosmic ray intensity and anisotropy in the minimum of the 23rd solar activity cycle. Advances in Space, Vol. 50, Issue 6,

September 2012, pp. 712-715.
[19] Sdobnov V. E. et al. Features of the cosmic ray 27-day variation within 2014 November-December. JJ. Phys.: Conf. Ser. 1181 012005, 2019J. Phys.: Conf. Ser. 1181 012005, 2019J. Phys.: Conf. Ser. 1181 012005, 2019J. Phys.: Conf. Ser. 1181 012005, 2019. https://iopscience.iop.org/article/10.1088/1742-6596/1181/1/012005/pdf
[20] Meyer P., Simpson J. A. Changes in Amplitude of the Cosmic-Ray 27-Day Intensity Variation with Solar Activity. Phys. Rev. 96, 1085 – Published 15 November, 1954 DOI:https://doi.org/10.1103/Phys Rev.96.1085

კოსმოსური სხივების 27-დღიანი ვარიაციები მზის აქტივობის 24-ე ციკლის აღმავალ და დაღმავალ ფაზაში

გ. ვანიშვილი, თ. ბაქრაძე, ე. ალანია, ტ. ერქომაიშვილი, ვ. ყავლაშვილი, მ. ღუღუნაშვილი, ო. ხაჯიშვილი

რეზიუმე

მზის აქტივობის 24-ე ციკლის აღმავალ და დაღმავალ ფაზაში, კოსმოსური სხივების მსოფლო ქსელის ორი (მოსკოვი და იაკუტსკი) სადგურის და თბილისის კოსმოფიზიკური ობსერვატორიის, კოსმოსური სხივების ნეიტრო- ნული კომპონენტის, 27 -დღიანი ვარიაციების შესწავლის საფუძველზე დადგენილია, რომ 27-დღიანი ვარიაციის პროფილი აღწერს კვაზისინუსოი- იდას. სინუსოიდალური წირიდან გადახრა განისაზღვრება მზის აქტივობის მოცემულ ფაზაში მზის ლაქების (2.2 აღმავალ ფაზაში და 81.8 დაღმავალ ფაზაში) რიცხვის, კოორდინატებისა და სიმძლავრის ცვლილების მიხედვით.

საკვანძო სიტყვები: კოსმოსური სხივების 27-დღიანი ვარიაციები, მზის ციკლი, ბარტელის ბრუნვის რიცხვი, კარინგტონის ბრუნვის რიცხვი, მზის აქტივობის აღმავალი და დაღმავალი ფაზები, კოსმოსური სხივების ნეიტრონული მონიტორების მსოფლიო ქსელი, კვაზი-სინუსოიდური მრუდი.

27-дневные вариации космических лучей в восходящей и нисходящей фазах 24-го цикла солнечной активности

Г. Ванишвили, Т. Бакрадзе, Е. Алания, Т. Эркомаишвили, В. Кавлашвили, М. Гугунашвили, О. Хаджишвили

Резюме

На основе исследования 27-дневных вариаций нейтронной компоненты космических лучей в восходящей и нисходящей фазе 24-го цикла солнечной активности на двух станциях Глобальной сети космических лучей (Москва и Якутск) и Тбилисской космофизической обсерватории установлено, что профиль 27-дневных вариаций описывает квазисинусоидальную кривую. Отклонение от синусоидальной кривой определяется изменением числа, координат и интенсивности солнечных пятен (2,2 в восходящей фазе и 81,8 в нисходящей фазе) в течение данной фазы солнечной активности.

Ключевые слова: 27-дневные вариации космических лучей, солнечный цикл, число вращения Бартельса, число вращения Каррингтона, восходящая и нисходящая фазы солнечной активности, всемирная сеть мониторов нейтронов космических лучей, квазисинусоидальная кривая.

Information for contributors

Papers intended for the Journal should be submitted in two copies to the Editor-in-Chief. Papers from countries that have a member on the Editorial Board should normally be submitted through that member. The address will be found on the inside front cover.

1. Papers should be written in the concise form. Occasionally long papers, particularly those of a review nature (not exceeding 16 printed pages), will be accepted. Short reports should be written in the most concise form not exceeding 6 printed pages. It is desirable to submit a copy of paper on a diskette.
2. A brief, concise abstract in English is required at the beginning of all papers in Russian and in Georgian at the end of them.
3. Line drawings should include all relevant details. All lettering, graph lines and points on graphs should be sufficiently large and bold to permit reproduction when the diagram has been reduced to a size suitable for inclusion in the Journal.
4. Each figure must be provided with an adequate caption.
5. Figure Captions and table headings should be provided on a separate sheet.
6. Page should be 20 x 28 cm. Large or long tables should be typed on continuing sheets.
7. References should be given in the standard form to be found in this Journal.
8. All copy (including tables, references and figure captions) must be double spaced with wide margins, and all pages must be numbered consecutively.
9. Both System of units in GGS and SI are permitted in manuscript
10. Each manuscript should include the components, which should be presented in the order following as follows:
    Title, name, affiliation and complete postal address of each author and dateline.
    The text should be divided into sections, each with a separate heading or numbered consecutively.
    Acknowledgements. Appendix. Reference.
11. The editors will supply the date of receipt of the manuscript.

CONTENTS - სარჩევი

საქართველოს გეოფიზიკური საზოგადოების ჟურნალი

მყარი დედამიწის, ატმოსფეროს, ოკეანისა და კოსმოსური პლაზმის ფიზიკა

ტომი 29, № 1

ჟურნალი იბეჭდება საქართველოს გეოფიზიკური საზოგადოების პრეზიდიუმის დადგენილების საფუძველზე

ტირაჟი 20 ცალი

JOURNAL OF THE GEORGIAN GEOPHYSICAL SOCIETY

Physics of Solid Earth, Atmosphere, Ocean and Space Plasma

Vol. 29, № 1

Printed by the decision of the Georgian Geophysical Society Board

Circulation 20 copies

ЖУРНАЛ ГРУЗИНСКОГО ГЕОФИЗИЧЕСКОГО ОБЩЕСТВА

Физика Твердой Земли, Атмосферы, Океана и Космической Плазмы

Том 29, № 1

Журнал печатается по постановлению президиума Грузинского геофизического общества

Тираж 20 экз

Tbilisi-თბილისი-Тбилиси
2026